Two-Stage Multi-Channel LED Driver with CLL Resonant Converter

Xuebing Chen

Thesis submitted to the Faculty of the
Virginia Polytechnic Institute and State University
in partial fulfillment of the requirements for the degree of

Master of Science
in
Electrical Engineering

Qiang Li, Chair
Fred C. Lee
Rolando Burgos

August 8th, 2014
Blacksburg, Virginia

Keywords: Multi-channel LED driver, two-stage LED driver, resonant converter, output current balance

Two-Stage Multi-Channel LED Driver with CLL Resonant Converter

Xuebing Chen

Abstract

LED is widely used in many applications, such as indoor lighting, backlighting and street lighting, etc. For these application, multiple LED strings structure is adopted for reasons of cost-effectiveness, reliability and safety concerns. Several methods and topologies have been proposed to drive multiple LED strings. However, the output current balance and efficiency are always the two major concerns for LED driver.

A simple two-stage multi-channel LED driver is proposed. It is composed of a buck converter as the first stage and a multi-channel constant current (MC^3) CLL resonant converter as the second stage. For the CLL resonant converter, the magnetizing inductance of the transformer can be as large as possible. Therefore, the magnetizing current of the transformer has little influence on the output currents. In addition, the currents of two LED strings driven by the same transformer is balanced by a DC blocking capacitor. As a result, the current balance among LED strings is very good, even if the load is severely unbalanced. Meanwhile, the current flowing through the external inductance L_{r1}, instead of the magnetizing current is used to help the primary-side switches to achieve ZVS. Therefore, large magnetizing inductance is good for current balance and properly designed L_{r1} is helpful for ZVS achievement. These properties of MC^3 CLL are preferred to drive multi-channel LED strings.

In the design procedure of MC^3 CLL resonant converter, the parasitic junction capacitor of the secondary-side rectifier is taken into account. It influences the operation during dead time significantly when the voltage step-up transformer is applied. The junction capacitors of the secondary-side rectifiers, and the output capacitors of the primary-side switches will resonate with the inductor L_{e2} during the dead time. Finally, this resonance impact the ZVS achievement of the primary-side switches. Therefore, the inductors L_{r1} and L_{e2} should be designed according the charge needed to achieve ZVS with considering the resonance.

Additionally, the control strategy for this two-stage structure is simple. Only the current of one specific LED string is sensed for feedback control to regulate the bus voltage, and the currents of other LED strings are cross-regulated. Furthermore, the MC^3 CLL is unregulated and always working around the resonant frequency point to achieve best efficiency. The compensator is designed based on the derived small signal model of this two-stage LED driver. Due to the special electrical characteristics of LED, the soft start-up process with a delayed dimming signal is adopted and investigated. With the soft start-up, there is no overshoot for the output current.

Finally, a prototype of the two-stage LED driver is built. The current balance capability of the LED driver is verified with the experiment. Good current balance is achieved under balanced and severely unbalanced load condition. In addition, the efficiency of the LED driver is also presented. High efficiency is guaranteed within a wide load range. Therefore, this two-stage structure is a very promising candidate for multi-channel LED driving applications.

Acknowledgments

First of all, I would like to express my sincere gratitude to my advisor, Dr. Qiang Li, for his advising, encouragement, and generous patience. It is him who guides me into the field of power electronics. I have learned a lot from his extensive thinking and his rigorous research attitude during the past two years. He often shares his philosophy with me, which is the most helpful to me. Without his help, none of the work showing here would be possible.

I am also grateful to Dr. Fred C. Lee, for his enthusiastic help during my research on LED driver. His insightful suggestions and creative ideas influence me deeply for my research. I also want to acknowledge Dr. Rolando Burgos for his support, comments and suggestions.

I would also like to thank all the great staff in CPES: Ms. Teresa Shaw, Ms. Marianne Hawthorne, Ms. Teresa Rose, Ms Linda Long, Mr. David Gilham, Dr. Wenli Zhang, Dr. Mingkai Mu, Dr. Xuning Zhang, and Dr. Zhiyu Shen.

It is such a pleasure to work in CPES and it is such an honor to be part of the great family. I would also like to thank all the people that have been part of my life: Dr. Yingyi Yan, Dr. Weiyi Feng, Dr. Daocheng Huang, Dr. David Reusch, Dr. Zheng Chen, Dr. Xin Ming, Dr. Weijing Du, Mr. Shu Ji, Mr. Yipeng Su, Mr. Pei-Hsin Liu, Mr. Bo Wen, Mr. Shuilin Tian, Mr. Wei Zhang, Mr. Xiucheng Huang, Mr. Dongbin Hou, Mr. Zhengyang Liu, Mr. Yuchen Yang, Mr. Yang Jiao, Mr. Sizhao Lu, Mr. Zheming Zhang, Mr. Zhongsheng Cao, Mr. Chao Fei, Ms. Yincan Mao, Mr. Syed Bari, Mr. Jun Wang, Mr. Fang Chen, Mr. Qiong Wang, Mr. Chi Li, Mr. Ming Lu, Mr. Bin Li, Mr. Tao Liu, Mr. Shishuo Zhao, Mr. Shuojie She, Ms. Han Cui, Ms. Bingyao Sun. I cherish the wonderful time together and the great friendship.

With the greatest love and gratitude to my parents, I would like to thank them for their selfless support to my study in the past twenty years. This is a wonderful journey for me in the past years.

I would like to thank Panasonic Corporation for the funding on the project “Current Driver for Solid State Light Sources with Wide Load Variation”. Special thanks go out to the CPES PMC mini-consortium members for the funding on my research. They are 3M Company, Altera - Enpirion Power, Chicony Power, CSR Zhuzhou Institute Co., Ltd., Delta Electronics, Huawei Technologies, International Rectifier, Linear Technology, Macroblock, Inc., Murata Manufacturing Co., Ltd., NEC TOKIN Corporation, NXP Semiconductors, Richtek Technology, Texas Instruments.

Table of Contents

List of Figures

List of Tables

Chapter 1. Introduction

1.1 LED Lighting

The light-emitting diode (LED) and organic light-emitting diode (OLED) both belong to solid state light source. LED is a two-lead semiconductor light source. It resembles a basic pn-junction diode, but it will emit light when it is activated. When a proper voltage is applied to the two terminals of LED, the electrons will recombine with the electron holes inside the device. Consequently, it will release the energy in the form of photons. Furthermore, the color of the light is determined by the energy band gap of the semiconductor [1]. Generally speaking, LEDs are small-point light sources, as Fig. 1.1 (a) shows.

OLED is a diffuse-area light source, as shown in Fig. 1.2 (b). It is also a light-emitting diode. However, it has an emissive electroluminescent layer which is composed by the organic compound. The organic film is situated between two electrodes. It will emit light when the electric current is flowing through it. Although the OLED technology is developing rapidly these days, there is still a long way for OLED to become a practical light source. At present, most of OLED products are used for small-area displays, such as smartphones and digital camera etc.

(a) LED lamp (b) OLED lamp

Fig. 1.1. Two kinds of solid state light source

Lighting accounts for approximately 15% of global electricity consumption. As the US Energy Information Administration (EIA) estimates that LEDs will produce more than 150 lumens per watt by 2020, comparing with the present performance of about 83 lumens per watt. In contrast, traditional incandescent lamps presently produce only 16 lumens of light output per watt, while halogen incandescent lamps produce nearly 20 lumens and equivalent compact fluorescent lamps (CFL) provide about 67 lumens. LEDs have higher efficacy than its rivals. In addition, the US Department of Energy (DOE) estimates that LEDs presently last 30,000 to 50,000 hours. However, the lifespan of CFLs is about 8,000 to 10,000 hours and 1,000 hours for a typical incandescent bulb. Therefore, LEDs have longer life time than conventional light sources.

For LED, it has higher luminous efficacy and longer life time than conventional light sources. Moreover, LEDs are eco-friendly and have good current rendering properties. Therefore, LEDs are very promising light sources and are widely used in many applications, such as indoor lighting, display backlighting and street lighting.

The electrical characteristics of the LED lamp is presented in Fig. 1.2. When the voltage applied to the LED reaches its threshold voltage, the LED starts to emit light. If the voltage is higher than the threshold voltage, the forward current will increase exponentially as the voltage goes up. In the same time, the voltage across the LED has negative coefficient. As the junction temperature rises, the voltage will decrease. Additionally, the brightness of the LED lamp is determined by the forward current. Therefore, the forward current of the LED lamp is regulated instead of the voltage to achieve dimming.

LED’s forward current is exponential to its forward voltage when the LED is lit. Therefore, a little variation of the forward voltage will result in a dramatic change of the forward current. How to drive LEDs? Since the forward current determines the brightness, the LEDs are in series and

they are driven by a constant current source. In this way, each LED can achieve uniform brightness and similar thermal performance. However, the number of LEDs in series can't be very large to avoid higher voltage needed. In practice, multiple LED strings' structure is widely adopted for reasons of cost-effectiveness, reliability and safety concerns. How to drive multiple LED strings at the same time? This is a challenge for multi-channel LED driver. Meanwhile, how to make the current of each LED string to be identical? This is another challenge for multi-channel LED driver.

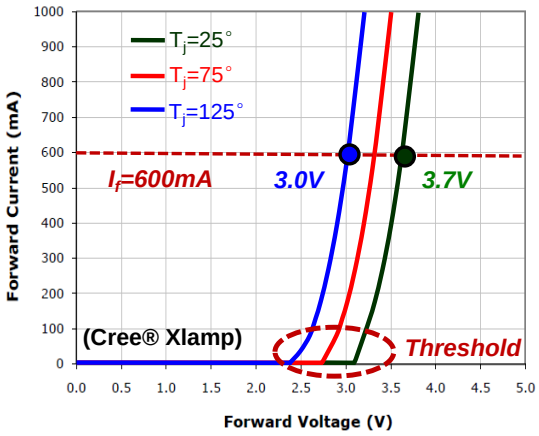

Fig. 1.2. Electrical characteristics of LED lamp

1.2 Current Balance Methods

Several methods have been proposed to achieve good current balance. Generally, these methods can be divided into two categories: passive methods and active methods. In active methods, for each LED string, there will be a switching mode converter or linear regulator to regulate the current individually [2], [3]. With these methods, the current of each string could be controlled precisely and there is no current imbalance issue. However, these methods require a dedicated drive circuit for each LED string. It will increase the system complexity and cost when a large number of parallel LED strings are driven at the same. In addition, the conversion efficiency is relatively low when the linear current regulator is used.

In passive methods, there will be passive components like resistors, capacitors or coupled inductors in series with each LED string [4]-[7]. These passive components are used to balance the currents among LED strings. The easiest way to balance the currents among parallel LED strings is to insert a series resistor in each branch. The voltage drop across the series resistor will compensate the voltage difference between LED strings. The drawbacks of this method is that the series resistor in each branch should be fine-tuned according to the voltage difference. Besides that, the power consumption on the resistors will be considerable when the voltage difference is large [4]. In [5], coupled inductor is used to balance the current among LED strings. It can drive 2^N LED strings at the same time. However, this method needs to provide the coupled inductor with AC voltage or AC current. In [6], the current balancing transformer is used to balance the currents of parallel LED strings. In order to weaken the influence of the magnetizing current, the impedance must be very large. In [7], the capacitive balancing mechanism is applied. For passive methods, the current balance capability is very sensitive to the impedance of passive components. The larger the impedance is, the better the current balance will be.

1.3 Topologies of Multi-Channel LED Driver

Several single-stage structures of multiple channel LED driver have been proposed recently. In [8] and [9], a single-stage multi-channel constant current (MC^3) LED driver is presented, as shown in Fig. 1.3. In the proposed MC^3 LED driver, the transformers are in series on the primary side. With the same magnetizing inductance and same turns ratio, the currents flowing through the secondary side windings of the transformer are identical. Therefore, the output current will be identical. Meanwhile, output inductors L_1, L_2 and L_n could be coupled with each other to improve the current balance among LED strings when the loads are unbalanced. From control point of view, the current of one specific LED string is sensed for feedback control, and the currents of other

LED strings are cross-regulated. The disadvantage of this structure is that one transformer only drives one LED string. More transformers are required for driving multiple LED strings. For the primary side switches, the switching loss will be significant since they are hard switching.

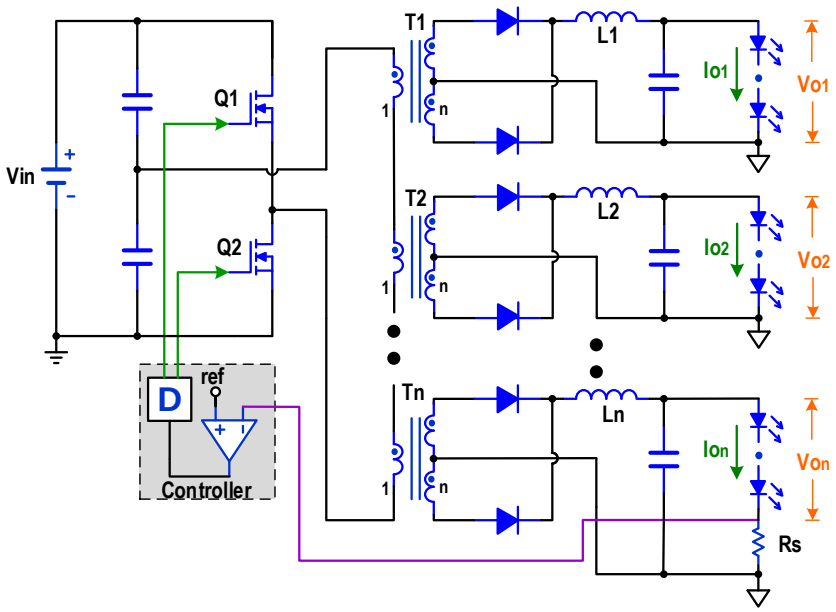

Fig. 1.3. Multi-channel constant current source (MC^3) LED driver [8], [9]

In [10], a 110-W multi-channel LED driver is proposed. It consists of boost PFC, buck converter and half-bridge DC transformer. The buck converter provides a controlled current source according to dimming requirement. And the half-bridge DC transformer is used for the isolation of four LED strings, as Fig. 1.4 shows. Meanwhile, the voltage-doubler structure is adopted on the secondary side. One transformer can drive two LED strings at the same time. Therefore, the number of the transformer can be reduced. In addition, a DC blocking capacitor is used to balance the currents between two LED strings driven by the same transformer.

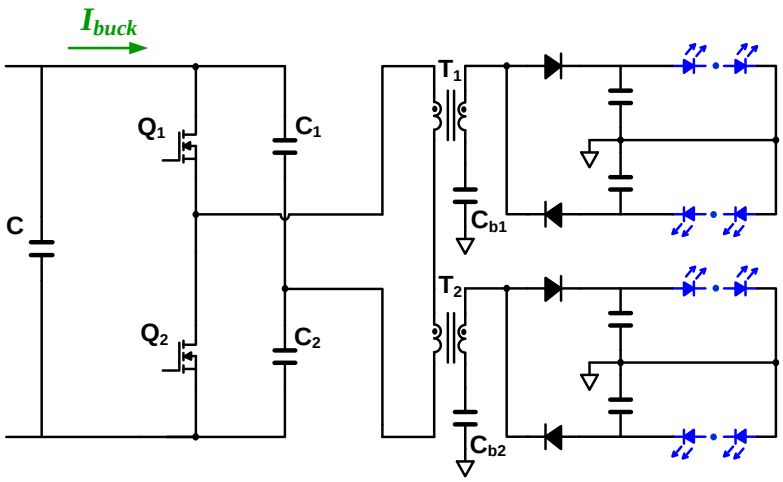

Fig. 1.4. Half-bridge DC transformer with voltage-doubler structure [10]

In [11], an LED driver based on the voltage-fed half-bridge topology is proposed, as Fig. 1.5 shows. One transformer drives two LED strings at the same time and the currents of two LED strings are balanced by the DC block capacitor. It is able to drive multiple LED strings with more transformers in series on the primary side. However, the operation of this LED driver is a little bit complicated, particularly when it is driving more than two LED strings at the same time. The structure on the primary side could be full-bridge or push-pull as well. On the secondary side, it could be also the bridge-type rectifier or current-doubler rectifier structures [12].

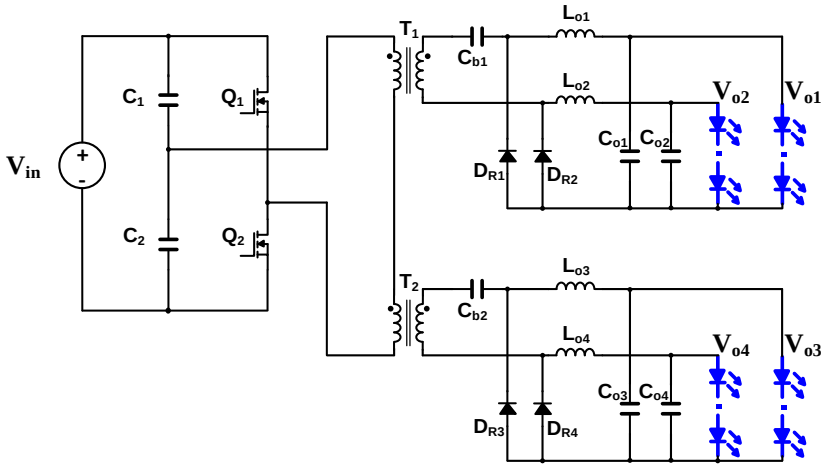

Fig. 1.5. Voltage-fed half-bridge topology for LED driving [11]

In [13], a capacitor-isolated LED driver based on LLC resonant converter is proposed, as Fig. 1.6 shows. One module drives two LED strings. The capacitors C_{r1} and C_{r2} play three roles. They provide isolation between the primary side and the secondary side. And they are used for the current balance between String 1 and String 2. In addition, they are also the resonant capacitors. For the current balance between different modules, the resonant inductor will be coupled. The basic structure of the capacitor-isolated LED driver is very attractive. However, the operation with more modules will be more complicated than the basic structure.

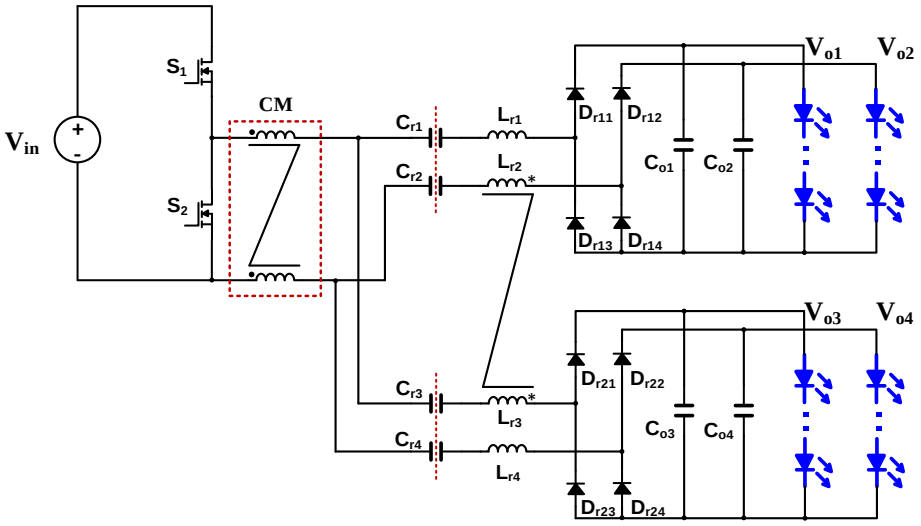

Fig. 1.6. Capacitor-isolated LED driver [13]

Resonant converter is also adopted for driving LED. LLC resonant converter is widely used for the power supplies of server, telecom etc. In [14], a MC^3 LLC resonant converter is proposed to drive multiple LED strings. The LLC resonant converter can achieve ZVS for the primary-side switches and ZCS for the secondary-side rectifiers, so that the switching loss will be significantly reduced. It can achieve high efficiency under the optimal working point. Meanwhile, the voltage-doubler structure is applied on the secondary side. Each transformer module can drive two LED strings at the same time.

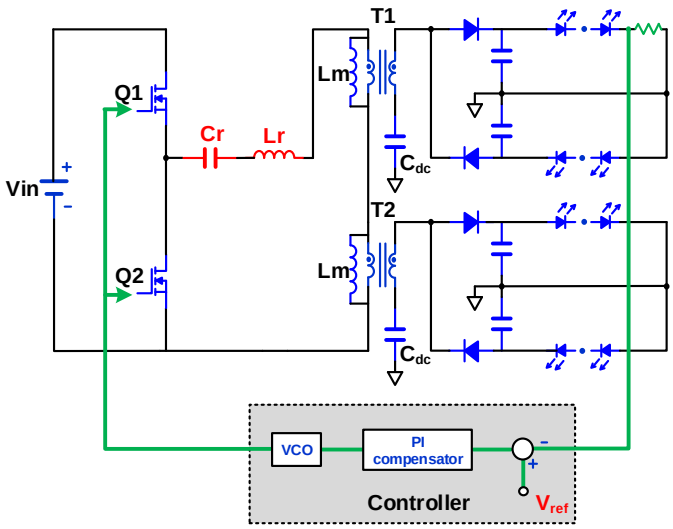

Fig. 1.7. MC^3 LLC resonant LED driver [14]

For these LLC-based single-stage structures, the switching frequency of LLC converter is regulated when the input voltage varies or the LED dims. Therefore, high efficiency can't be guaranteed with input voltage variation or dimming because the LLC does not always work at the optimum point.

In [15], a two-stage multi-channel LED driver is proposed. It contains a buck converter as the first stage and a MC^3 LLC resonant converter as the secondary stage, as Fig. 1.8 shows. The current of one specific LED string is sensed for feedback control to regulate the bus voltage. The MC^3 LLC resonant converter is always working at the resonant frequency to achieve best efficiency. On the secondary side, the voltage-doubler structure is adopted and one transformer drives two LED strings. This structure can adapt to the load variation easily. Furthermore, low dimming can be achieved conveniently by tuning the bus voltage.

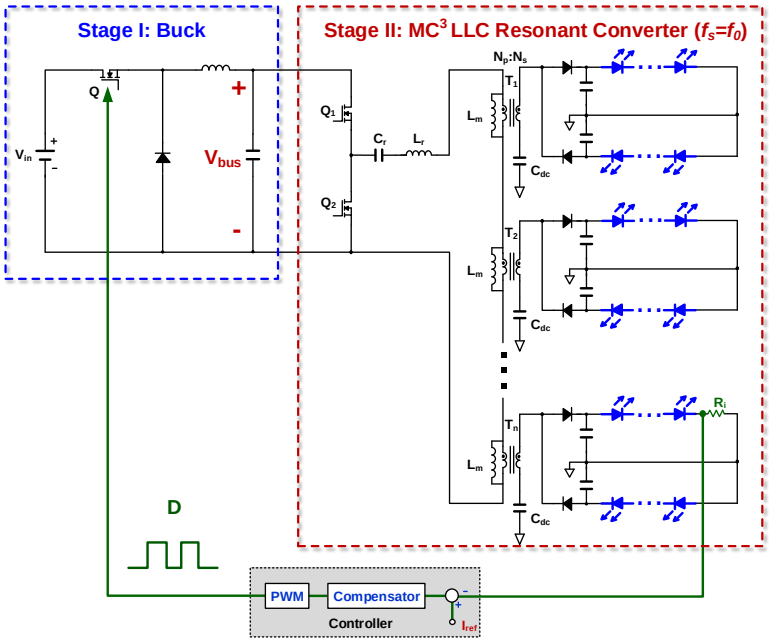

Fig. 1.8. Two-stage LED driver with MC^3 LLC resonant converter [15]

1.4 Objectives and Thesis Outline

LED is very promising in many applications, such as indoor lighting, display backlighting, and street lighting etc. With the development of the DC distribution system and the energy storage technology, the LED driver could be directly connected to the high voltage DC-bus. This thesis is focus on a multi-channel LED driver, whose input comes from the output of PFC or the high voltage DC-bus, as Fig. 1.9 shows. The specifications for this LED driver are presented in Table 1.1.

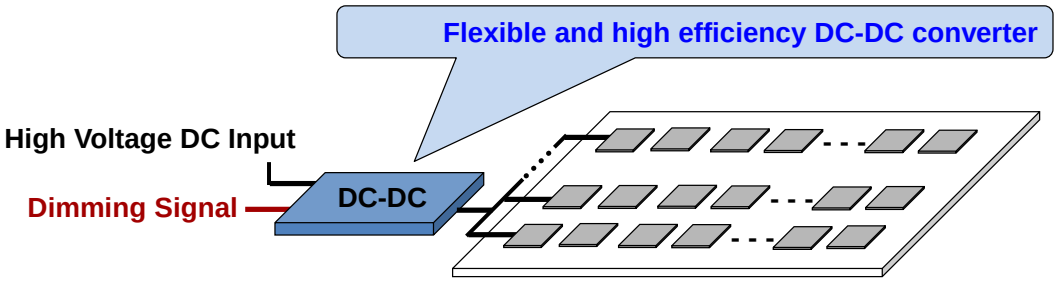

Fig. 1.9. Multi-channel LED driver with wide load variation

Table 1.1. Specifications of the LED driver

DC Input Voltage V_{in}	380V ±10%
Output voltage of channel	20~90V (Variable)
Normal output current of channel	300mA ±5%
Number of LED strings	2~10 (Variable)
Dimming Capability	5%~100%

The challenges for this LED driver are as follows:

1. Wide load variation (the number of LED and LED string can vary);

2. Good current balance among the LED strings (balanced load and unbalanced load);

3. High efficiency from 20% dimming to full load condition.

The outline of this thesis is as follows:

Chapter 1 introduces the basic characteristics of LED. The current balance mechanisms in multiple LED strings application are discussed. Meanwhile, several topologies used for driving multiple LED strings are also presented. At last, the objective of this thesis is also illustrated.

In Chapter 2, the current balance capability of the two-stage LED driver with MC^3 LLC resonant converter is discussed. Since the magnetizing inductor is critical for both ZVS of primary-side switches and current balance, it is difficult to find an optimal inductance to meet these two requirements. A two-stage LED driver with MC^3 CLL resonant converter is proposed. The characteristics of LLC are also presented.

Chapter 3 discusses the design considerations of the two-stage LED driver. The key point focuses on the MC^3 CLL resonant converter. The complete design procedure of MC^3 CLL resonant is illustrated. From the switches and the turns ratio of transformer, to the optimal dead time and

CLL resonant tank, a feasible design example is presented. In addition, the impact of junction capacitor of the secondary-side rectifier is investigated deeply for the voltage step-up application.

Chapter 4 presents the small-signal model of this two-stage LED driver. It combines the small-signal model of buck converter and CLL resonant converter. The analytical small signal model of the LED driver is verified with simulation. The PI compensator is designed based on the derivative model and the start-up process of the LED driver is also investigated.

Chapter 5 presents the experimental results of this two-stage LED driver. The current balance capability under balanced load and unbalanced load conditions is illustrated. Meanwhile, the efficiencies of the two-stage LED driver and MC^3 CLL resonant converter are presented respectively.

Chapter 6 summarizes the two-stage LED driver and discusses some possibilities for future work.

Chapter 2. Proposed Two-Stage LED Driver with CLL Resonant Converter

2.1 Two-Stage LED Driver with MC^3 LLC Resonant Converter

In order to achieve lower dimming ratio conveniently, a two-stage LED driver based on LLC resonant converter is proposed previously. It consists of a buck converter as the first stage and a MC^3 LLC resonant converter as the second stage, as Fig. 2.1 shows. The bus voltage V_{bus} is tuned to make the LEDs work at the required dimming condition. Additionally, the MC^3 LLC resonant converter is unregulated and it works like a DC transformer (DCX). Comparing with the conventional one-stage MC^3 LLC resonant converter [14], this two-stage LED driver can be implemented easily.

Usually, the best efficiency for LLC resonant converter can be achieved when switching frequency f_s is equal to resonant frequency f_0. Therefore, LLC working at resonant frequency point is preferred in practice. Based on this consideration, the switching frequency of MC^3 LLC resonant converter is fixed and it is always around the resonant frequency f_0. For this two-stage LED driver, one transformer module drives 2 LED strings. If there are more than 2 LED strings, more transformer modules could be plugged in, as shown in Fig. 2.2. Besides that, the current of one specific LED string is sensed for feedback control, and the currents of other LED strings are cross-regulated.

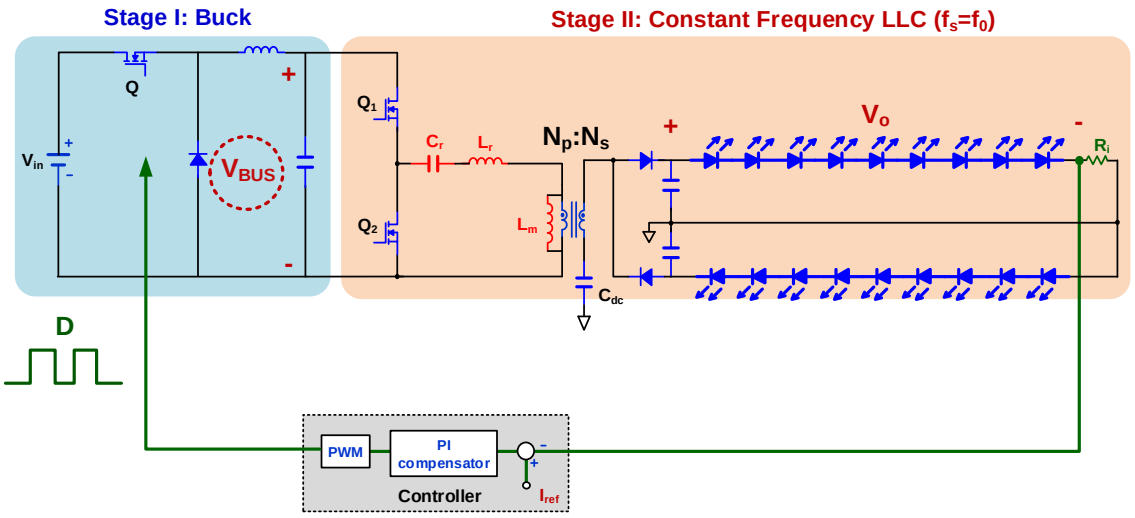

Fig. 2.1. Two-stage structure of LED driver with LLC resonant converter

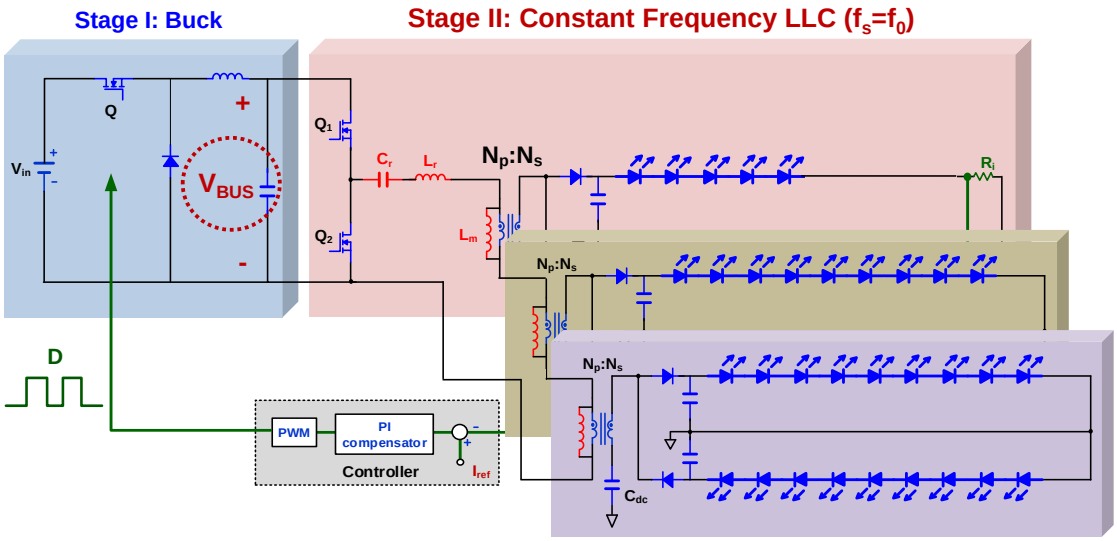

Fig. 2.2. Two-stage LED driver with more LED strings

2.2 Current Imbalance Issue of the MC^3 LLC Resonant Converter

The current balance capability is very critical for multiple LED strings application. How about the current balance capability of the MC^3 LLC resonant converter? For one transformer module, it drives 2 LED strings at the same time. If there is any voltage difference between these 2 LED strings, the DC block capacitor C_{dc} will balance the difference [16]. As a result, the forward

currents of these LED strings will be almost the same. For more transformer modules, since only one specific LED string's current is sensed for feedback control, the currents of the other LED strings are cross-regulated. Since each transformer module is in series at the primary side, the current flowing through the primary side winding of each transformer is the same. The current flowing through the secondary side winding of each transformer is expected to be the same as well. Therefore, good current balance could be achieved.

Take this LED driver with balanced load as an example, there are 5 transformer modules and 10 LED strings. The LED number of each string is identical and each string has 28 LEDs, as Fig. 2.3 shows. The current of one LED string driven by #1 transformer is sensed for feedback control. Under the full load condition (I_o=300mA), the forward voltage of this LED string is about 90V. Similarly, the currents and forward voltages of other LED strings are also about 300mA and 90V respectively. The turns ratio of the transformer is 1:3. Therefore, the voltage reflected onto the primary side is about 30V. The forward current of these LED strings are presented in Fig. 2.4.

In conclusion, the forward current of each string is identical, and the forward voltage of each string is identical as well. Furthermore, the magnetizing current of each transformer is also identical. Therefore, the current balance capability under the balanced load is excellent.

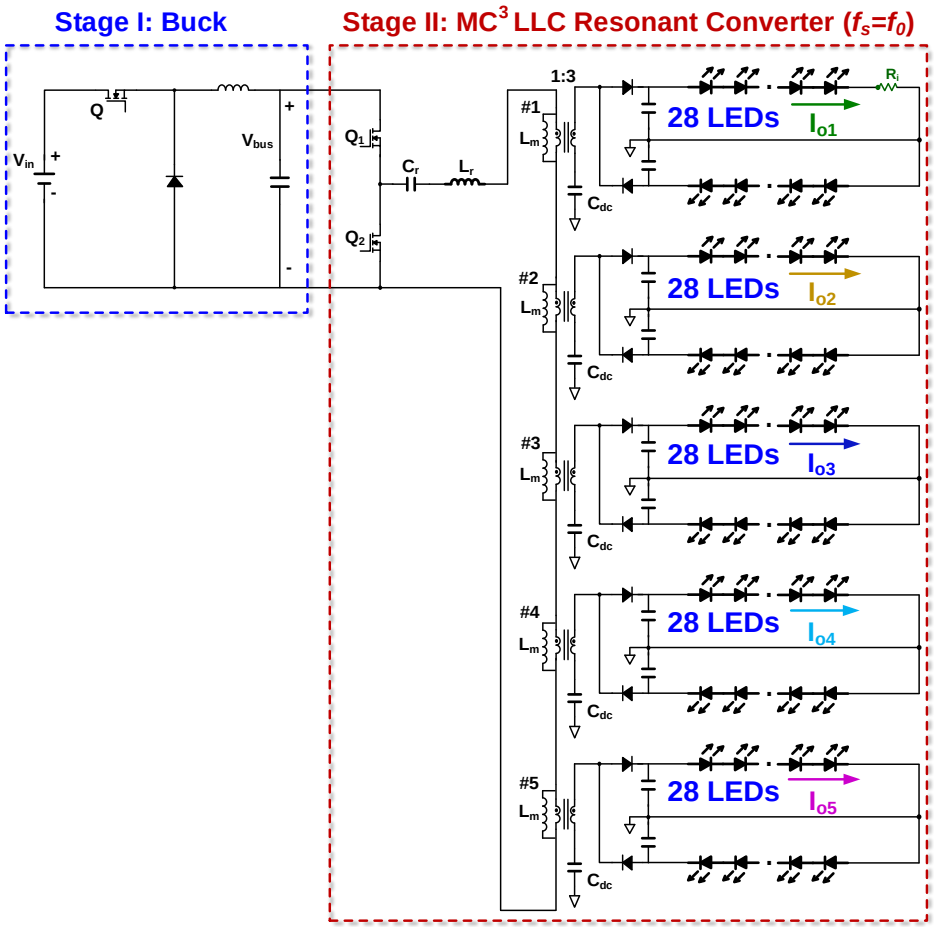

Fig. 2.3. LED driver with balanced load (10 strings)

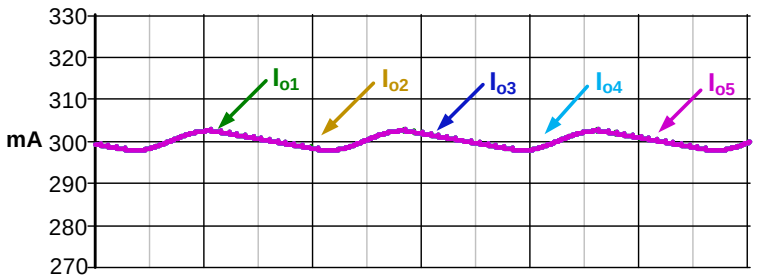

Fig. 2.4. LED string currents with balanced load (10 strings)

In practice, the LED number of each string is not always the same. The LED number of each string could be different according to the application. Even though the LED number of each string is the same, failure of LEDs could happen which usually results in short circuit. This will cause

the actual LED number in each string is different. It is preferred for the LED driver to maintain good current balance capability under such unbalanced load conditions.

For LLC resonant converter, we must pay much attention to the design of the magnetizing inductance of the transformer. The magnetizing current of the transformer is used to charge and discharge the output capacitors of primary side switches to help them to achieve ZVS during dead time. For this 2-stage LED driver, the magnetizing inductance is chosen as 20uH according to the ZVS requirement. Therefore, ZVS of primary side switches is guaranteed at full load condition regardless of the number variation of transformers.

For example, there are 5 transformers, and 2 LED strings driven by the same transformer have 10, 16, 19, 22 and 28 LEDs per string respectively, as Fig. 2.5 shows. The current of one LED string with 10 LEDs is sensed for feedback control. In this circumstance, the current of LED string with 10 LEDs is about 300mA (full load). The currents of other LED strings with less LED number will be less than 300mA, as Fig. 2.6 shows. The LED string with 28 LEDs will have the lowest current and it is about 240mA. Therefore, the current variation is about 20%.

What causes such huge current difference? Take the case with 2 transformers under unbalanced loads condition as example. There are 4 LED strings. The 2 strings driven by #1 transformer have 10 LEDs per string, and the other 2 strings driven by #2 transformer only have 28 LEDs per string, as Fig. 2.7 presents. The current of one LED string with 10 LEDs is sensed for feedback control. In this circumstance, the current of LED string with 10 LEDs is about 300mA (full load). The LED string with 28 LEDs will have the lowest current and it is about 240mA, as Fig. 2.8 shows. At the same time, the forward voltages of these LED strings have huge differences. They are 30V and 90V respectively. As a result, the voltages reflected onto the primary side of the transformers are 10V and 30V respectively. The magnetizing currents flowing through the

primary-side windings are totally different comparing with i_{Cr}, as Fig. 2.9 shows. Consequently, the currents flowing through the secondary side windings are with huge difference, as Fig. 2.10 shows. This results in the current variation among LED strings.

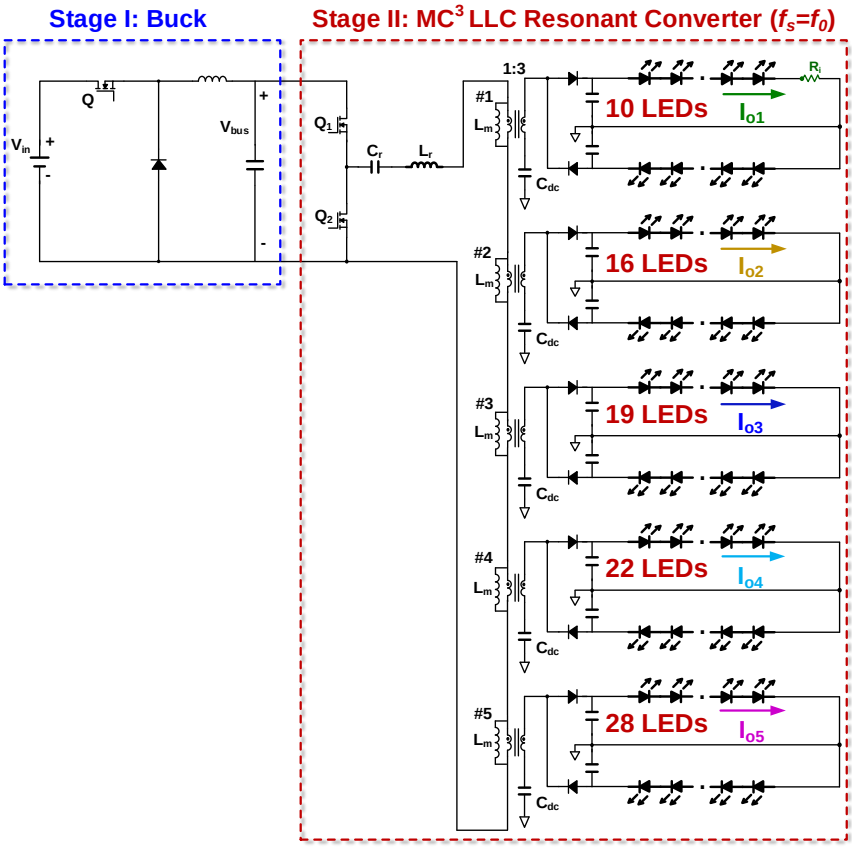

Fig. 2.5. LED driver with unbalanced load (10 strings)

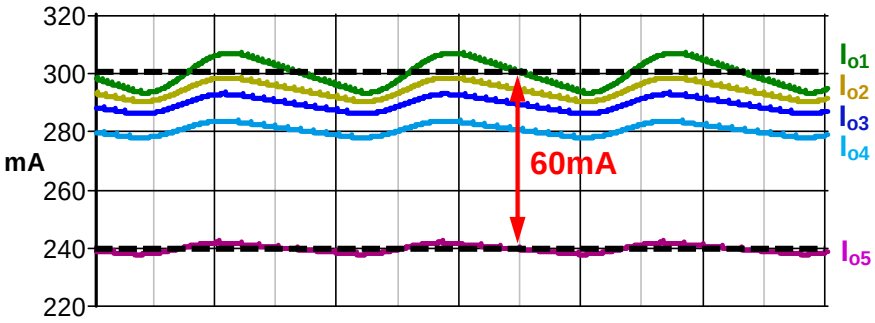

Fig. 2.6. LED string currents under unbalanced load (10 strings)

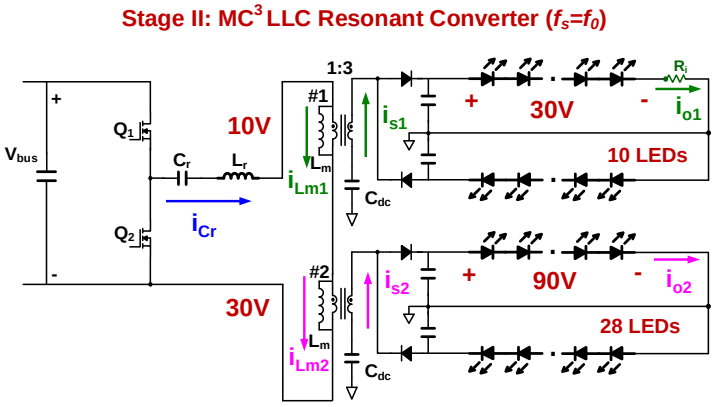

Fig. 2.7. LED driver with unbalanced load (4 strings)

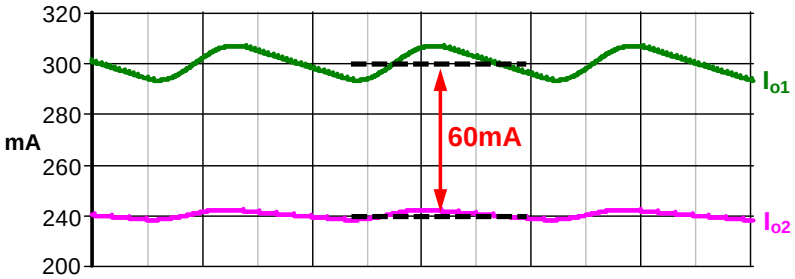

Fig. 2.8. LED string currents under unbalanced load (4 strings)

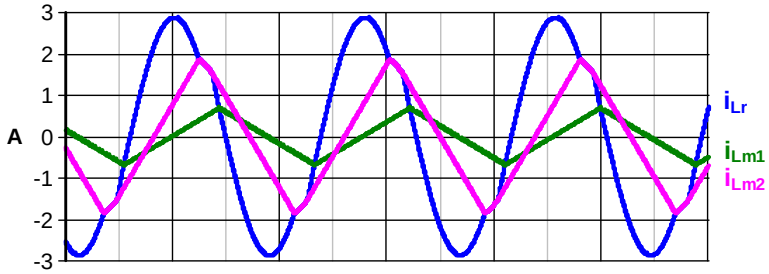

Fig. 2.9. Primary side current and the magnetizing currents under unbalanced loads (4 strings)

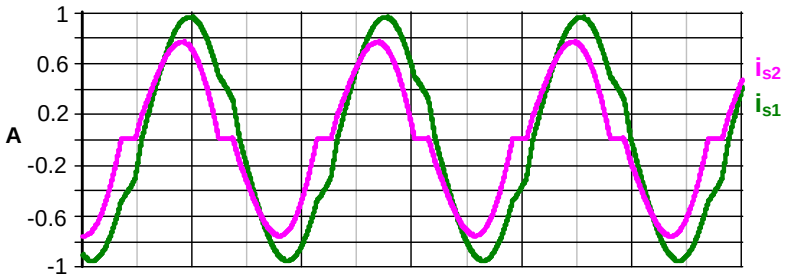

Fig. 2.10. Secondary side currents (4 strings)

In short, the current balance capability deteriorates under unbalanced load condition due to a small magnetizing inductance. In order to tackle this issue, the transformer with larger magnetizing inductance is preferred. Simply, we can make the magnetizing inductance of the transformer as large as possible. In practice, the magnetizing inductance could be increased to 160uH. For example, there are 5 transformers, and 2 LED strings driven by the same transformer have 10, 16, 19, 22 and 28 LEDs per string, as Fig. 2.5 shows. The current of the LED string with 10 LEDs is sensed for feedback control. In this circumstance, the current of the LED string with 10 LEDs is about 300mA (full load). The currents of other LED strings with more LED number will be a little bit lower than 300mA, as Fig. 2.11 shows. However, the current variation is only about 3.7mA (1.3%). Although the voltages across the primary side of the transformers have huge difference and the magnetizing currents are different as well, the amplitude of the magnetizing current is very small comparing with the amplitude of the resonant current, as Fig. 2.12 shows. The influence of the different magnetizing currents is negligible. The current balance capability of the LED driver with larger magnetizing inductance is excellent. However, for LLC, if the magnetizing inductance is very large, ZVS of the primary side switches is very hard to achieve, as Fig. 2.13 shows. Here is a dilemma. For the ease of achieving ZVS, a smaller magnetizing inductance is preferred. However, for good current balance capability, a larger magnetizing inductance is favored. In a word, LLC resonant converter is not a good candidate for the multiple LED strings driving application.

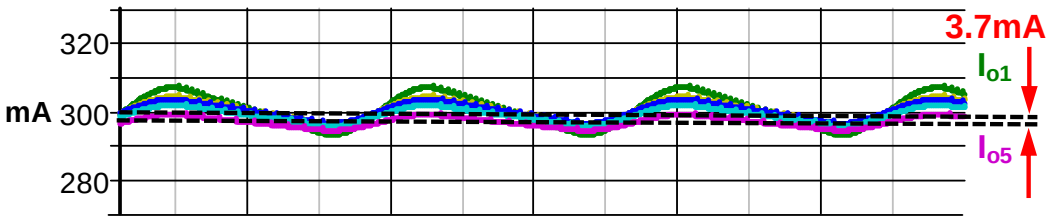

Fig. 2.11. Output currents under unbalanced load (large Lm)

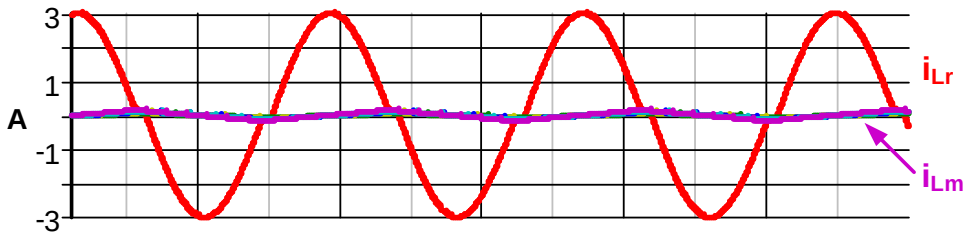

Fig. 2.12. Primary side current and the magnetizing currents under unbalanced loads (large Lm)

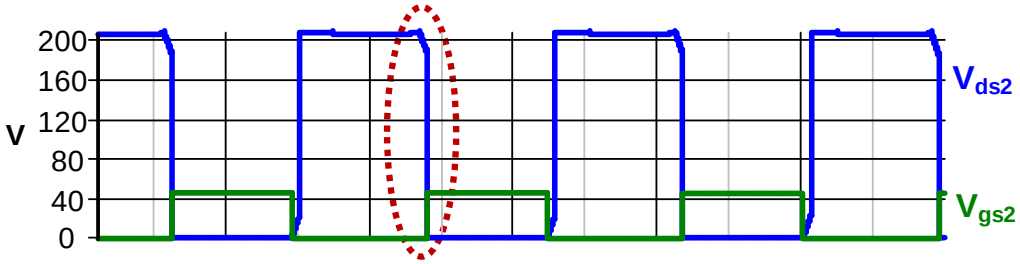

Fig. 2.13. Lose ZVS during dead time (large Lm)

If the LLC resonant converter is with large magnetizing inductance, ZVS of the primary side switches, which should be one of the good properties for LLC, is lost. This will significantly increase the turn on loss of the primary side switches. When one of the primary side switches turns on, the energy stored in its output capacitor will dissipated on the $R_{ds(on)}$ of its conduction channel. At the same time, the bus voltage V_{bus} will charge the output capacitor of the other switch almost from 0 to V_{bus}. The charging current also flows through the conduction channel of the switch which has just turned on, as Fig. 2.14 shows.

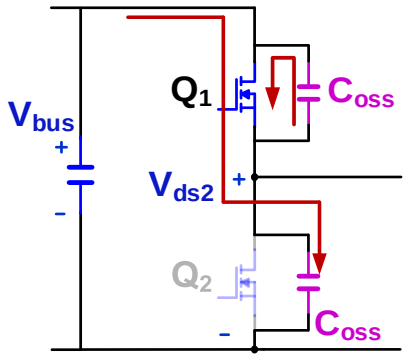

Fig. 2.14. Current flowing direction when Q_1 turns on (hard switching)

The total turn on loss of Q_1 and Q_2 can be calculated from the following equation:

$$P_{turn\_on} = 2 \cdot 2 f_s \int_0^{V_{bus}} v \cdot c_{oss}(v) dv . \tag{2.1}$$

For ST's device STB11NM60FD, the total turn on loss of Q_1 and Q_2 with hard switching is presented in Fig. 2.15. When there are 5 transformers in series at the primary side, the total turn on loss is approximately 4.6W. This additional turn on loss will make the efficiency drop 1.5% at the full load condition.

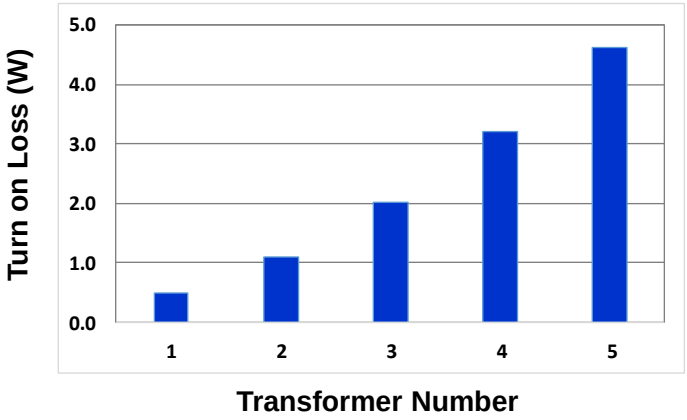

Fig. 2.15. Turn on loss of Q_1 and Q_2 with hard switching

2.3 Proposed Two-Stage LED Driver with MC^3 CLL Resonant Converter

2.3.1 Basic Characteristics of CLL Resonant Converter

Is there any topology not only with large magnetizing inductance, but also it achieves ZVS easily during the dead time? CLL resonant converter is a variant of LLC, as shown in Fig. 2.16. For CLL, the magnetizing inductance can be as large as possible. Meanwhile, ZVS of the primary side switches can be attained with a properly designed external inductor L_{r1}. Its characteristics are investigated in [17] and [18].

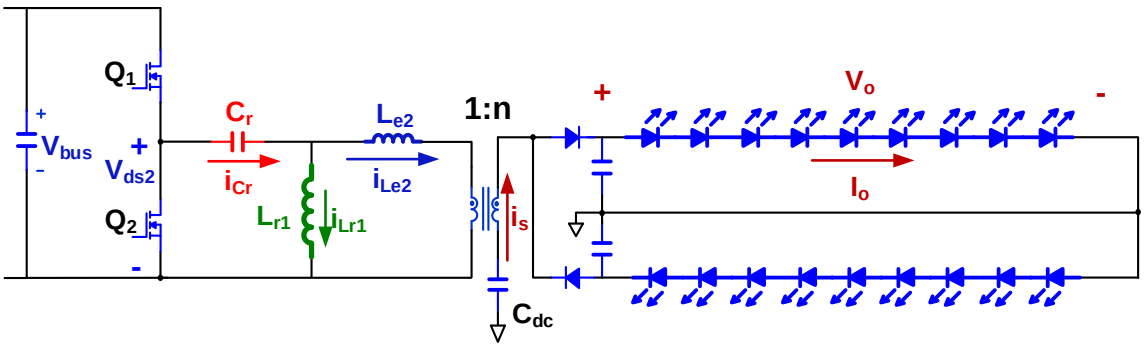

Fig. 2.16. CLL resonant converter for LED driving

For CLL resonant converter, C_r is in series with 2 inductors L_{r1} and L_{e2}. Meanwhile, L_{r1} and L_{e2} are in parallel. Therefore, these 3 components make up the resonant tank, as shown in Fig. 2.16. Under normal operation, C_r resonates with L_{r1} and L_{e2}. After the secondary side current i_s reaches 0, C_r will only resonate with L_{r1}. This is the basic operation principle of CLL.

The voltage gain of CLL is calculated from the following equation:

$$M = \frac{V_o / n}{V_{bus} / 2}. \tag{2.2}$$

The series resonant frequency of CLL is obtained as

$$f_0 = \frac{1}{2\pi\sqrt{C_r L_{r\_eq}}}, \tag{2.3}$$

where $L_{r\_eq} = \dfrac{L_{r1} \cdot L_{e2}}{L_{r1} + L_{e2}}$.

The quality factor of CLL resonant converter can be written as

$$Q = \frac{\sqrt{L_{r\_eq} / C_r}}{R_o / n^2}, \tag{2.4}$$

where $R_o = \frac{V_o}{2I_o}$.

The parallel resonant frequency of CLL is as follows:

$$f_{02} = \frac{1}{2\pi\sqrt{C_r L_{r1}}}. \tag{2.5}$$

The voltage gain of CLL converter is presented in Fig. 2.17. There are 2 operation zones for CLL. One is ZCS zone, and the other is ZVS zone. The boundary for these 2 zones is the dashed line, which covers the series resonant frequency and the parallel resonant frequency. For CLL, it working at the series resonant frequency point is preferred as well. The primary side switches can achieve ZVS and the secondary side rectifiers can achieve ZCS at the resonant frequency, as Fig. 2.18 shows. Besides that, the voltage gain of CLL at the series resonant frequency point is $1+1/L_n$, where $L_n=L_{r1}/L_{e2}$. This boost gain characteristic is very useful for the voltage step-up application.

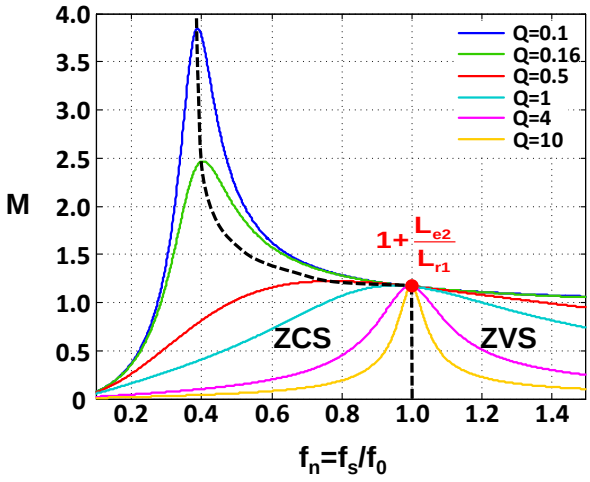

Fig. 2.17. Voltage gain of CLL resonant converter

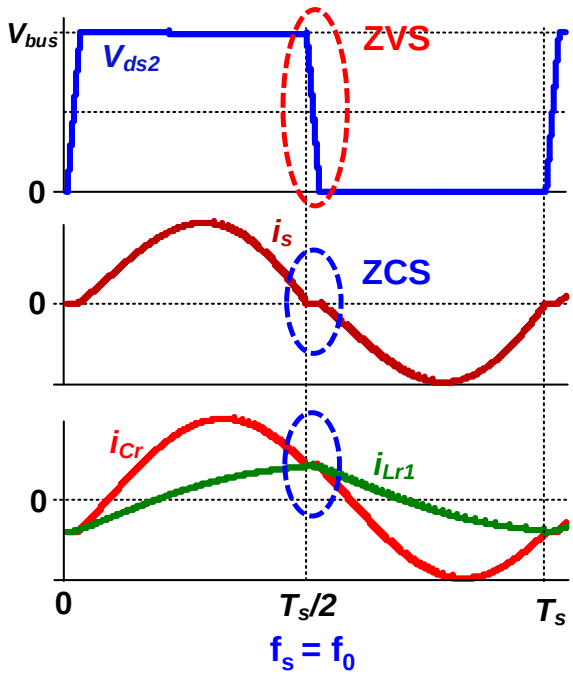

Fig. 2.18. Waveforms of the CLL at the resonant frequency

For CLL, the current flowing through L_{r1} instead of the magnetizing current of transformer is used to charge and discharge the output capacitors of the primary side switches to achieve ZVS during dead time. Therefore, L_{r1} is very critical for the ZVS requirement, and it needs to be designed properly.

2.3.2 Performance of Two-Stage LED Driver with MC^3 CLL Resonant Converter

For example, there are 5 transformers, and 2 LED strings driven by the same transformer have 10, 16, 19, 22 and 28 LEDs per string, as Fig. 2.19 shows. Meanwhile, the magnetizing inductance is about 160uH. The current of one LED string with 10 LEDs is sensed for feedback control. In this circumstance, the current of the LED string with 10 LEDs is about 300mA (full load). The currents of other LED strings with less LED number are very close to 300mA, as Fig. 2.20 shows. The current variation is about 4.0mA (1.3%). Although the voltages across the primary side of the transformers are totally different and magnetizing currents are different as well, the amplitude of

the magnetizing current is very small comparing with the amplitude of the resonant current. Therefore, the current balance capability is very good. Besides that, ZVS of primary side switches can be achieved by optimizing L_{r1}. In this case, L_{r1} is set to be 86.7uH and ZVS is attained, as Fig. 2.21 shows. The current flowing through L_{r1} plays an important role in achieving ZVS of Q_1 and Q_2 during dead time. The waveform of i_{Lr1} is shown in Fig. 2.22. CLL is a good candidate for driving multiple LED strings.

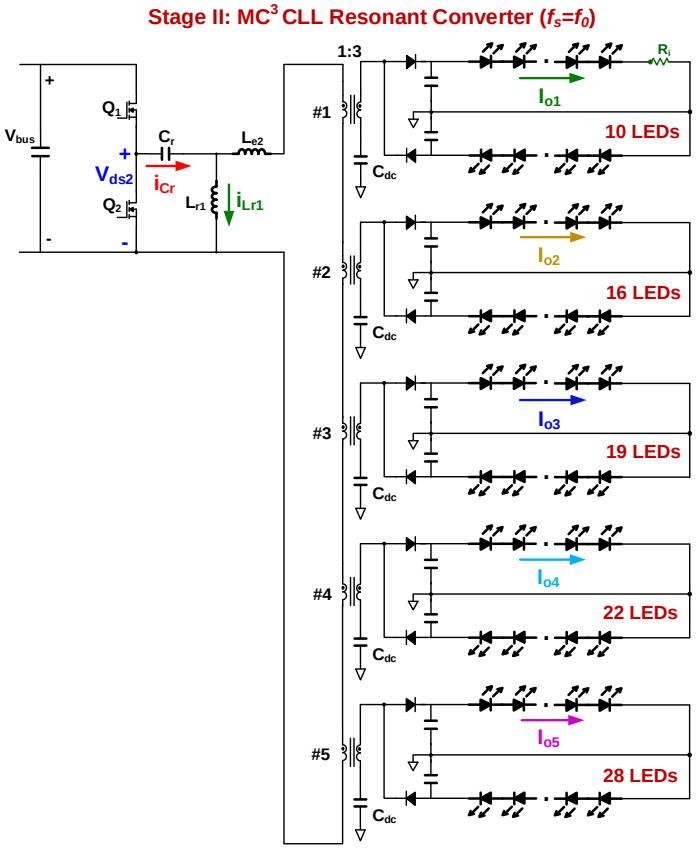

Fig. 2.19. LED driver with unbalanced loads (CLL)

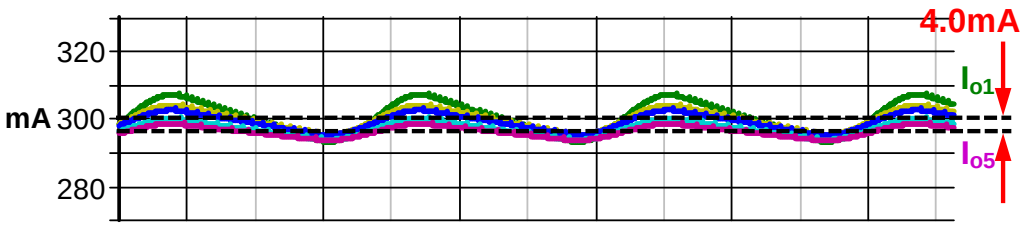

Fig. 2.20. Output currents under unbalanced load (CLL)

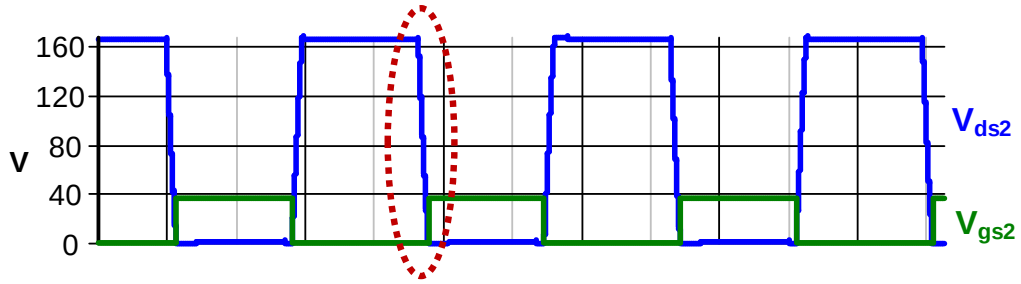

Fig. 2.21. ZVS during dead time (CLL)

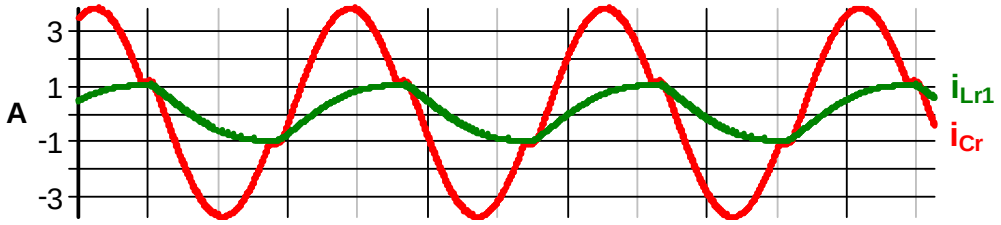

Fig. 2.22. Primary side current and current flowing through L_{r1} (CLL)

2.3.3 Benefits of MC^3 CLL Resonant Converter for Driving Multiple LED Strings

For LLC resonant converter, L_r and C_r are in series resonance when electrical energy is transferred from the primary side to the secondary side. There are 2 elements in resonance. When the secondary side rectifier is off, the magnetizing inductance L_m will mingle with L_r to resonate with C_r. At that moment, there are 3 elements in resonance. In addition, the voltage gain of LLC at series resonant frequency is 1. During dead time, the magnetizing current of transformer is used to charge and discharge the output capacitors of the primary side switches to achieve ZVS. Therefore, L_m is very critical for designing LLC resonant converter. Meanwhile, in MC^3 CLL resonant converter, larger L_m is desired for good current balance. It is difficult to find an optimal L_m to meet ZVS achievement and good current balance.

For CLL, C_r resonates with L_{r1} and L_{e2} when power is delivered from the primary side to the secondary side. There are 3 elements in resonance. However, when the secondary side rectifier is off, C_r will only resonate with L_{r1}. At that moment, there are 2 elements in resonance. This

operation scenario is a little different from LLC's. Besides that, the voltage of CLL at series resonant frequency is $1+1/L_n$, where $L_n=L_{r1}/L_{e2}$. Therefore, the voltage gain is higher than 1, which is a good virtue for the voltage step-up application. In contrast to LLC, the magnetizing inductance of CLL can be as large as possible, which is not critical for ZVS achievement. This property is very useful for multiple LED strings application to achieve good current balance as aforementioned. For CLL, we ignore the magnetizing current of transformer in some circumstances. Instead, the current flowing through L_{r1} is used to charge and discharge the output capacitors of the primary side switches to achieve ZVS. Therefore, L_{r1} is very critical to accomplish ZVS for CLL.

Generally speaking, CLL is peer to LLC. They have similar characteristics and performance. However, CLL with larger magnetizing inductance is preferred for multiple LED strings application. Meanwhile, CLL can achieve ZVS during dead time easily by adjusting the value of external inductor L_{r1}. This is very helpful to obtain high efficiency. In sum, CLL resonant converter is a good candidate for driving multiple LED strings. It is able to meet the ZVS requirement and good current balance at the same time.

Chapter 3. Design Considerations

3.1 Buck Converter

3.1.1 Switches Selection

For buck converter, the input voltage is DC 380V ±10%. Therefore, the voltage rating for the high side MOSFET and the low side freewheeling diode is 600V. A 600V SiC Schottky diode is used as the freewheeling diode. There is almost no reverse recovery current for the SiC Schottky diode, so this will be helpful to reduce the turn on loss of the high side MOSFET. The main parameters of C3D06060G are presented in Table 3.1. Lower capacitive charge Q_C can help to reduce the turn on loss of high side MOSFET.

Table 3.1. Main parameters of C3D06060G

SiC Diode	**C3D06060G**
V_{RRM}	600V
V_F (I_F=1.0A)	1.0V
I_{F_max}(T_c<150℃)	6A
Q_C (V_R=600V)	16nC

In this application, the maximum current through the high side switch is about 1.2A. The power MOSFET is selected based on the F.O.M (Figure of Merit) with $R_{ds(on)}$·C_{oss}. There are 2 candidates. One is IPB65R280C6 from Infineon, and the other is STB11NM60FD from STMicroelectronics. The key parameters of these 2 devices are shown in Table 3.2.

Since the RMS value of input current is less than 1.0A, the conduction loss of the high side MOSFET is less than 0.5W even with STB11NM60FD. For hard switching, the switching loss of high side MOSFET is the dominant loss. Therefore, STB11NM60FD is adopted due to its smaller

C_{oss}, which is strongly related to the turn on loss and turn off loss of the high side MOSFET. Briefly, smaller C_{oss} means smaller switching loss.

Table 3.2. Key parameters of IPB65R280C6 and STB11NM60FD

Power MOSFET	**IPB65R280C6**	**STB11NM60FD**
$\mathbf{V_{(BR)DSS}}$	650V	600V
$\mathbf{R_{DS(on)}}$	0.28Ω	0.45Ω
$\mathbf{I_{DS\_max}(T_c=100\ ℃)}$	8.7A	7A
$\mathbf{Q_g}$	45nC	28nC
$\mathbf{Q_{gd}}$	24nC	13nC
$\mathbf{C_{OSS\_er[a]}}$	47pF	41pF

[a] C_{OSS_er} is a fixed capacitance that gives the same stored energy as C_{OSS} while V_{DS} is rising from 0 to 400V

3.1.2 Inductor Design

The normal output current of the buck converter I_{oN} is about 0.9A. The inductor current is shown in Fig. 3.1. In order to guarantee the buck converter is working at CCM (continuous current mode) most of the time, the inductor must meet the following inequality

$$L \geq \frac{V_o(1-D)T_s}{\Delta i_L} = \frac{V_{in}D(1-D)T_s}{\Delta i_L}, \tag{3.1}$$

The maximal current ripple is 60% of the normal output current I_{oN}, namely

$$\Delta i_{L\_\max} = 60\% \cdot I_{oN} = 0.54\text{A}. \tag{3.2}$$

The right hand side of (3.1) reaches its maximal value when V_{in}=418V and D=0.5. So we get $L \geq 1.94mH$. In practice, we choose $L = 2.0mH$.

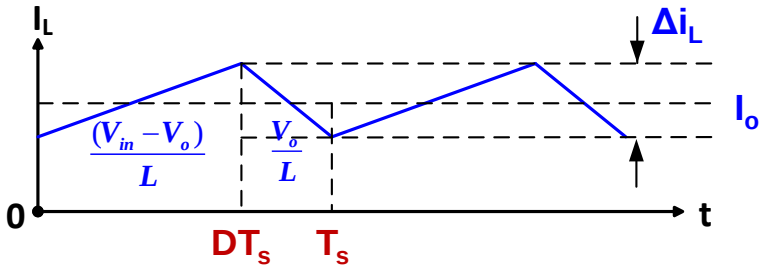

Fig. 3.1. Inductor current of buck converter

The current ripple Δi_L versus the duty cycle D is presented in Fig. 3.2. The current ripple reaches its maximal value when D=0.5. When D is lower than 0.5 or higher than 0.5, the current ripple will decrease correspondingly.

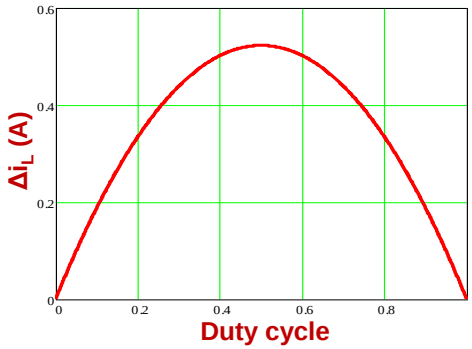

Fig. 3.2. Current ripple Δi_L versus the duty cycle D (V_{in}=418V & L=2.0mH)

The performance factor ($f \times B_{max}$) of several kinds of ferrite core material at a certain loss level (P_V=500mW/cm^3 @ 100℃) is presented in Fig. 3.3. Since the switching frequency of buck converter is 100kHz, it is feasible to use 3C96 for buck inductor to achieve lower core loss. In addition, RM10/I core is adopted for the buck converter.

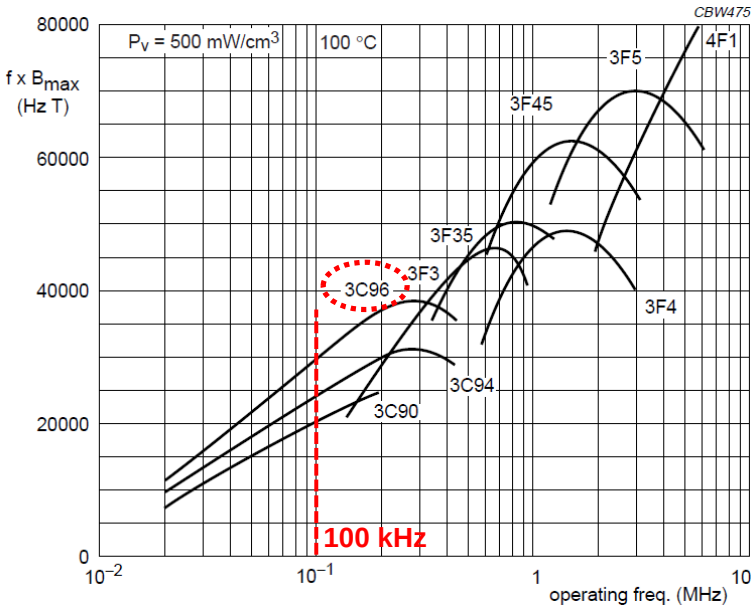

Fig. 3.3. Performance factor ($f \times B_{max}$) of power ferrite materials [19]

RM10/I is with a height of 18.6mm. The effective core parameters of RM10/I are presented in Table 3.3.

Table 3.3. Effective core parameters of RM10/I

Symbol	Parameter	Value
$\mathbf{V_e}$	Effective volume	3360 mm^3
$\mathbf{A_e}$	Effective area	99.1 mm^2

For buck inductor, there is a DC bias current I_o flowing through it, as shown in Fig. 3.4. This DC current will cause a DC bias magnetic field H_{DC}. In order to prevent H_{DC} from saturating the core, an air gap is needed for the magnetic path. The B-H characteristic of the magnetic core with an air gap can be represented with a straight line approximately, as Fig. 3.4 shows.

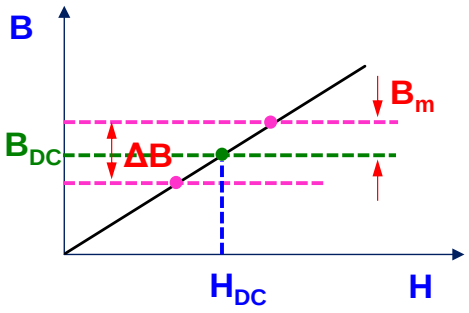

Fig. 3.4. B-H characteristic of magnetic core with air gap (B=μ·H)

The key parameters of 3C96 are presented in Table 3.4.

Table 3.4. Key parameters of 3C96

Symbol	Value
B_{sat} (100 ℃)	440 mT
P_V(100 ℃; 100kHz; B_m=70mT)	20 kW/m^3

Assume that B_{DC}=230mT which is half of B_{sat} when the DC bias current is 0.9A, then we have

$$\Delta B = B_{DC}\frac{\Delta i_L}{I_{oN}} = 138mT\,, \tag{3.3}$$

where $\Delta i_L = 0.54A$.

The winding turns of buck inductor can be derived from the following equation

$$N_L = \frac{L\cdot\Delta i_L}{\Delta B\cdot A_e} \approx 81, \tag{3.4}$$

B_m is the peak value of ΔB, and its value is $B_m = \Delta B/2 = 69mT$.

The penetration depth of copper conductor at 100kHz is about

$$\delta = \frac{75}{\sqrt{f}} = 0.24mm\,, \tag{3.5}$$

The parameters of buck inductor are presented in Table 3.5.

Table 3.5. Key parameters of buck inductor

L	B_m	Air Gap	Wire	Turns
2.0 mH	69 mT	0.42 mm	50/40 Litz wire	81.5

The loss of buck inductor is shown in Table 3.6.

Table 3.6. Loss of buck inductor based on analytical calculation (@Full Load)

Core Loss	Rdc Loss	Rac Loss
0.172 W	0.329W	0.035 W

The total loss of buck inductor is about 0.54W under full load condition.

3.2 CLL Resonant Converter

The complete design procedure of the MC^3 CLL resonant converter is presented in Fig. 3.5. The switching frequency is determined according to the desired power density. In this case, it is 300 kHz to achieve low profile.

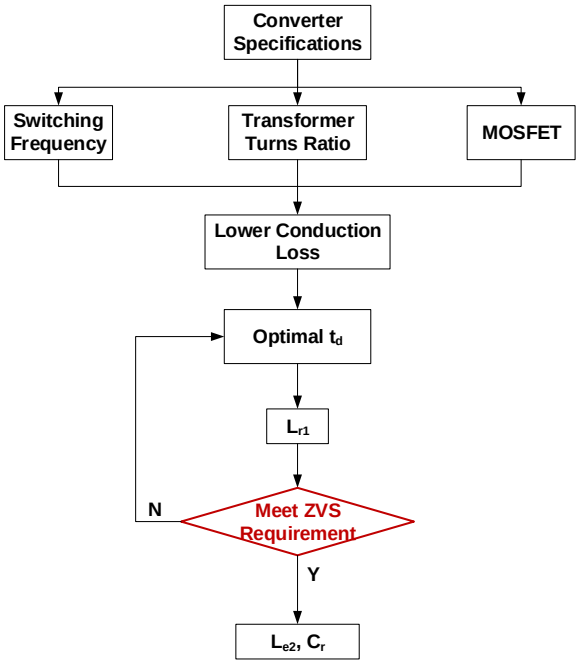

Fig. 3.5. Complete design procedure of MC^3 CLL resonant converter

Meanwhile, the turns ratio of the transformer is determined by the worst case (V_{in_min}, V_{o_max}). The input of the 2-stage LED driver comes from the output of PFC or the high-voltage DC bus. It is 380V ±10%, so the minimal input voltage is about 342V. When there are 10 LED strings, and each string has 28 LEDs, as Fig. 3.6 shows. As the LEDs are working under full-load condition (I_o=300mA), the output voltage is about 90 V, which is the maximal value. Since the turns ratio of each transformer is the same, the minimal input voltage and the maximal bus voltage should meet the following inequality

$$V_{in\_\min} \geq V_{bus\_\max} = 5 \times \frac{N_p}{N_s} \times V_{o\_\max} \times 2, \tag{3.6}$$

According to (3.6), the turns ratio should be less than or equal to 0.38. In practice, the turns ratio of the transform is set to be 1:3. Therefore, the maximal bus voltage is about 300 V.

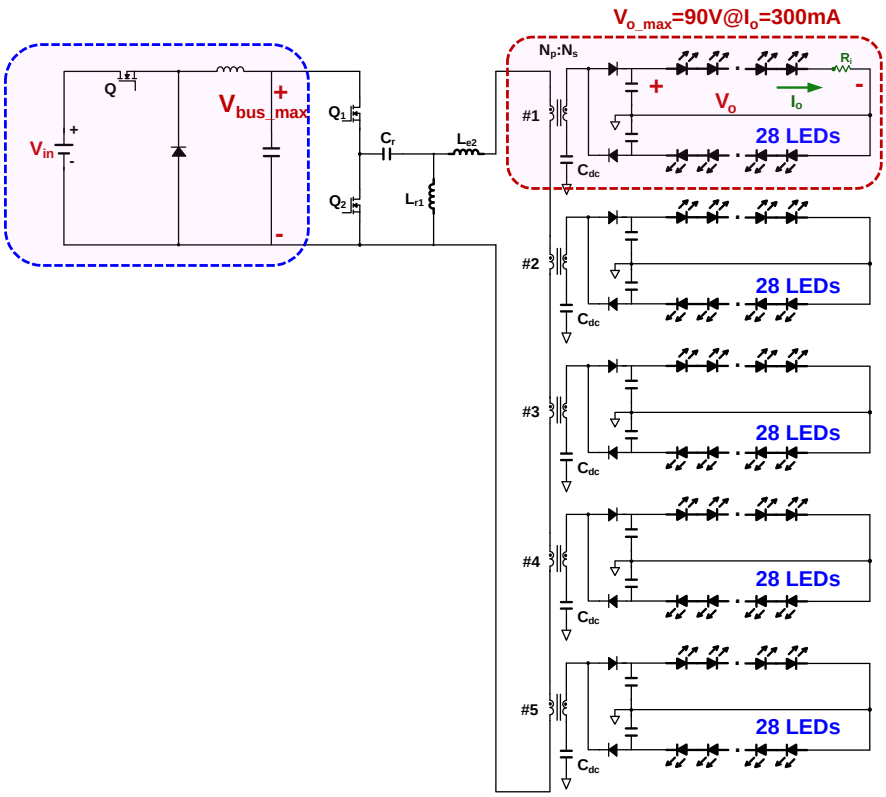

Fig. 3.6. Multiple LED strings (10 strings) working under full load condition

3.2.1 Switches Selection

The input voltage of CLL converter varies from 5.7V to 300V. Therefore, a 600V MOSFETs are chosen for this application. It is STB11NM60FD from STMicroelectronics, and the parameters of this device is presented in Table 3.7.

Table 3.7. Key parameters of STB11NM60FD

Items	STB11NM60FD
$\mathbf{V_{(BR)DSS}}$	600 V
$\mathbf{R_{DS(on)}}$	0.45 Ω
$\mathbf{I_{DS\_max}(T_c=100\ ℃)}$	7 A
$\mathbf{Q_g}$	28 nC
$\mathbf{C_{OSS\_tr[b]}}$	100 pF

[b] C_{OSS_tr} is a fixed capacitance that gives the same charging time as C_{OSS} while V_{DS} is rising from 0 to 400V

The output capacitance C_{oss} of MOSFET is a nonlinear capacitance, and it strongly depends on V_{DS}. $C_{oss\_tr}(V_{DS})$ is a fixed capacitance that gives the same charging time as C_{oss} while V_{ds} is rising from 0 to V_{DS}. The effective C_{oss} of MOSFET at a specific V_{DS} is obtained from the following equation

$$C_{oss\_tr}(V_{DS}) = \frac{1}{V_{DS}} \int_0^{V_{DS}} C_{oss}(v_{ds}) dv_{ds} \,. \tag{3.7}$$

$C_{oss\_tr}(V_{DS})$ of STB11NM60FD at 60V and 300V are shown in Table 3.8.

Table 3.8. $C_{oss\_tr}(V_{DS})$ of STB11NM60FD at 60V and 300V

Items	STB11NM60FD
$\mathbf{C_{oss\_tr}(60V)}$	470 pF
$\mathbf{C_{oss\_tr}(300V)}$	150 pF

The maximal output voltage is 90V. The schottky diode PDS3200 is adopted to achieve lower conduction loss. The key parameters of the schottky diode are presented in Table 3.9.

Table 3.9. Key parameters of PDS3200

Items	**PDS3200**
$\mathbf{V_{RRM}}$	200 V
$\mathbf{V_F@I_F=1A}$	0.55 V
$\mathbf{C_{j[c]}}$	100 pF

[c] C_j is the effective junction capacitance while the reverse voltage across the diode is rising from 0 to 180V

3.2.2 Relationship Between L_p (L_{r1} & L_{e2}) and Dead Time t_d

During the dead time, the voltages across the output capacitors of the primary-side switches change. In order to achieve ZVS, one changes from 0 to V_{bus}, and the other changes from V_{bus} to 0. Besides that, the voltages across the junction capacitors of the secondary-side rectifiers will also vary. One changes from 0 to $2V_o$, and the other changes from $2V_o$ to 0.

CLL is an LLC-type resonant converter. LLC resonant converter is widely used in the power supplies for telecoms, servers and many other electronic devices [21]. For these applications, the LLC is usually used for reducing the input voltage. Thus the turns ratio of the transformer is greater than 1. The junction capacitors can be reflected onto the primary side for the analysis during dead time. However, since the turns ratio is greater than 1, the equivalent junction capacitor reflected onto the primary side is much less than its real value on the secondary side. Meanwhile, if the equivalent junction capacitor is much less than the output capacitor of the primary-side switches, the influence of the junction capacitor of the secondary-side rectifier can be ignored [22]. Generally speaking, the junction capacitors of the secondary-side rectifiers are not taken into account for the voltage step-down application.

A. One transformer module

Since the turns ratio of the transformer is 1:3, the transformer is used for voltage step-up application. When the junction capacitor C_j is reflected onto the primary side, its value will be 9

times larger than its real value. Thus the influence of C_j is considerable comparing with that of C_{oss}. Take the case with one transformer module as an example, the operation principles of CLL resonant converter before and during the dead time are presented in Fig. 3.7. The current flowing through L_{r1} is almost invariable during the dead time, so it can be regarded as a constant current source. In addition, the voltage across C_r has little variation as well, so it can be regarded as a voltage source. Thus, the equivalent circuit of CLL resonant converter is shown in Fig. 3.8. $2n^2C_j$ is the equivalent junction capacitor on the primary side. During the dead time, v_p will change from $+nV_o$ to $-nV_o$.

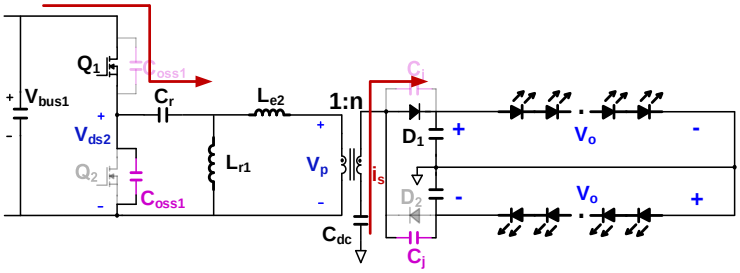

(a) Before the dead time (Q_1 is on and Q_2 is off)

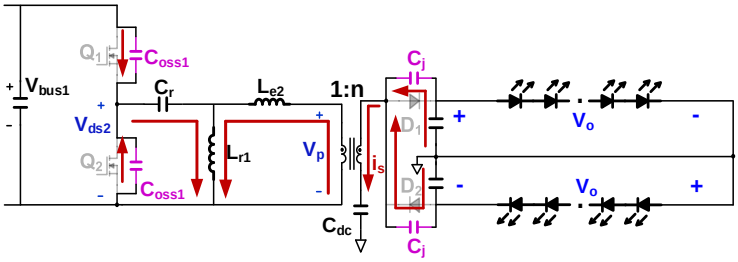

(b) During the dead time (Q_1 and Q_2 are both off)

Fig. 3.7. Operation principles of CLL resonant converter

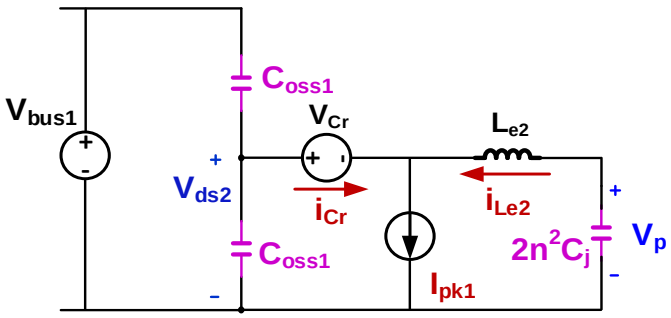

Fig. 3.8. Equivalent circuit of CLL resonant converter during dead time

The peak value of i_{Lr1} with one transformer can be obtained from the following equation

$$I_{pk1} = \frac{V_{bus1}}{2} \cdot \frac{T_0}{4} \cdot \frac{1}{L_p}, \tag{3.8}$$

where $L_p = \frac{L_{r1}^2}{L_{r1} + L_{e2}}$.

According to KCL, I_{pk1} is the sum of i_{Cr} and i_{Le2} during dead time, namely

$$\boldsymbol{I}_{pk1} = \boldsymbol{i}_{Cr} + \boldsymbol{i}_{Le2}. \tag{3.9}$$

Therefore, I_{pk1} not only provides charge to help the primary-side switch achieve ZVS, but also provides enough charge to reverse the polarity of the voltage across the equivalent junction capacitors. If the primary-side switches achieve ZVS and the rectifier's junction capacitor reverses the polarity of the voltage across it during the dead time, the following inequality should be met

$$I_{pk1} \cdot t_d \geq V_{bus1} \cdot 2C_{oss1} + \frac{2V_o}{n} \cdot 2n^2 C_j. \tag{3.10}$$

Combine with (3.8), we can obtain

$$L_p \leq \frac{t_d \cdot T_0}{16(C_{oss1} + M \cdot n^2 \, C_j)}. \tag{3.11}$$

where M is the voltage gain of CLL resonant converter.

The maximal L_p for one transformer module to realize ZVS at a given dead time t_d is

$$L_{p\_\max} = \frac{t_d \cdot T_0}{16(C_{oss1} + M \cdot n^2 C_j)}. \tag{3.12}$$

B. Five transformer modules

The circuit diagram with 5 transformer modules is presented in Fig. 3.9.

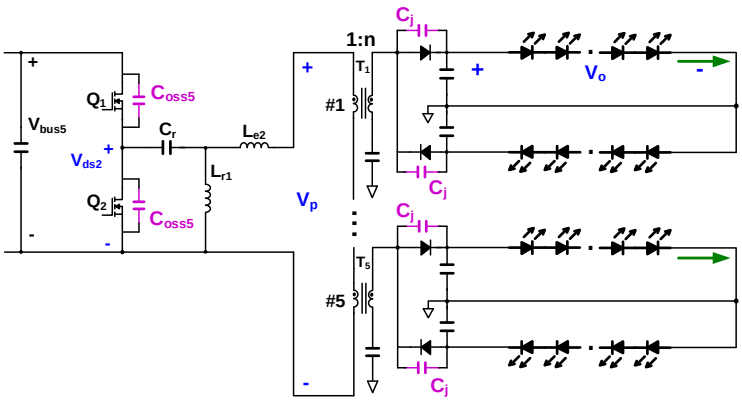

Fig. 3.9. MC^3 CLL resonant converter with five transformer modules

The equivalent circuit during the dead time is shown in Fig. 3.10. There will be an equivalent junction capacitor for each transformer, which is $2n^2C_j$. Since there are five transformer modules, there will be five equivalent capacitor in series on the primary side. Therefore, the total equivalent capacitor on the primary side is $2n^2C_j/5$. During the dead time, the voltage across the capacitor will change from $+5nV_o$ to $-5nV_o$. Although the equivalent capacitor is one fifth of that with one transformer, the voltage across the capacitor is five times of that with one transformer. The total charge needed for reversing the voltage across the junction capacitor is the same for both cases. It is

$$\frac{2V_o}{n} \cdot 2n^2 C_j = \frac{2 \cdot 5V_o}{n} \cdot \frac{2n^2 C_j}{5} = 4nV_o C_j. \tag{3.13}$$

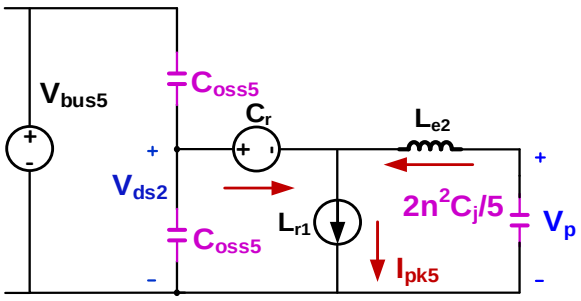

Fig. 3.10. Equivalent circuit of MC^3 CLL resonant converter during dead time (5 transformers)

The peak value of i_{Lr1} with five transformers can be obtained from the following equation

$$I_{pk5} = \frac{V_{bus5}}{2} \cdot \frac{T_0}{4} \cdot \frac{1}{L_p}, \tag{3.14}$$

where $L_p = \frac{L_{r1}^2}{L_{r1} + L_{e2}}$.

According to KCL, I_{pk5} is the sum of i_{Cr} and i_{Le2} during dead time, namely

$$\boldsymbol{I}_{pk5} = \boldsymbol{i}_{Cr} + \boldsymbol{i}_{Le2}. \tag{3.15}$$

If the primary-side switches achieve ZVS and the equivalent junction capacitor reverses the polarity of the voltage across it during the dead time, the following inequality should be met

$$I_{pk5} \cdot t_d \geq V_{bus5} \cdot 2C_{oss5} + \frac{2V_o}{n} \cdot 2n^2 C_j. \tag{3.16}$$

Combine with (3.14), we can obtain

$$L_p \leq \frac{t_d \cdot T_0}{16(C_{oss5} + M \cdot n^2 \, C_j / 5)}. \tag{3.17}$$

The maximal L_p for five transformer modules to realize ZVS at a given dead time t_d is

$$L_{p\_max} = \frac{t_d \cdot T_0}{16(C_{oss5} + M \cdot n^2 \, C_j / 5)}. \tag{3.18}$$

3.2.3 Relationship Between Current RMS Value and Dead Time t_d

For one LED string, it can be replaced with a resistor when it is working at steady state condition, as Fig. 3.11 shows. The resistor can be obtained according to (3.19).

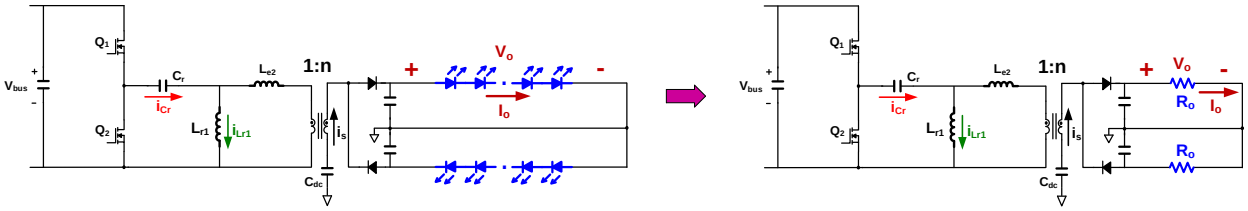

Fig. 3.11. Replace one LED string with an equivalent resistor

$$R_o = \frac{V_o}{I_o}. \tag{3.19}$$

Since one transformer module drives two LED strings at the same time, the equivalent resistor for two LED strings in parallel is denoted by R_L, which is $R_o/2$. The ideal waveforms of i_{Cr} and i_{Lr1} are presented in Fig. 3.12.

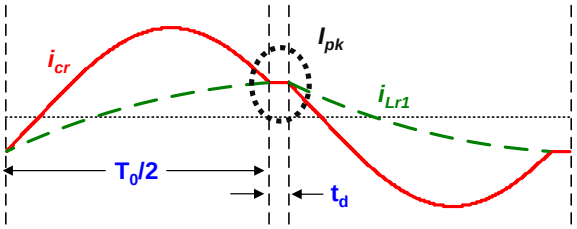

Fig. 3.12. Waveforms of i_{Cr} and i_{Lr1} in one switching period

According to Fig. 3.12, the primary-side current $i_{Cr}(t)$ can be expressed as follows

$$i_{Cr}(t) = \sqrt{2} I_{Cr\_RMS} \sin(\omega_o t + \Phi). \tag{3.20}$$

Meanwhile, the current $i_{Lr1}(t)$ approximates to a triangular wave, so we have

$$i_{Lr1}(t) \approx -\frac{N_{tr} \cdot V_o}{n \cdot L_p} \cdot \frac{T_o}{4} + \frac{N_{tr} \cdot V_o}{n \cdot L_p} \cdot t, \tag{3.21}$$

where N_{tr} is the number of the transformers.

The RMS value of the primary side current $i_{Cr}(t)$ can be derived from the following equation

$$\frac{\int_0^{\frac{T_o}{2}}\left[i_{Cr}(t)-i_{Lr1}(t)\right]dt}{T_s/2}=\frac{nV_o}{R_L}. \tag{3.22}$$

Solve (3.22), we can get

$$I_{Cr\_RMS}=\frac{1}{4\sqrt{2}}\frac{nV_o}{R_L}\sqrt{\frac{N_{tr}^2R_L^2T_o^2}{n^4L_p^2}+4\pi^2+\frac{16\pi^2(T_ot_d+t_d^2)}{T_o^2}}. \tag{3.23}$$

Substitute L_p with its maximal value $\frac{t_d\cdot T_0}{16(C_{oss}+M\cdot n^2\,C_j/N_{tr})}$, we have

$$I_{Cr\_RMS}=\frac{1}{4\sqrt{2}}\frac{nV_o}{R_L}\sqrt{\frac{256N_{tr}^2R_L^2(C_{oss}+M\cdot n^2\,C_j/N_{tr})^2}{n^4t_d^2}+4\pi^2+\frac{16\pi^2(T_ot_d+t_d^2)}{T_o^2}}. \tag{3.24}$$

In the similar way, the RMS value of the secondary side current can be derived by the following equation:

$$I_{s\_RMS}=\frac{1}{n}\sqrt{\frac{\int_0^{\frac{T_o}{2}}\left[i_{Cr}(t)-i_{Lr1}(t)\right]^2dt}{T_s/2}}. \tag{3.25}$$

Solve (3.25), we can get

$$I_{s\_RMS}=\frac{\sqrt{6}}{24\pi}\frac{V_o}{R_L}\sqrt{\frac{(5\pi^2-48)N_{tr}^2{R_L}^2{T_o}^3}{n^4L_p^2(T_o+2t_d)}+\frac{12\pi^4T_o}{T_o+2t_d}+\frac{48\pi^4({t_d}^2+t_dT_o)}{T_o(T_o+2t_d)}}. \tag{3.26}$$

Substitute L_p with its maximal value $\frac{t_d\cdot T_0}{16(C_{oss}+M\cdot n^2\,C_j/N_{tr})}$, we have

$$I_{s\_RMS}=\frac{\sqrt{6}}{24\pi}\frac{V_o}{R_L}\sqrt{\frac{256(C_{oss}+M\cdot n^2\,C_j/N_{tr})^2(5\pi^2-48)N_{tr}^2R_L{}^2T_o}{n^4t_d{}^2(T_o+2t_d)}+\frac{12\pi^4T_o}{T_o+2t_d}+\frac{48\pi^4(t_d{}^2+t_dT_o)}{T_o(T_o+2t_d)}}. \quad (3.27)$$

The total conduction loss of the primary-side switches and the secondary-side rectifiers is strongly related to t_d, and it can be obtained from (3.28).

$$P_{con}=R_{DS}I_{Cr\_RMS}^2+N_{tr}\cdot V_F I_{s\_RMS}. \quad (3.28)$$

The MC^3 CLL resonant converter is designed with five transformers, and high efficiency is expected when there are five transformer modules. The RMS values of the primary-side current and the secondary-side current can be written as

$$I_{Cr\_RMS}=\frac{1}{4\sqrt{2}}\frac{nV_o}{R_L}\sqrt{\frac{256\times25R_L^2(C_{oss5}+M\cdot n^2\,C_j/5)^2}{n^4t_d^2}+4\pi^2+\frac{16\pi^2(T_ot_d+t_d^2)}{T_o^2}}. \quad (3.29)$$

$$I_{s\_RMS}=\frac{\sqrt{6}}{24\pi}\frac{V_o}{R_L}\sqrt{\frac{256\times25(C_{oss5}+M\cdot n^2\,C_j/5)^2(5\pi^2-48)R_L{}^2T_o}{n^4t_d{}^2(T_o+2t_d)}+\frac{12\pi^4T_o}{T_o+2t_d}+\frac{48\pi^4(t_d{}^2+t_dT_o)}{T_o(T_o+2t_d)}}. \quad (3.30)$$

According to Table 3.8, C_{oss5}=150pF when V_{bus}=300V. Therefore, I_{Cr_RMS} vs. t_d and I_{s_RMS} vs. t_d are presented in (a) and (b) of Fig. 3.13 respectively.

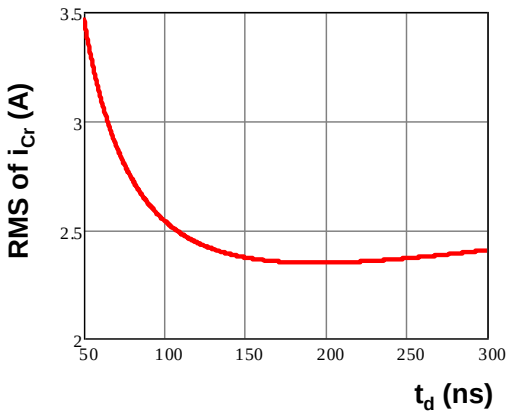

(a) i_{Cr_RMS} vs. t_d

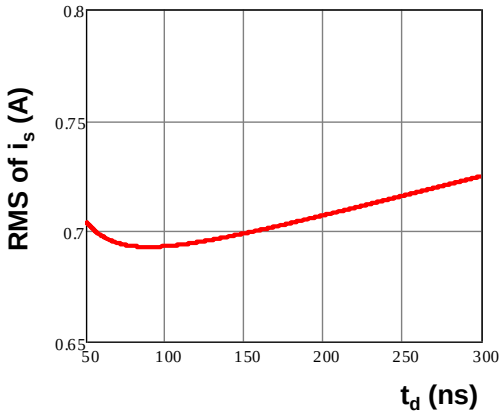

(b) i_{s_RMS} vs. t_d

Fig. 3.13. RMS value of primary-side current and secondary-side current vs. t_d (STB11NM60FD)

According to Table 3.7 and Table 3.9, $R_{DS(on)}$=0.45Ω and V_F=0.55V. Meanwhile, there are five transformers. The relationship between conduction loss and t_d is shown in Fig. 3.14. There is an optimal zone for the dead time. From 150ns to 250ns, the conduction loss is the lowest. In practice, t_d is selected to be 150ns in order to achieve high efficiency.

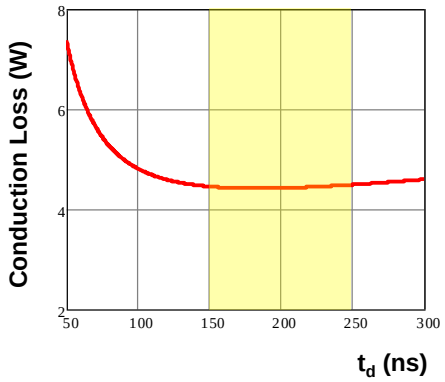

Fig. 3.14. Total conduction loss vs. t_d (STB11NM60FD)

3.2.4 Determine L_{r1}, L_{e2} and C_r

L_p can be designed according to (3.12) and (3.18). Since the transformer is a voltage step-up transformer, the junction capacitors of rectifiers play an important role in the operation during dead time. Therefore, the operation during dead time is a little bit different from the conventional CLL resonant converter with voltage step-down transformer. There is a resonance among L_{e2}, C_{oss} and C_{jp} during dead time. This resonance will influence the ZVS achievement of the primary-side switches and the normal operation of CLL. As a result, the resonance during the dead time will impact the selection of L_{r1}, L_{e2} and C_r. In the following paragraphs, the operation during dead time will be analyzed in details. Take the case with five transformers as an example.

In practice, high efficiency of CLL resonant converter is desired. Therefore, ZVS of the MC^3 CLL resonant converter should be guaranteed. The parameters of the CLL resonant tank are designed based on this consideration. Since the transformer is a voltage step-up transformer, the

junction capacitors of rectifiers play an important role in the operation during dead time. Therefore, the operation during dead time is a little bit different from the conventional CLL resonant converter with voltage step-down transformer. There is a resonance among L_{e2}, C_{oss} and C_{jp} during dead time. It also influences the normal CLL resonance since it changes the initial condition of CLL resonance. However, the principle for the ZVS achievement is the same. The total charge provided by i_{Cr} should be greater than Q_{oss}. L_{r1} can be roughly determined by the maximal value of L_p. Then with a given L_{r1}, the relationship between Q_{Cr} and L_{e2} can be established. L_{e2} is selected from the areas that ZVS of the primary-side switches can be achieved. After L_{r1} and L_{e2} are both determined, C_r can be determined according to the resonant frequency.

The equivalent circuit of CLL resonant converter during dead time is presented in Fig. 3.15. During the dead time, L_{e2} will resonate with C_{oss} and C_{jp} which is the lumped capacitor of all the junction capacitors reflected onto the primary side. For the case with five transformer modules, $C_{jp}=2n^2C_j/5$. At the beginning of dead time, $i_{Cr}=I_{pk}$ and $i_{Le2}=0$. Meanwhile, $v_p=+5V_o/n$ or $-5V_o/n$.

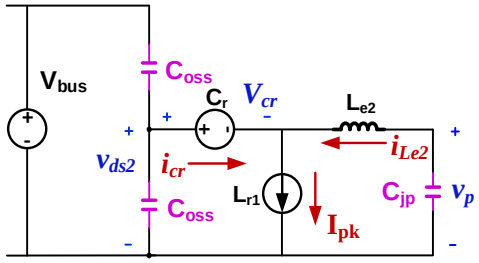

Fig. 3.15. Equivalent circuit of CLL resonant converter during dead time

Based on Fig. 3.15, the state equations describing the equivalent circuit can be written as

$$\frac{dv_{ds2}}{dt} = -\frac{i_{cr}}{2C_{oss}}. \tag{3.31}$$

$$\frac{dv_p}{dt} = -\frac{i_{Le2}}{C_{jp}}. \tag{3.32}$$

$$\frac{di_{Le2}}{dt} = -\frac{1}{L_{e2}}(v_{ds2} - V_{cr} - v_p). \tag{3.33}$$

According to KCL, the following relationship can be established

$$I_{pk} = i_{cr} + i_{Le2}. \tag{3.34}$$

The initial conditions of the equivalent circuit are as follows:

$I_{pk} = \frac{5V_o}{nL_{r1}} \cdot \frac{T_0}{4}$;

$V_{cr} = \frac{V_{bus}}{2} + \frac{n^2 v_p(0)}{5R_L} \cdot \frac{\pi}{2} \cdot \omega_0 L_{e2}$;

$v_{ds2}(0)=V_{bus}$;

$v_p(0)=5V_o/n$;

$i_{cr}(0)=I_{pk}$.

Solve the state equations with (3.34) and the initial conditions, we can get the following expressions in time domain

$$i_{Cr}(t) = I_{pk} - \frac{A}{G} - 2V_e \cos(\omega_d t + \theta), \tag{3.35}$$

$$i_{Le2}(t) = \frac{A}{G} + 2V_e \cos(\omega_d t + \theta), \tag{3.36}$$

$$v_{ds2}(t) = v_{ds2}(0) - \frac{I_{pk}}{2C_{oss}} \cdot t + \frac{A}{2C_{oss}G} \cdot t + \frac{2V_e}{2C_{oss}\omega_d}\left[\sin(\omega_d t + \theta) - \sin(\theta)\right], \tag{3.37}$$

$$v_p(t) = v_p(0) - \frac{A}{C_{jp}G} \cdot t - \frac{2V_e}{C_{jp}\omega_d}\left[\sin(\omega_d t + \theta) - \sin(\theta)\right], \tag{3.38}$$

where $\mathrm{A} = \dfrac{I_{pk}}{2C_{oss}L_{e2}}$,

$\mathrm{B} = \dfrac{v_p(0)+V_{Cr}-V_{bus}}{L_{e2}}$,

$G = \dfrac{2C_{oss}+C_{jp}}{2C_{oss}C_{jp}} \cdot \dfrac{1}{L_{e2}}$,

$\omega_d = \sqrt{G}$,

$\mathrm{V}_e = \dfrac{\sqrt{A^2+(\mathrm{B}\,\omega_d)^2}}{2G}$,

$\theta = \text{-}\cos^{-1}\left(\dfrac{-A}{\sqrt{A^2+(\mathrm{B}\,\omega_d)^2}}\right)$.

The total charge provided by i_{Cr} during dead time t_d can be obtained by the integration of (3.35), so it is

$$Q_{Cr} = \int_0^{t_d} i_{Cr}(t)\mathrm{d}t = I_{pk}t_d - \frac{A}{G}\cdot t_d - \frac{2V_e}{\omega_d}\left[\sin(\omega_d t_d+\theta)-\sin(\theta)\right]. \tag{3.39}$$

The coefficients of Q_{Cr} are strongly related to L_{r1}, L_{e2} and t_d. When there are 10 LED strings and LEDs are working at full-load condition, the bus voltage is about 300V and the output capacitor of STB11NM60FD is about 150pF. The total charge needed for the ZVS achievement is as follows

$$Q_{Coss} = V_{bus}\cdot 2C_{oss} = 90nC\,. \tag{3.40}$$

If the ZVS of the primary-side switches could be achieved during dead time, the following inequality should be met.

$$Q_{Cr} \geq Q_{Coss} = 90nC\,. \tag{3.41}$$

According to (3.18), the maximal L_p can be obtained and L_{p_max}=94.7uH. In practice, L_{r1} is set to be 95.6uH. When L_{r1} is fixed to be 95.6uH and t_d=150ns, Q_{Cr} only pertains to L_{e2}. The relationship between Q_{Cr} and L_{e2} are presented in Fig. 3.16. ZVS of the primary side switches can be guaranteed when L_{e2} falls into some particular regions, such as the intersection of the red curve and the blue curve, the area that the red curve is above the blue curve. When 0.86uH<L_{e2}<1.68uH, ZVS of the primary-side switches can't be achieved within 150ns since the charge provided by i_{Cr} is less than Q_{oss}. In contrast to the area that 1.68uH≤L_{e2}≤3.42uH, ZVS of the primary-side switches can be achieved within 150ns since the charge provided by i_{Cr} is greater than Q_{Coss}. When L_{e2} is less than 0.89uH, the influence of the resonance during the dead time is little. However, when L_{e2} is greater than 0.89uH, the impact is more significant as L_{e2} increases gradually. Three cases with different L_{e2} are discussed with derivation results and simulation results in the following paragraphs.

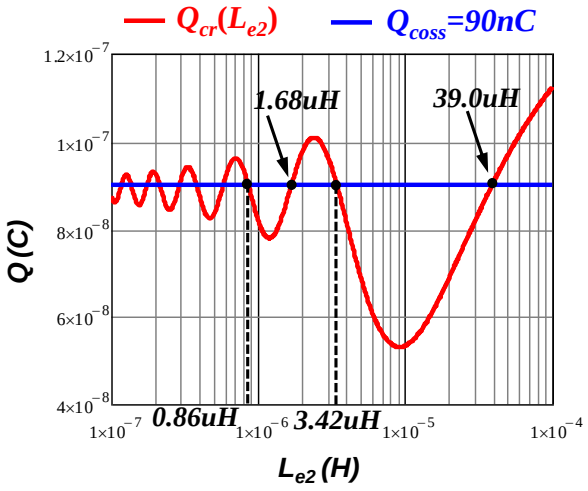

Fig. 3.16. Q_{Cr} vs. L_{e2} (L_{r1}=95.6uH)

Case 1: L_{r1}=95.6uH, L_{e2}=3.4uH and C_r=85.2nF

The waveforms of v_{ds2} and v_p based on (3.37) and (3.38) are presented in Fig. 3.17. The low-side switch Q_2 achieves ZVS around 150ns and the voltage across the equivalent junction capacitor almost reverses its polarity at 150ns. The simulation results are also shown in Fig. 3.18. Compare Fig. 3.17 and Fig. 3.18, the theoretical analysis and the simulation results match well. ZVS of the primary-side switches is achieved at the end of dead time.

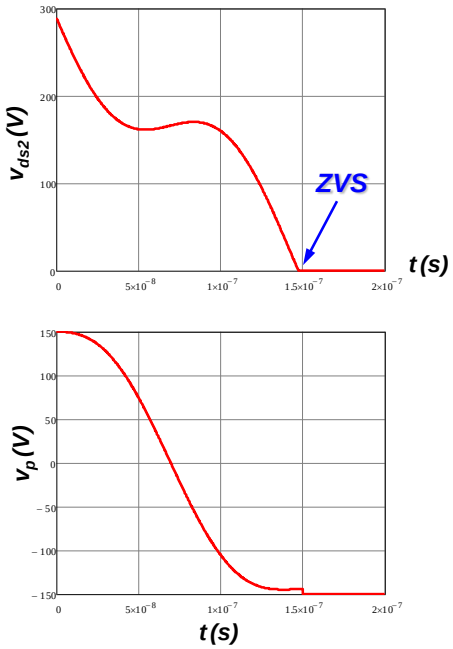

Fig. 3.17. Waveforms of v_{ds2} and v_p based on derivation (L_{e2}=3.4uH)

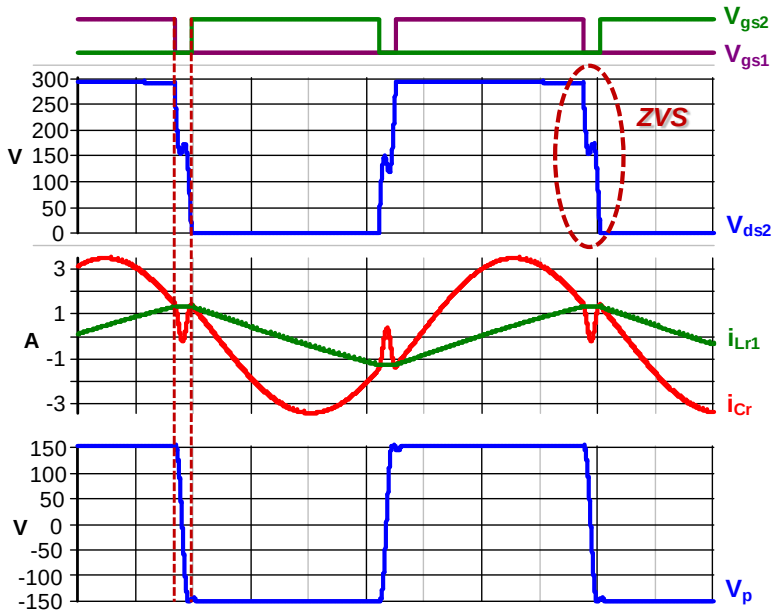

Fig. 3.18. Waveforms of v_{ds2} and v_{j2} based on simulation (L_{e2}=3.4uH)

For this case, L_{r1} and L_{e2} are in the area that the red curve is above the blue curve, as Fig. 3.16 shows. Therefore, with this design, ZVS of the primary-side switches is achieved within 150ns.

Case 2: L_{r1}=95.6uH, L_{e2}=2.4uH and C_r=120nF

The waveforms of v_{ds2} and v_p based on (3.37) and (3.38) are presented in Fig. 3.19. The low-side switch Q_2 is able to achieve ZVS around 136ns which is less than 150ns, and the voltage across the equivalent junction capacitor can't reverse its polarity within 150ns. Since i_{Le2} does not provide enough charge to reverse the voltage across the equivalent junction capacitor within 150ns, the output capacitor of Q_2 will reach zero before 150ns. The simulation results are shown in Fig. 3.20. Since v_{ds2} reaches zero around 136ns, the dead time could be reduced to 135ns to achieve full ZVS at that time point.

For this case, L_{e2} is in the area that the red curve is below the blue curve, as Fig. 3.16 shows. The voltage across the equivalent junction capacitor is reversed after 150ns.

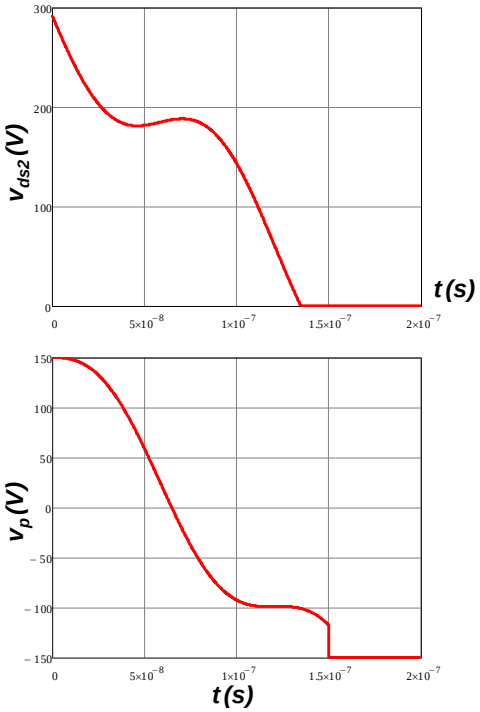

Fig. 3.19. Waveforms of v_{ds2} and v_p based on derivation (L_{e2}=2.4uH)

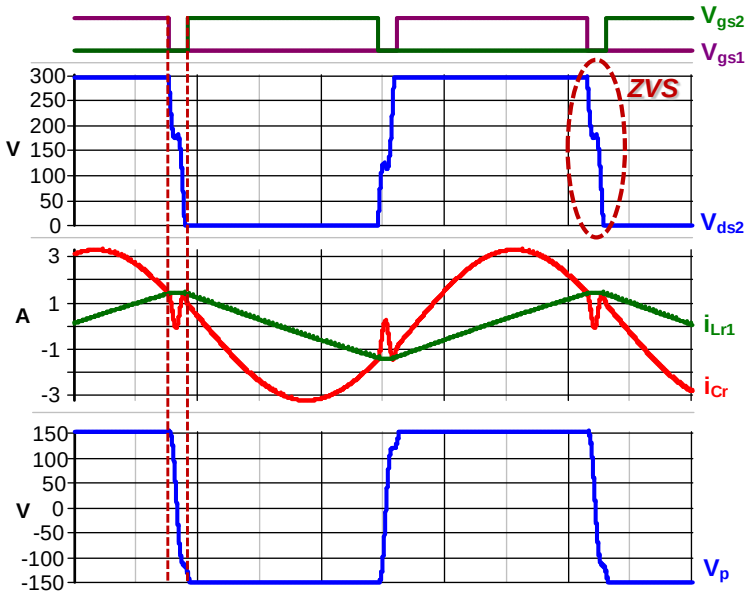

Fig. 3.20. Waveforms of v_{ds2} and v_p based on simulation (L_{e2}=2.4uH)

Case 3: L_{r1}=95.6uH, L_{e2}=6.6uH and C_r=45.6nF

The waveforms of v_{ds2} and v_p based on (3.37) and (3.38) are presented in Fig. 3.21. The low-side switch Q_2 can't achieve ZVS within 150ns and the voltage across the equivalent junction capacitor reverses its polarity around 118ns, which is much less than 150ns. After the voltage across the junction capacitor is reversed, the secondary-side rectifier will conduct earlier than the primary-side switch does. This makes it harder for the primary-side switch to achieve ZVS. The simulation results are also shown in Fig. 3.22. Compare Fig. 3.21 and Fig. 3.22, the theoretical analysis and the simulation results match well. Only partial ZVS of the primary-side switches is achieved at the end of dead time.

For this case, L_{r1} and L_{e2} are in the area that the red curve is below the blue curve, as Fig. 3.16 shows. Therefore, with this design, ZVS of the primary-side switches can't be achieved within 150ns.

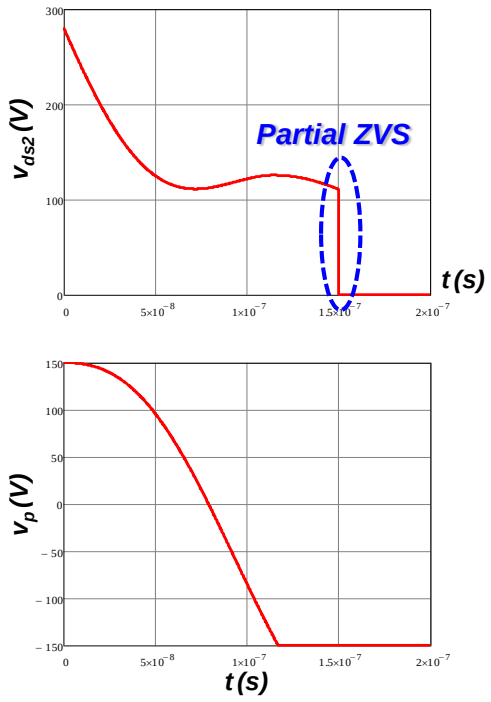

Fig. 3.21. Waveforms of v_{ds2} and v_p based on derivation (L_{e2}=6.6uH)

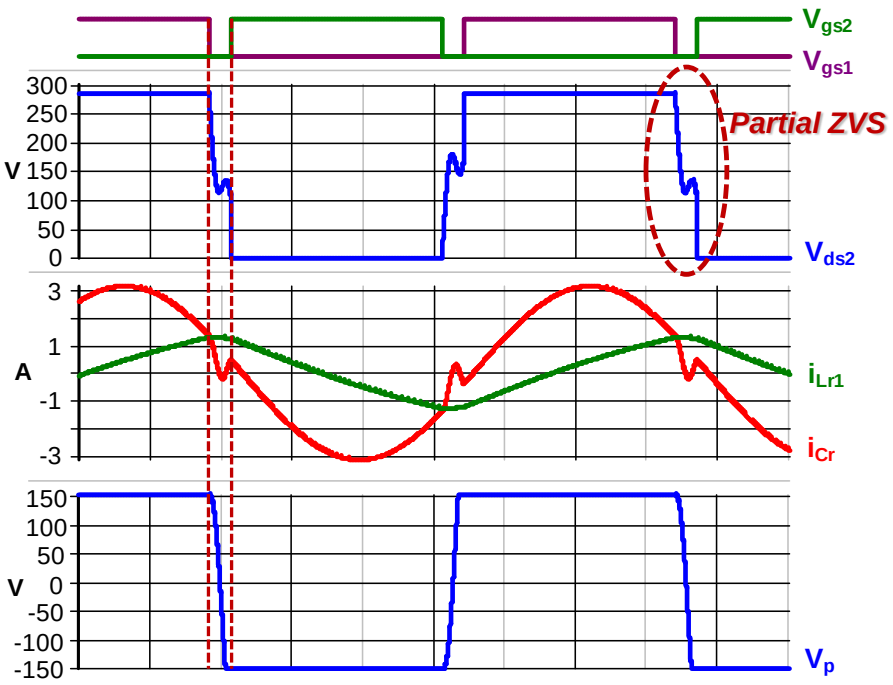

Fig. 3.22. Waveforms of v_{ds2} and v_{j2} based on simulation (L_{e2}=6.6uH)

The maximal L_p can be got according to (3.18) and it is about 94.7uH. The values of L_{r1} and L_{e2} should meet this requirement ($L_p=L_{r1}^2/(L_{r1}+L_{e2})$) at first. L_{r1} can be roughly determined by the maximal value of L_p. For a given L_{r1}, the relationship between Q_{Cr} and L_{e2} can be established. A figure like Fig. 3.16 can be got. Then L_{e2} can be chosen in the areas where $Q_{Cr} \geq Q_{Coss}$. L_{e2} can be determined with this method. After L_{r1} and L_{e2} are both determined, C_r can be determined according to the resonant frequency.

For example, when L_{r1}=95.6uH, the relationship between Q_{Cr} and L_{e2} is presented in Fig. 3.16. Then L_{e2}=3.35uH and the ZVS requirement is met. With known L_{r1} and L_{e2}, C_r can be designed according to the resonant frequency. In this case, C_r=89nF. The experiment results are presented in Fig. 3.23. ZVS of the primary-side switches is achieved.

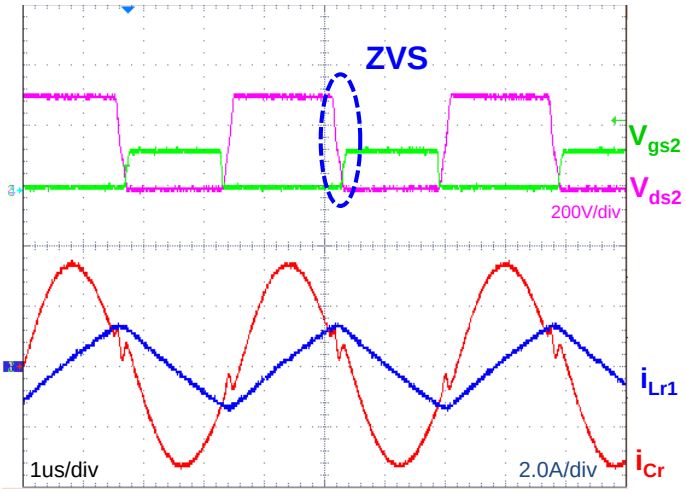

Fig. 3.23. The experiment results (L_{r1}=95.6uH & L_{e2}=3.35uH)

According to Fig. 2.17, the DC voltage gain of CLL resonant converter can be divided into two operation zones for the primary-side switches. One is the ZVS zone, the other is ZCS zone. For power MOSFET, it is desired to working in the ZVS zone. This will impose some constraints on the parameters of CLL resonant converter.

For example, when there are 5 transformer modules, L_{r1}=95.6uH, L_{e2}=3.35uH ($L_{e2}=L_{r2}+5L_k$, L_{r2}=2.90uH and L_k=0.09uH) and C_r=87nF. In this circumstance, L_n=28.5 and the voltage gain of CLL resonant converter is presented in Fig. 3.24. The quality factors of CLL resonant converter under 5% dimming and full load conditions can be obtained according to (2.8). They are 0.004 and 0.073 respectively. From 5% dimming to full load, the CLL resonant converter is always working in the ZVS zone, as shown in Fig. 3.24.

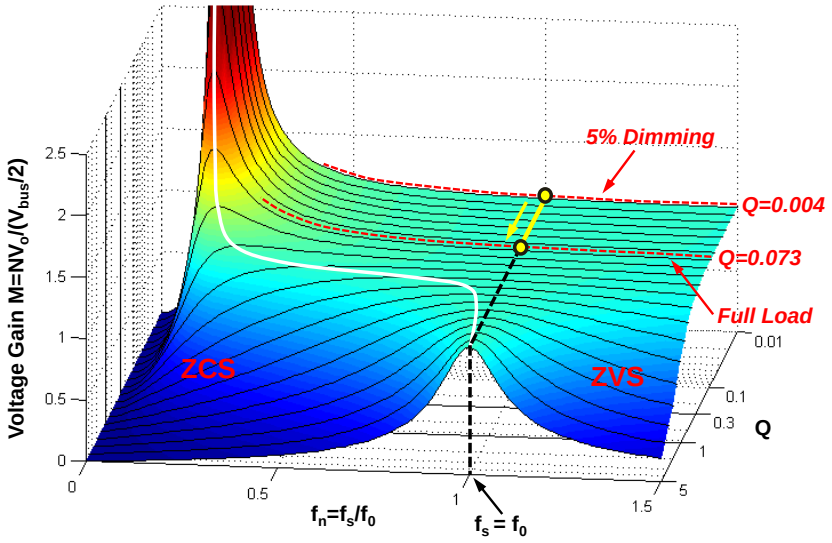

Fig. 3.24. Working points of full load and 5% dimming (5 transformer modules)

When there is only 1 transformer module, L_{r1}=95.6uH, L_{e2}=2.99uH ($L_{e2}=L_{r2}+L_k$, L_{r2}=2.90uH and L_k=0.09uH) and C_r=87nF. In this circumstance, L_n=32.0 and the voltage gain of CLL resonant converter is presented in Fig. 3.25. The quality factors of CLL resonant converter under 5% dimming and full load conditions can be obtained according to (2.8). They are 0.021 and 0.346 respectively. From 5% dimming to full load, the CLL resonant converter is always working in the ZVS zone, as Fig. 3.25 shows.

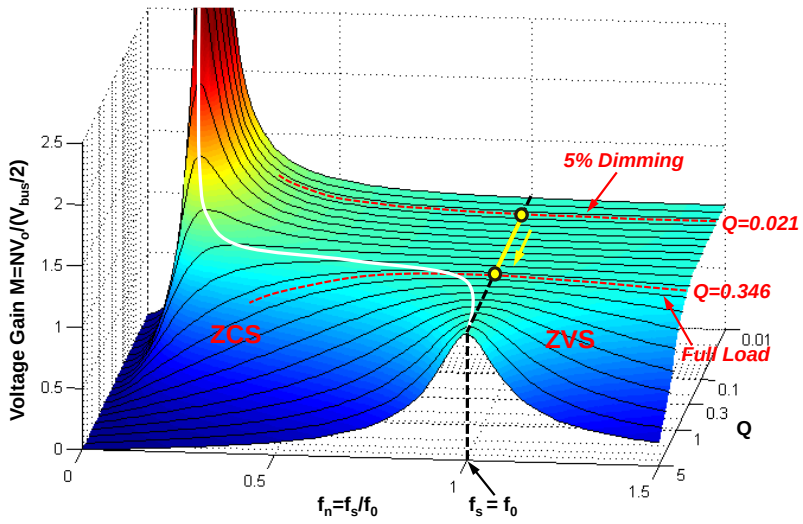

Fig. 3.25. Working points of full load and 5% dimming (1 transformer modules)

3.2.5 Transformer Design

The turns ratio of transformer is 1:3. For the transformer modularization, the PCB windings are adopted to construct the planar transformer. Furthermore, there are 6 turns for the primary side winding and 18 turns for the secondary side winding in order to make loss of the transformer lower. Besides that, the primary side winding and the secondary side winding are interleaved to achieve lower winding loss. The configuration of the planar transformer is presented in Fig. 3.26. In order to keep the transformer module low profile, core set EER 25 (combination of ER 25/6/15 with ER 25/6/15) is adopted. The key parameters of EER 25 are presented in Table 3.10.

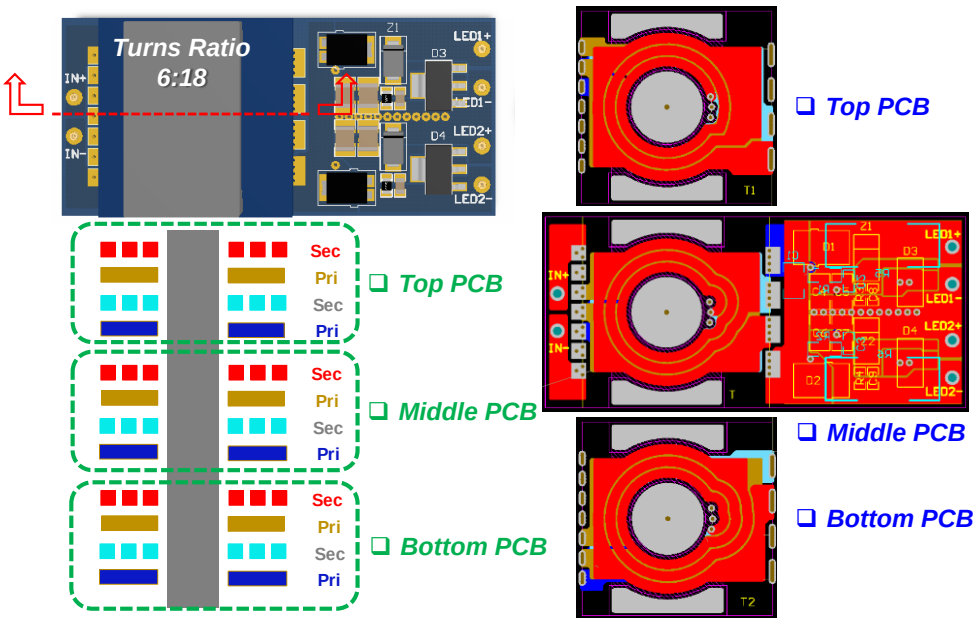

Fig. 3.26. Configuration of the planar transformer

Table 3.10. Effective core parameters of EER 25

Symbol	Parameter	Value
V_e	Effective volume	2414 mm^3
L_e	Effective length	34.1 mm
A_e	Effective area	70.8 mm^2

For the transformer design, an optimal ΔB should be found, which leads to minimal total core loss and winding loss. For this planar transformer, N97 is adopted. The key parameters of N97 are shown in Table 3.11.

Table 3.11. Key parameters of N97

Symbol	**Value**
B_{sat} (100 ℃)	410 mT
P_V(100 ℃; 100kHz; B_m=60mT)	150 kW/m^3

ΔB can be obtained from the following equation

$$\Delta B = \frac{V_o \cdot T_o}{2N_s \cdot A_e} = 117mT \tag{3.42}$$

B_m is half of ΔB, namely B_m=ΔB/2=58.5mT.

Since the magnetizing inductance of the transformer should be very large, there is no air gap for the core. The key parameters of the transformer are presented in Table 3.12.

Table 3.12. Key parameters of transformer with PCB winding

L_m	**L_k**	**$C_{interwinding}$**	**B_m**	**Air Gap**	**Primary Turns (N_p)**	**Secondary Turns (N_s)**
160 μH	150 nH	420pF	58.5 mT	0	6	18

The loss of the transformer based on theoretical analysis is presented in Table 3.13. .

Table 3.13. Loss of transformer based on theoretical analysis

Core Loss	**Winding Loss**
0.362 W	0.274 W

The total loss for the transformer is about 0.636W. The prototype of one transformer module is presented in Fig. 3.27.

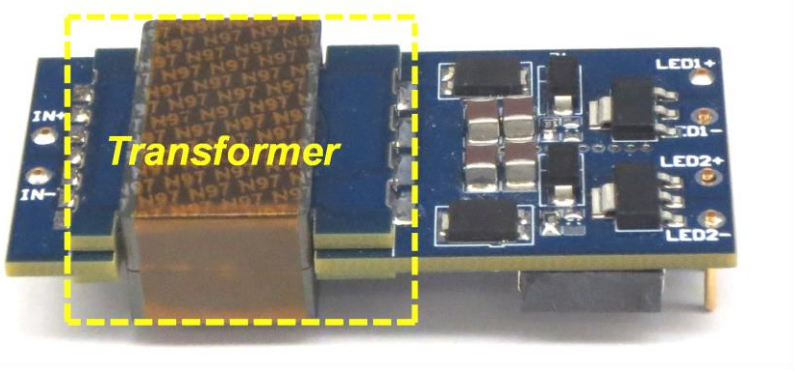

Fig. 3.27. Prototype of one transformer module with planar transformer

In order to achieve lower leakage inductance and lower inter-winding capacitor, the transformer is also designed with Litz wire, as Fig. 3.28 presents. The primary side winding is with 44/180 Litz wire and the secondary side winding is with 44/100 Litz wire. The key parameters of the transformer are presented in Table 3.14. The transformer with Litz wire has lower leakage inductance and lower inter-winding capacitance.

Table 3.14. Key parameters of transformer with Litz wire winding

L_m	L_k	$C_{inter\text{-}winding}$	B_m	Air Gap	Primary Turns (N_p)	Secondary Turns (N_s)
160 μH	90 nH	70pF	58.5 mT	0	6	18

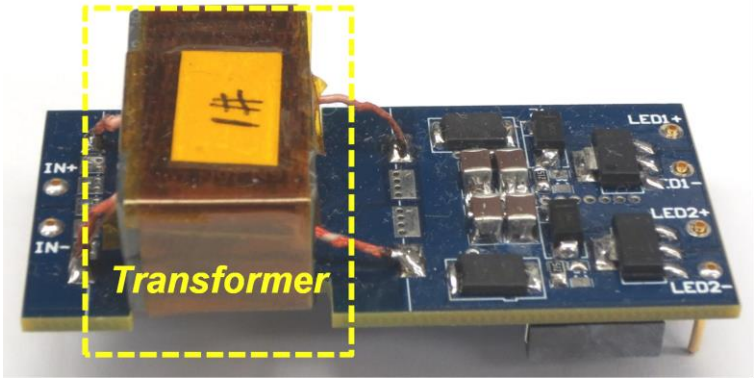

Fig. 3.28. Prototype of one transformer module with Litz wire

The loss of the transformer based on theoretical analysis is presented in Table 3.15.

Table 3.15. Loss of transformer based on theoretical analysis

Core Loss	**Winding Loss**
0.362 W	0.221 W

The core loss is the same as the transformer with PCB winding, but the winding loss of the transformer with Litz wire is lower. The total loss for the transformer is about 0.583W. In practice, the transformer with Litz wire is adopted to achieve better performance.

Chapter 4. Small Signal Model and Control

4.1 Small Signal Model

4.1.1 Small Signal Model of Buck Converter

For buck converter, its small signal model can be derived according to the three terminal model [27], [28]. The topology of buck converter is shown in Fig. 4.1. In buck converter, the switching network is the non-linear part. It can be substituted with a linear block to get its small signal model. The linear blocks are shown Fig. 4.2. With these linear blocks, the small signal model of buck converter under CCM and DCM can be both derived. The transfer functions of duty cycle to bus voltage under CCM and DCM are shown in (4.1) and (4.2) respectively.

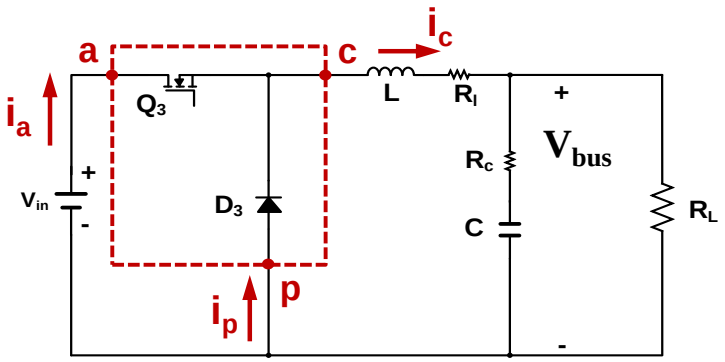

Fig. 4.1. Topology of buck converter

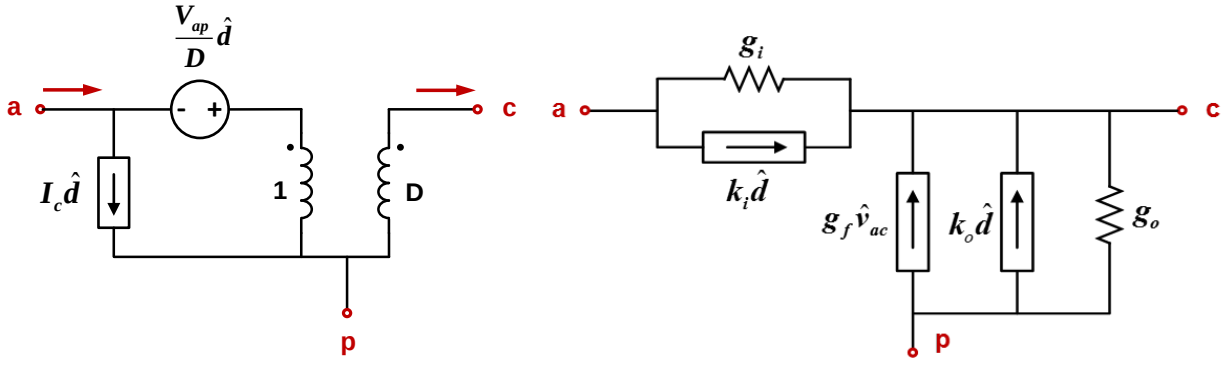

(a) CCM (b) DCM

Fig. 4.2. Three terminal small signal model of switching network

When buck converter is working under DCM, the waveforms of i_a and i_P are presented in Fig. 4.3.

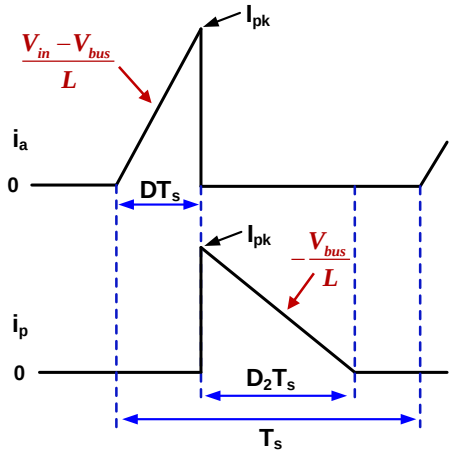

Fig. 4.3. Waveforms of i_a and i_p under DCM

$$G_{vd\_CCM}(s)=\frac{\hat{v}_{bus}(s)}{d(s)}=V_{in}\frac{1+sR_cC}{\frac{s^2}{\omega_{o1}^2}+\frac{1}{Q\omega_{o1}}s+1} \tag{4.1}$$

$$G_{vd\_DCM}(s)=\frac{\hat{v}_{bus}(s)}{d(s)}=H_d\frac{1+sR_cC}{a_2s^2+a_1s+1} \tag{4.2}$$

where $\omega_{o1}=\frac{1}{\sqrt{LC}}$, $Q=\frac{1}{\omega_{o1}}\frac{1}{\frac{L}{R_L}+(R_l+R_c)C}$,

$I_a=\frac{I_{pk}}{2}D$, $I_P=\frac{I_{pk}}{2}D_2$,

$$r=\frac{1}{\frac{I_a}{V_{in}-V_{bus}}+\frac{I_p}{V_{bus}}+\frac{2I_p}{V_{in}-V_{bus}}},$$

$$H_d = \frac{2I_o}{D}\frac{rR_L}{r+R_L+R_l},$$

$$a_1 = \frac{L}{R_l+r+R_L} + C\left[R_c + R_L // \left(r+R_l\right)\right],$$

$$a_2 = LC\frac{R_c+R_L}{r+R_L+R_l}.$$

I_a and V_{in} are the averages of input current and input voltage. C is output capacitor and R_c is the ESR of output capacitor. L is buck inductor and R_l is the DCR of buck inductor. I_p is the average of i_p. V_{bus} is the average of bus voltage. R_L is the load of buck converter.

4.1.2 Small Signal Model of CLL Resonant Converter

For CLL resonant converter, the equivalent small signal model can be derived with the method proposed in [29] and [30]. The topology of CLL resonant converter is shown in Fig. 4.4 and its equivalent small signal circuit model is shown in Fig. 4.5.

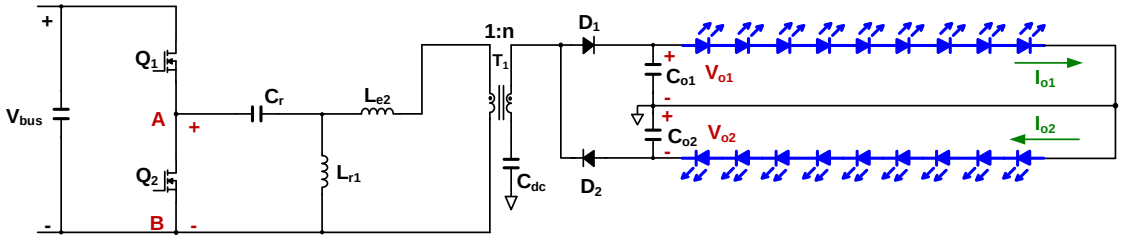

Fig. 4.4. Topology of CLL resonant converter

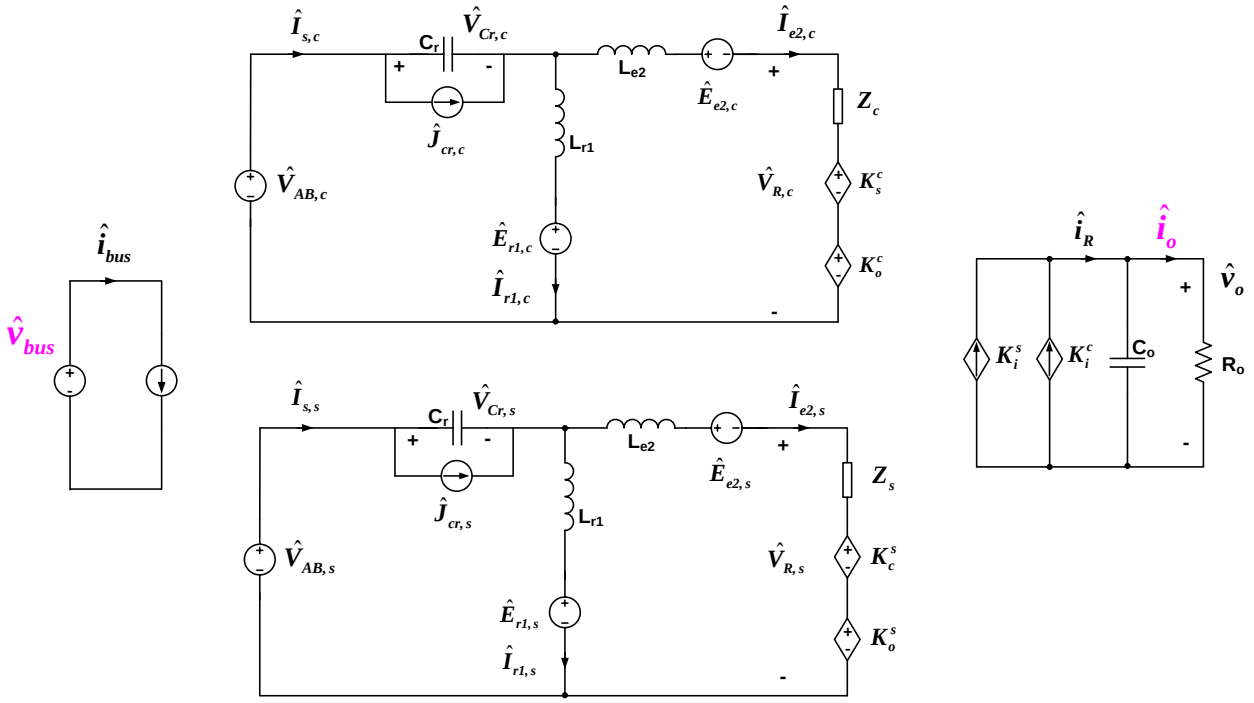

Fig. 4.5. Equivalent small signal model of CLL resonant converter

The terms in Fig. 4.5 are defined as follows:

$$\text{资}_{Cr,c} = \omega_s C_r V_{Cr,s},\ \text{资}_{Cr,s} = -\omega_s C_r V_{Cr,c};$$

$$\text{资}_{r1,c} = \omega_s L_{r1} I_{r1,s},\ \text{资}_{r1,s} = -\omega_s L_{r1} I_{r1,c};$$

$$\text{资}_{e2,c} = \omega_s L_{e2} I_{e2,s},\ \text{资}_{e2,s} = -\omega_s L_{e2} I_{e2,c};$$

$$Z_c = \frac{4V_{out}}{\pi}\frac{I_{e2,s}^2}{\left(I_{e2,c}^2 + I_{e2,s}^2\right)^{\frac{3}{2}}},\ Z_s = \frac{4V_{out}}{\pi}\frac{I_{e2,c}^2}{\left(I_{e2,c}^2 + I_{e2,s}^2\right)^{\frac{3}{2}}};$$

$$k_s^c = k_c^s = -\frac{4V_{out}}{\pi}\frac{I_{e2,s}I_{e2,c}}{\left(I_{e2,c}^2 + I_{e2,s}^2\right)^{\frac{1}{2}}};$$

$$k_o^c = \frac{4}{\pi}\frac{I_{e2,c}}{\left(I_{e2,c}^2 + I_{e2,s}^2\right)^{\frac{1}{2}}},\ k_o^s = \frac{4}{\pi}\frac{I_{e2,s}}{\left(I_{e2,c}^2 + I_{e2,s}^2\right)^{\frac{1}{2}}};$$

$$k_i^c = \frac{2}{\pi}\frac{I_{e2,c}}{\left(I_{e2,c}^2 + I_{e2,s}^2\right)^{\frac{1}{2}}},\ k_i^s = \frac{2}{\pi}\frac{I_{e2,s}}{\left(I_{e2,c}^2 + I_{e2,s}^2\right)^{\frac{1}{2}}}.$$

Meanwhile, $C_o=2C_{o1}$ and R_o is half of the AC equivalent resistance of one LED string.

According to the small signal model, the transfer functions of the input impedance and the bus voltage to output current are derived when switching frequency f_s equals to resonant frequency f_0.

The input impedance of CLL resonant converter is

$$Z_{in}(s) = \frac{\hat{v}_{bus}(s)}{\hat{i}_{bus}(s)} = \frac{4L_{r1}^2 R_o}{n^2\left(L_{r1}+L_{e2}\right)^2}\frac{\frac{s^2}{\omega_{o2}^2}+\frac{s}{\omega_{o2}Q_2}+1}{C_o R_o s+1} \tag{4.3}$$

The transfer function of bus voltage to output current is

$$G_{v2io}(s) = \frac{\hat{i}_{o1}(s)}{\hat{v}_{bus}(s)} = \frac{n\left(L_{r1}+L_{e2}\right)}{4R_o L_{r1}}\frac{1}{\frac{s^2}{\omega_{o2}^2}+\frac{s}{\omega_{o2}Q_2}+1} \tag{4.4}$$

where $\omega_{o2} = \frac{1}{\sqrt{\left(L_{r1}+L_{e2}\right)\frac{L_{e2}}{L_{r1}}\frac{n^2\pi^2 C_o}{4}}}$,

$$Q_2 = \frac{\frac{8R_o}{n^2\pi^2}}{\sqrt{\left(L_{r1}+L_{e2}\right)\frac{L_{e2}}{L_{r1}}\cdot\frac{16}{n^2\pi^2 C_o}}}.$$

$\hat{i}_{o1}(s)$ is equal to half of $\hat{i}_o(s)$ and the transformer's turns ratio is 1:n.

4.1.3 Small Signal Model of Two-Stage LED Driver

Since the CLL resonant converter is the load of the first stage buck converter, the transfer function of control to bus voltage in the first stage can be derived with $Z_{in}(s)$, which is the input impedance of CLL resonant converter. Combine with the transfer function of bus voltage to output current, the transfer function of control to output current in the two-stage LED driver can be derived as follows:

$$G_{d2io}(s)=\frac{\hat{v}_{bus}(s)}{d(s)}|_{R_L=z_{in}}\times\frac{\hat{i}_{o1}(s)}{\hat{v}_{bus}(s)} \tag{4.5}$$

$$G_{d2io}(s)=V_{in}\frac{n(L_{r1}+L_{e2})}{4R_oL_{r1}}\times\frac{R_cCs+1}{\frac{s^4}{\omega_{o1}^2\omega_{o2}^2}+\frac{s^3}{Q_2\omega_{o1}^2\omega_{o2}}+\left(\frac{1}{\omega_{o1}^2}+\frac{1}{\omega_{o2}^2}+\frac{LC_o\cdot n^2(L_{r1}+L_{e2})^2}{4L_{r1}^2}\right)s^2+\left(\frac{1}{Q_2\omega_{o2}}+\frac{L\cdot n^2(L_{r1}+L_{e2})^2}{4L_{r1}^2R_o}\right)s+1}$$

The derived model is verify with the simulation. From full load (I_{o1}=300mA) and light load (5% dimming, namely I_{o1}=15mA) with one transformer, the Bode plots of derived model and simulation are shown in Fig. 4.6 and Fig. 4.7 respectively.

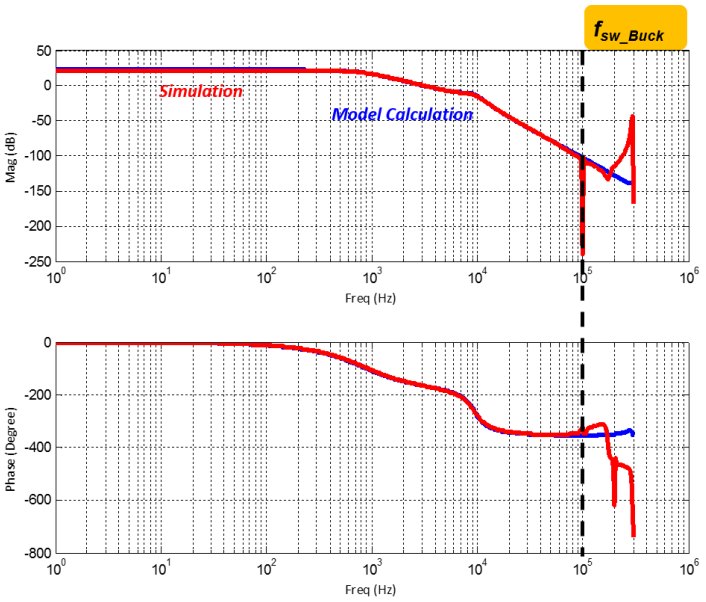

Fig. 4.6. Bode plot of control to output current (one transformer and full load)

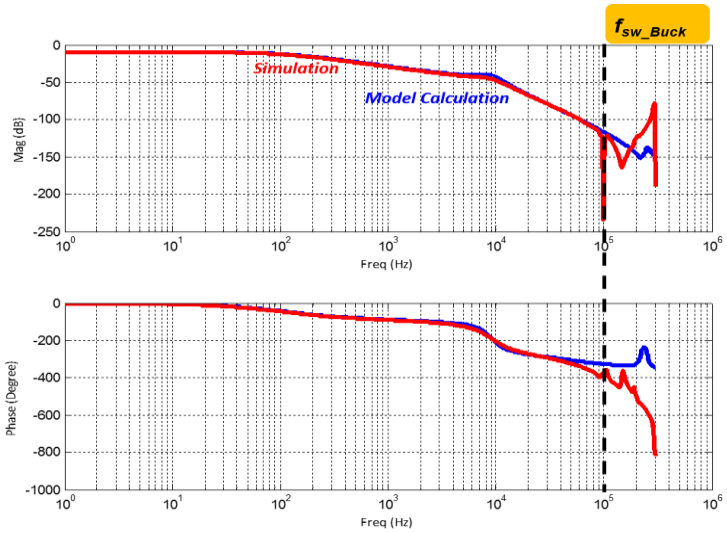

Fig. 4.7. Bode plot of control to output current (one transformer and 5% dimming)

According to Fig. 4.6 and Fig. 4.7, the derived analytical model with one transformer is accurate up to the switching frequency of buck converter (f_{sw_buck}=100kHz). This good enough for the feedback compensator design. In practice, the transformer modules of this two-stage LED driver could vary from 1 to 5. Therefore, it is necessary to derive the small signal model with multi-transformers. According to Fig. 4.5, when switching frequency of CLL resonant converter equals to resonant frequency, the transfer function of control to output current is

$$G_{d2io}(s)=\frac{\hat{v}_{bus}(s)}{d(s)}|_{R_L=z_{in}}\times\frac{\hat{i}_{o1}(s)}{\hat{v}_{bus}(s)}, \tag{4.6}$$

$$G_{d2io}(s)=V_{in}\frac{n(L_{r1}+L_{e2})}{4NR_oL_{r1}}\times\frac{R_cCs+1}{\frac{s^4}{\omega_{o1}^2\omega_{o3}^2}+\frac{s^3}{Q_3\omega_{o1}^2\omega_{o3}}+\left(\frac{1}{\omega_{o1}^2}+\frac{1}{\omega_{o3}^2}+\frac{LC_o\cdot n^2(L_{r1}+L_{e2})^2}{4L_{r1}^2}\right)s^2+\left(\frac{1}{Q_3\omega_{o3}}+\frac{L\cdot n^2(L_{r1}+L_{e2})^2}{4NL_{r1}^2R_o}\right)s+1}$$

where N is the number of transformers and

$$\omega_{o3}=\frac{1}{\sqrt{(L_{r1}+L_{e2})\frac{L_{e2}}{L_{r1}}\frac{n^2\pi^2C_o}{4N}}},$$

$$Q_3 = \frac{\frac{8NR_o}{n^2\pi^2}}{\sqrt{(L_{r1}+L_{e2})\frac{L_{e2}}{L_{r1}}\Big/\frac{n^2\pi^2 C_o}{16N}}}.$$

Compare (4.6) with (4.5), the difference of these two transfer functions is only the number of transformers. Similarly, the derived model is verified with simulation. In the case with five transformers, the Bode plots of control to output current under full load and 5% dimming are presented in Fig. 4.8 and Fig. 4.9 respectively.

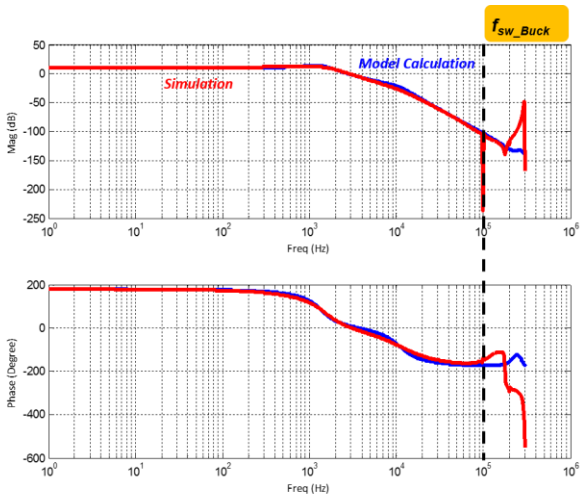

Fig. 4.8. Bode plot of control to output current (five transformer and full load)

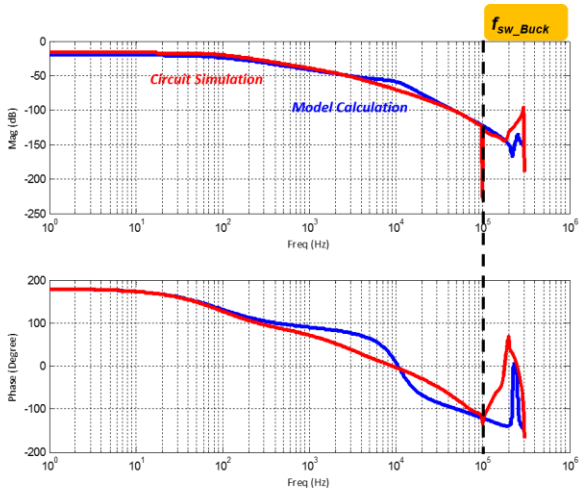

Fig. 4.9. Bode plot of control to output current (five transformer and 5% dimming)

The Bode plots of the two-stage LED driver with one transformer and five transformers under full load and 5% dimming are shown in Fig. 4.10.

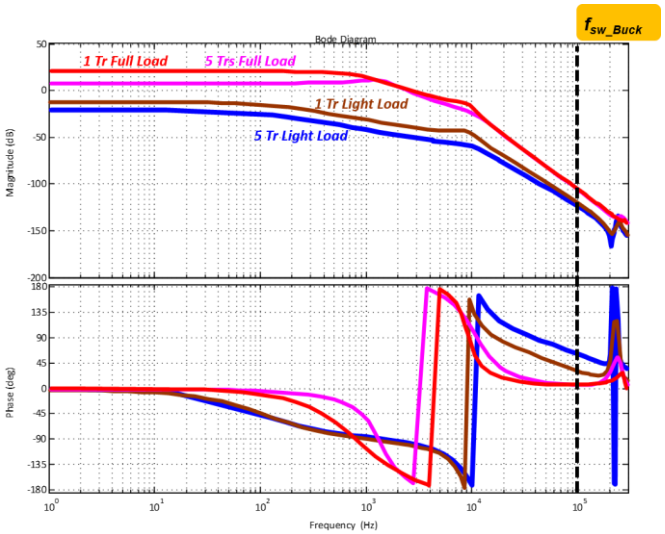

Fig. 4.10. Comparison of Bode plots with one transformer and five transformers

According to Fig. 4.10, the DC gain of one transformer under the full load condition is the highest. Therefore, the compensator should be designed under this condition so that the feedback control loop will be stable under other else conditions. There will be enough gain margin and phase margin.

4.2 PI Compensator Design

For simplicity, PI compensator is adopted for feedback control, as shown in Fig. 4.11.

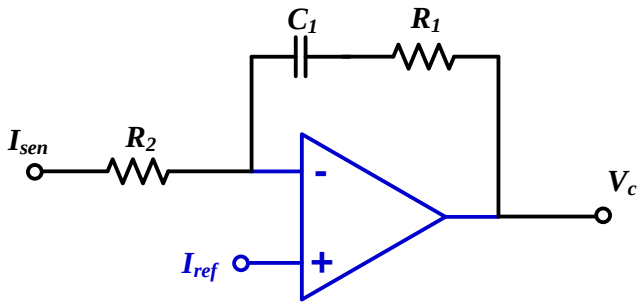

Fig. 4.11. PI compensator

With one transformer under full load condition, the open loop Bode plot is shown in Fig. 4.12. There are two double poles located at 642 Hz and 9.44 kHz respectively. Therefore, the zero of PI compensator is put at 300 Hz to obtain enough phase margin.

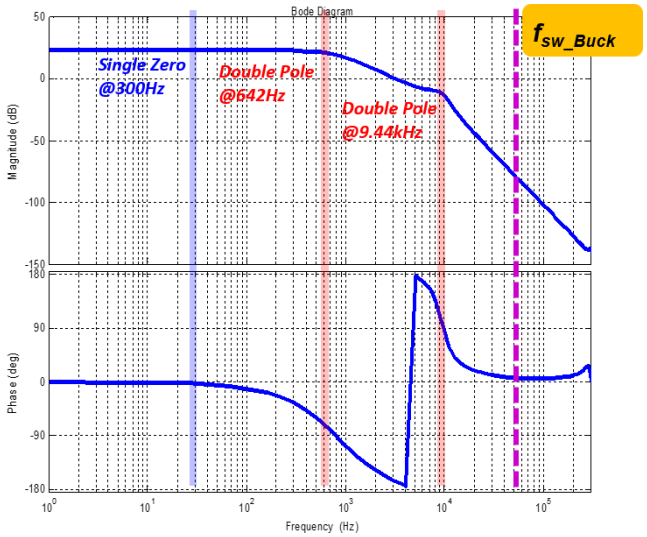

Fig. 4.12. Open loop Bode plot (one transformer & full load)

With the PI compensator, the closed loop Bode plot of control to output current is shown in Fig. 4.13. The crossover frequency is 738Hz. The phase margin is 73 degrees and gain margin is about 20dB.

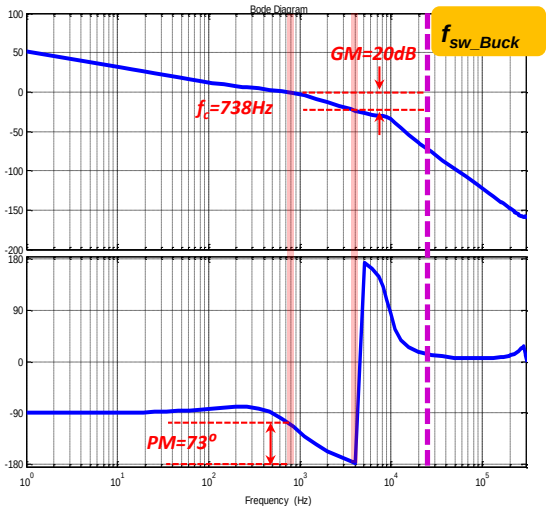

Fig. 4.13. Closed loop Bode plot with PI compensator (one transformer & full load)

The closed loop Bode plot with five transformers is shown in Fig. 4.14, where the crossover frequency is 100Hz. Meanwhile, the phase margin is 111 degrees and the gain margin is about 20dB. It is obvious that the two-stage LED driver is stable with the same PI compensator.

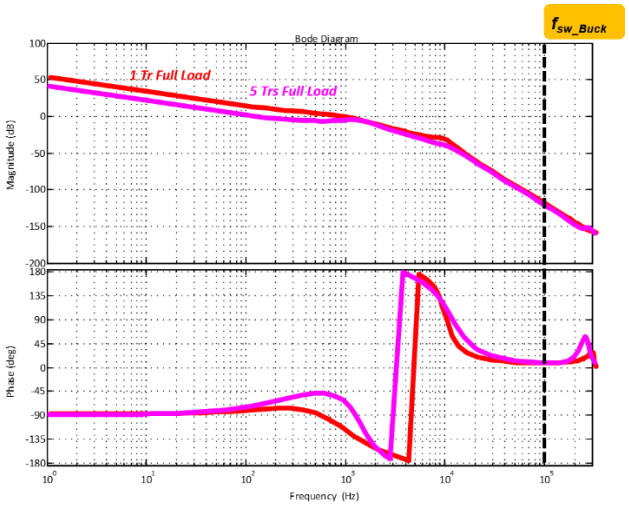

Fig. 4.14. Closed loop Bode plot with PI compensator (five transformers & full load)

4.3 Start-up Process

The complete two-stage LED driver with PI compensator is presented in Fig. 4.15. During the startup, the driving signals to the CLL resonant converter are applied immediately. Furthermore, the switching frequency of the driving signal is fixed and CLL resonant converter is unregulated. Meanwhile, the current reference signal I_{ref} will be also applied. Therefore, V_c which compares with saw tooth wave to generate PWM (pulse width modulation) signal, will be regulated. Then the bus voltage, output voltage and output current will be built up gradually. However, during the startup, the output current will present severe overshoot, as Fig. 4.16 shows. The bus voltage has overshoot, and it causes the overshoot of output current. This is unacceptable since the overcurrent is harmful to the lifetime of LED and LED will flash during the startup.

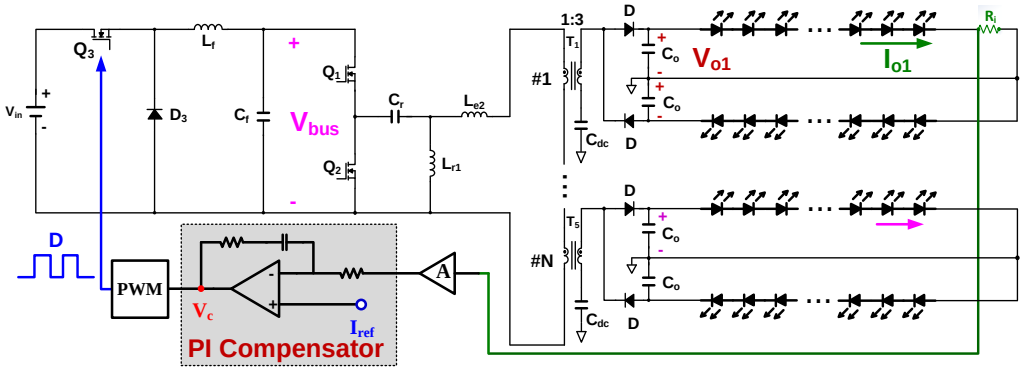

Fig. 4.15. Two-stage LED driver with PI compensator

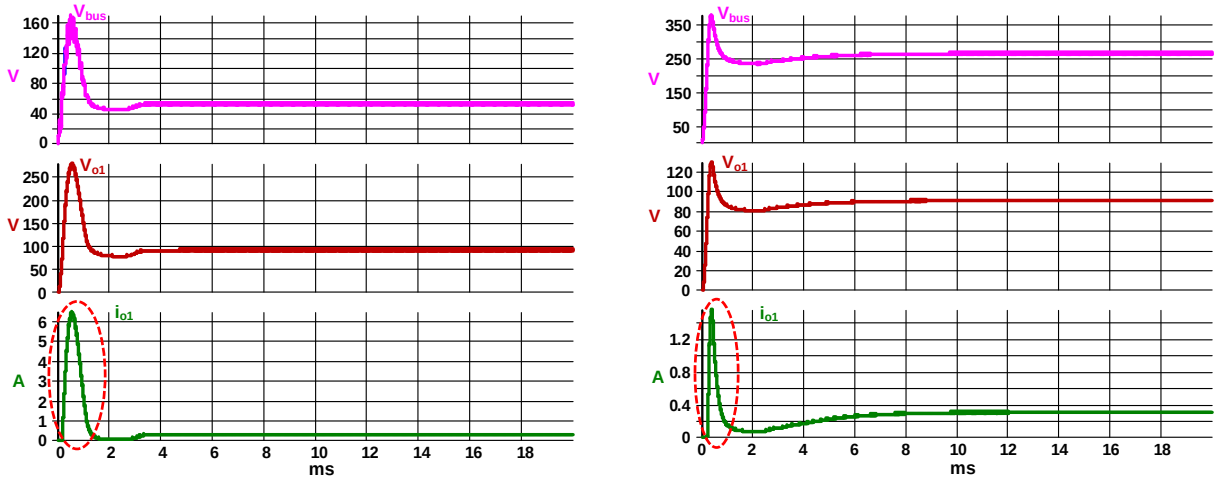

(a) One transformer & full load

(b) Five transformers & full load

Fig. 4.16. Output current overshoot during the startup

In order to realize soft startup without current overshoot, a RC network is added to the loop of current reference signal, as shown in Fig. 4.17.

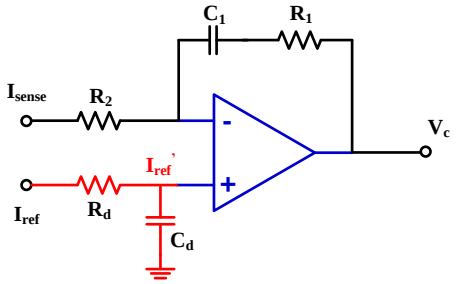

Fig. 4.17. PI Compensator with a RC network in I_{ref} loop

I-V curve of LED is shown in Fig. 4.18. Before the forward voltage reaches the threshold voltage, the forward current is almost zero and LED can be regarded as open circuit. After the forward voltage is greater than the threshold voltage, the forward current increases rapidly as the forward voltage rises and LED can be regarded as a variable resistor. According to this characteristic, the startup process of LED driver can be divided into two stages.

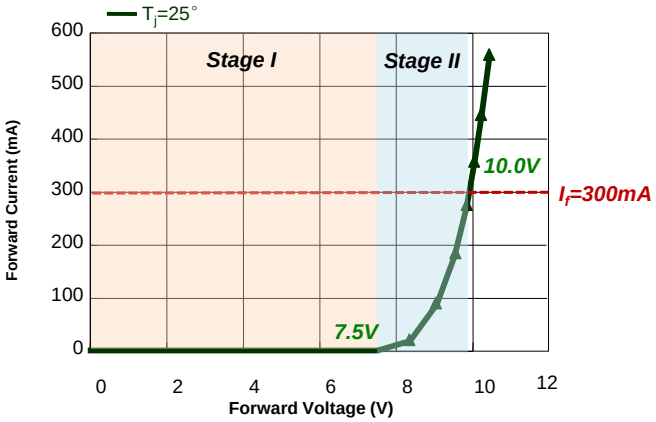

Fig. 4.18. I-V curve of LED string (3 LEDs/String)

Take the case with one transformer under light load as an example, the schematic is shown in Fig. 4.19. In stage I, the current flowing through LED is almost zero. Therefore, the output capacitor is charged and the LED driver starts up with no load. When the output voltage is larger than the threshold voltage, the LED driver is in stage II. The output current will increase as the output voltage rises. At the end of stage II, the output current reaches its steady state, as shown in Fig. 4.20. Meanwhile, v_c is the output of PI compensator, and it compares with saw tooth wave to generate PWM signal to drive buck converter. Therefore, the duty cycle of buck's driving signal is proportional to v_c. In addition, i_{outn} is the normalized output current and it can be derived from

$$i_{outn} = \frac{i_{out}}{I_{ss}}, \tag{4.7}$$

where I_{ss} is the steady state value of the output current.

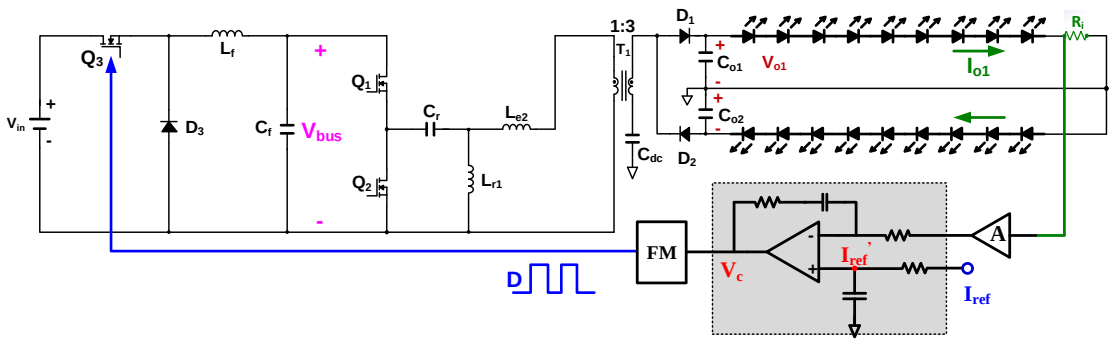

Fig. 4.19. Two-stage LED driver with one transformer

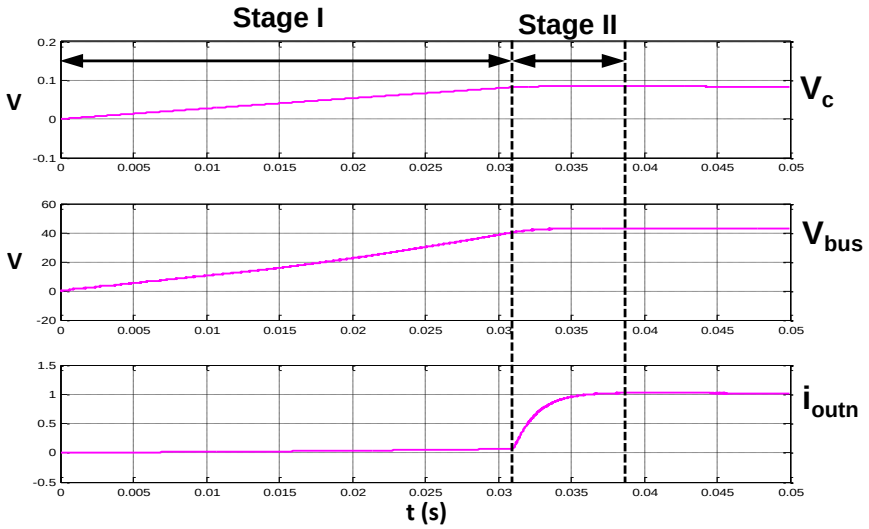

Fig. 4.20. Soft startup process (one transformer & light load)

4.3.1. Comparison of Full Load and Light Load

The stage I startup processes of one transformer under full load and light load are shown in Fig. 4.21. The stage I of light load is much longer than that of full load. The reason is that v_c increases slowly under light load condition. As a result, V_{bus} is also built up slowly. Therefore, it takes longer time for the output voltage to reach the threshold voltage. According to Fig. 4.17, during the startup, v_c can be derived as follows

$$v_c(t) = \frac{1}{C_1 R_2}\int\left(i_{ref}^{'} - i_{sense}\right)dt + \left(1+\frac{R_1}{R_2}\right)i_{ref}^{'} - \frac{R_1}{R_2}i_{sense}. \tag{4.8}$$

Since i_{sense} is equal to zero in the stage I, v_c can be written as

$$v_c(t) = \frac{1}{C_1 R_2}\int\left(i_{ref}^{'}\right)dt + \left(1+\frac{R_1}{R_2}\right)i_{ref}^{'} \ . \tag{4.9}$$

Meanwhile, during the startup, $i_{ref}^{'}$ can be obtained from

$$i_{ref}^{'} = I_{ref}\left(1-e^{-\frac{t}{R_d C_d}}\right). \tag{4.10}$$

Combine (4.9) and (4.10), v_c is got as follows

$$v_c(t) = \frac{I_{ref}}{C_1 R_2}t + \left(1+\frac{R_1}{R_2}+\frac{R_d C_d}{C_1 R_2}\right)I_{ref}\left(1-e^{-\frac{t}{R_d C_d}}\right). \tag{4.11}$$

According to (4.11), $v_c(t) \propto I_{ref}$. Therefore, v_c under full load will increase faster than that under light load. With one transformer, the output voltage reaches the threshold voltage earlier under full load condition.

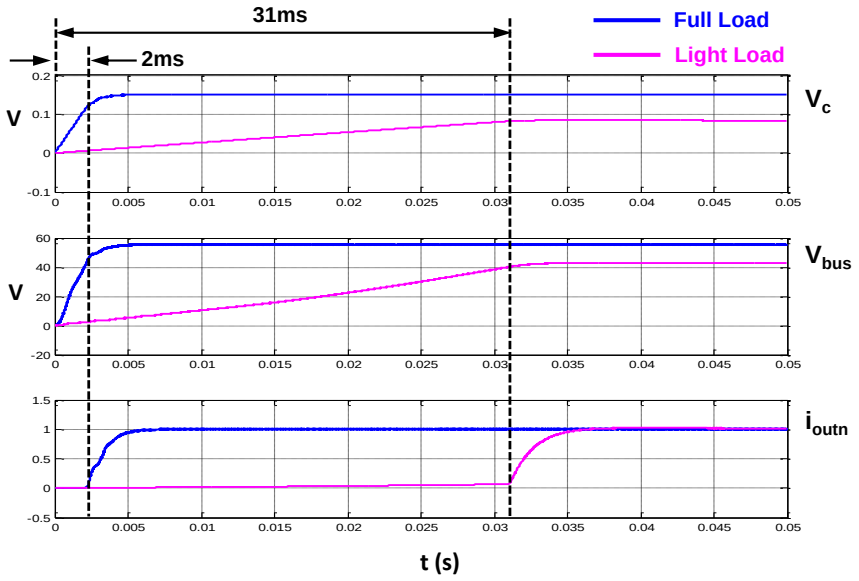

Fig. 4.21. Stage I of the startup process with one transformer

In stage II, the output voltage is greater than the threshold voltage. The output current increases as the output voltage rises. Therefore, i_{sense} is no longer equal to zero and it must be taken into account. According to (4.8), i'_{ref} and i_{sense} will impact on v_c at the same time. The influence of I_{ref} is also dominant in this stage. Therefore, the larger I_{ref} is, the faster v_c will reach the steady state. The stage II startup processes of one transformer under full load and light load are shown in Fig. 4.22. In a word, as the LED strings and the LED number per string are kept the same, the duration of the startup will be shorter with a larger I_{ref}.

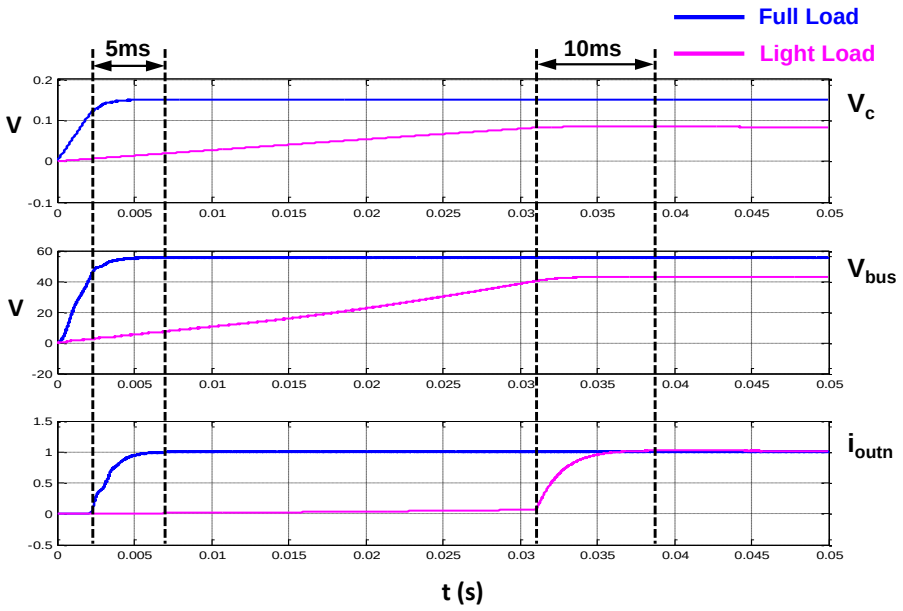

Fig. 4.22. Stage II of startup process with one transformer

4.3.2. Comparison of One Transformer and Five Transformers

The schematic diagram of the two-stage LED driver with five transformers is presented in Fig. 4.23. The stage I startup processes with one transformer and five transformers under full load condition are shown in Fig. 4.24. The stage II startup processes under full load are shown in Fig. 4.25. Although I_{ref} is the same in both cases, the bus voltage with five transformers will be five times of the bus voltage with one transformer. Therefore, the stage I with five transformers is about

five times of that with one transformer, as Fig. 4.24 shows. Meanwhile, the stage II with five transformers is also longer than that with one transformer, as Fig. 4.25 shows.

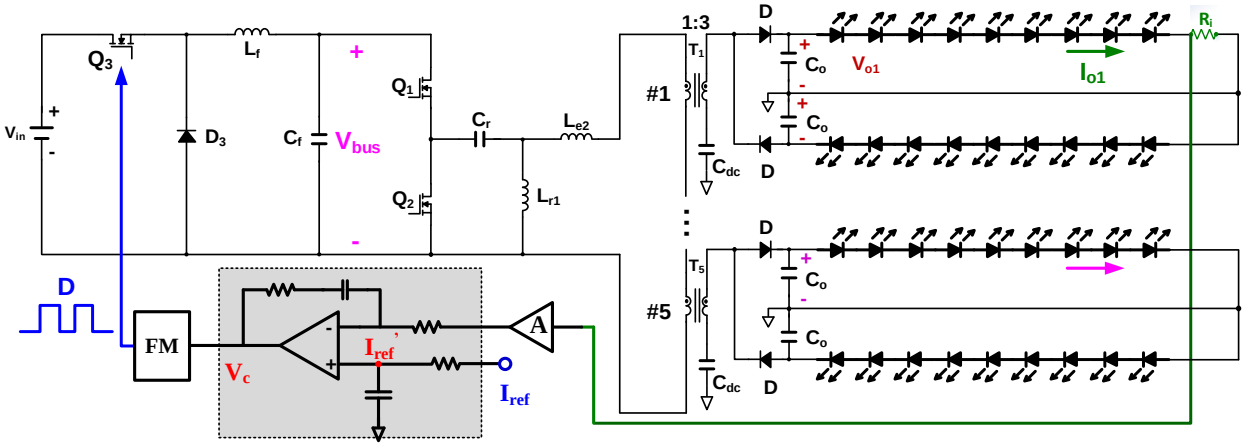

Fig. 4.23. Two-stage LED driver with five transformers

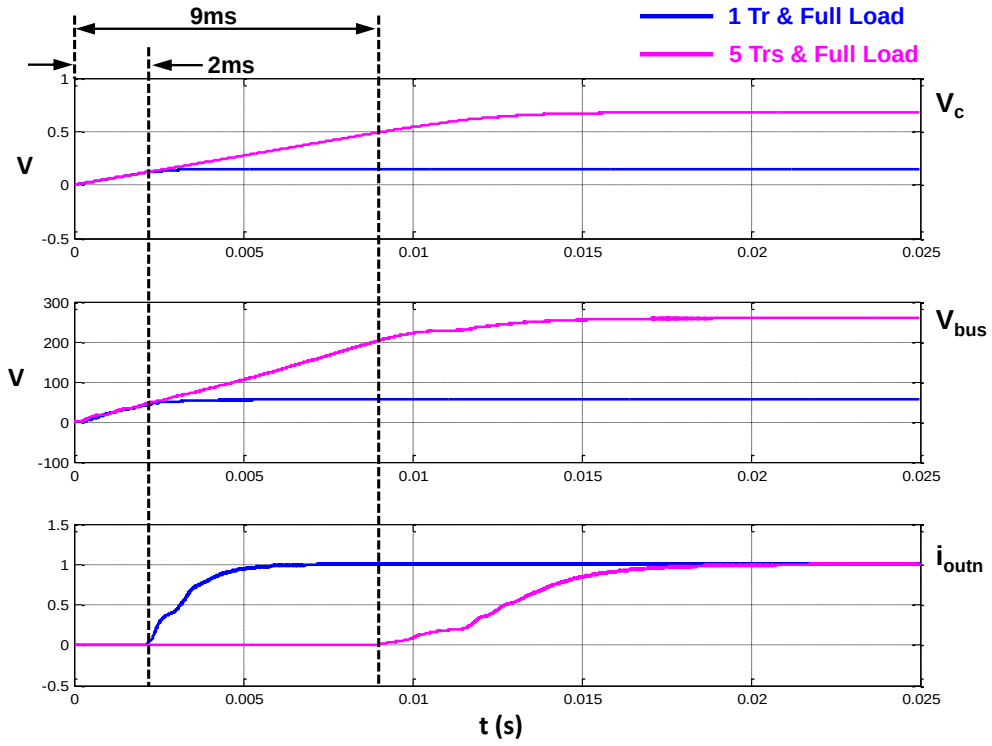

Fig. 4.24. Stage I of startup processes with one transformer and five transformers

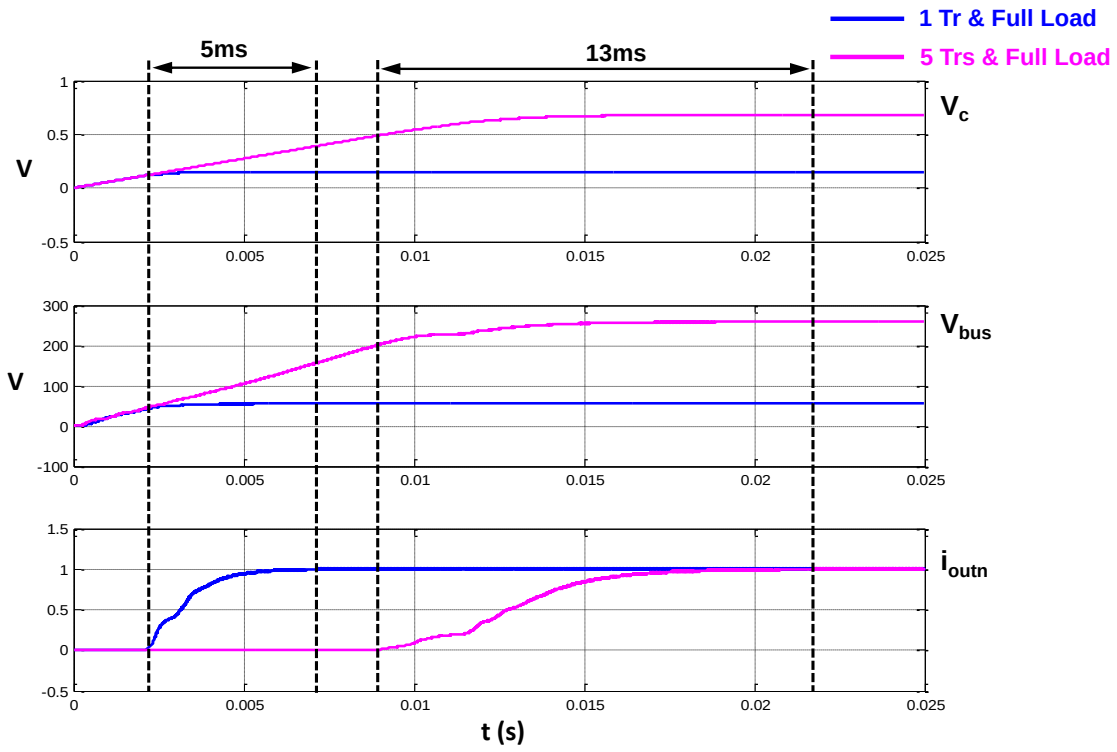

Fig. 4.25. Stage II of startup processes with one transformer and five transformers

The startups of the LED driver with one transformer and five transformers under full load condition are presented in Fig. 4.26 and Fig. 4.27 respectively. For the case with five transformers, the duration of stage I and stage II is much longer than that with one transformer. Moreover, besides these two stages, there is another stage called stage A before the stage I. The stage A is determined by the buck controller (UCC25702). The controller will not generate PWM signal until v_c reaches 2V. The actual startup begins after the stage A. Eventually, the soft startup is achieved with an extra RC network. The overshoot of the output current during startup can be avoided with this method.

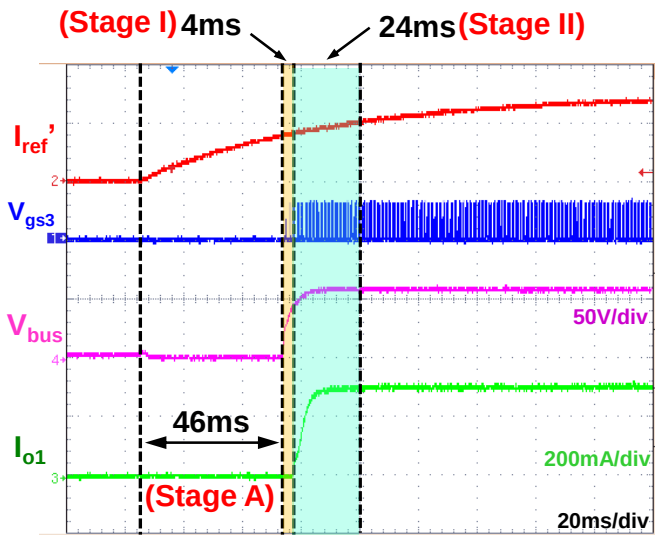

Fig. 4.26. Test result of soft startup with one transformer under full load

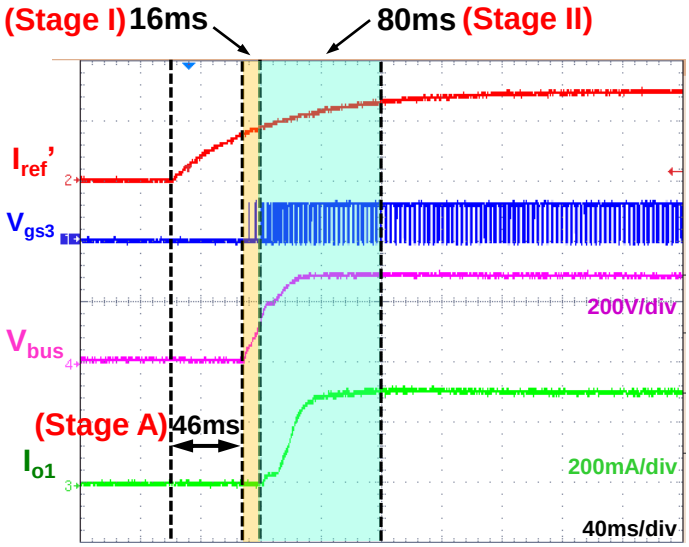

Fig. 4.27. Test result of soft startup with five transformers under full load

Chapter 5. Experiment Results

5.1 Prototype of Two-Stage LED Driver

The prototype of 2-stage LED driver is built in the Lab, as Fig. 5.1 shows. It contains a buck converter as the first stage and a MC^3 CLL resonant converter as the second stage. Each transformer module drives 2 LED strings at the same time. The load could vary from 1 LED string to 10 LED strings, and the transformer modules vary according to the load variation. This 2-stage structure is very flexible for load change.

The forward current of the first LED string is sensed for feedback control to regulate the bus voltage V_{bus}. For CLL, it is unregulated and its switching frequency is a little bit higher than the resonant frequency to achieve higher efficiency within a wide load range.

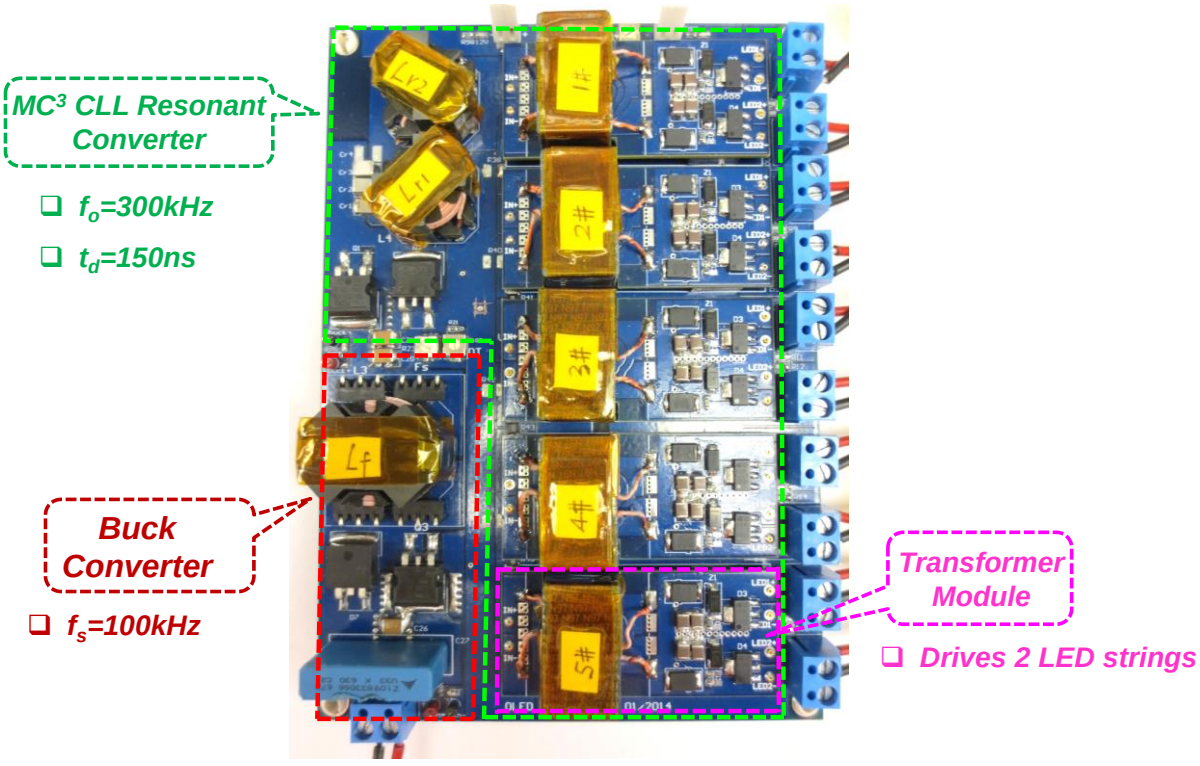

Fig. 5.1. Prototype of 2-stage LED driver

The key parameters of the prototype are listed in Table 5.1.

Table 5.1. Key parameters of the 2-stage prototype

Items	Symbol	Value
Input Capacitor of buck	C_{in}	0.99uF
Output Inductor of buck	L_f	2.0mH
Output Capacitor of buck	C_f	2.82uF
Resonant Capacitor of CLL	C_r	87nF
Resonant Inductor 1 of CLL	L_{r1}	95.6uH
Resonant Inductor 2 of CLL	L_{r2}	3.35uH
Magnetizing Inductor of Tr	L_m	160uH
DC Block Capacitor	C_{dc}	3.3uF
Output Capacitor of Channel	C_o	6.6uF

5.2 Current Balance Capability

The current balance capability is very critical for multiple LED string application, especially when the LED strings are unbalanced. For this 2-stage LED driver, CLL resonant converter with larger magnetizing inductance is adopted. Therefore, the magnetizing current has little influence on the current flowing through the secondary side winding of the transformer. Due to the primary side windings of transformers be in series, the current flowing through the primary side of the transformer is the same. The current flowing through the secondary side winding of the transformer is almost the same. Besides that, the currents flowing through these 2 LED strings driven by the same transformer is balanced by the DC block capacitor which is in series with the secondary side winding.

For this 2-stage LED driver, just the current of one specific LED string is sensed for feedback to regulate the bus voltage. The other strings' currents are cross-regulated. The control scheme is very simple. In addition, the dimming signal I_{ref} is generated by linear voltage regulator SC431, as

Fig. 5.2 shows. I_{ref} will vary from 0.150V to 3.000V by adjusting the value of resistance trimmer R100. Therefore, the output current of LED string could vary from 15mA (5% dimming) to 300mA (full load) correspondingly if the closed-loop PI compensation is applied. The current balance with different LED string and different LED number in each string are discussed in following sections.

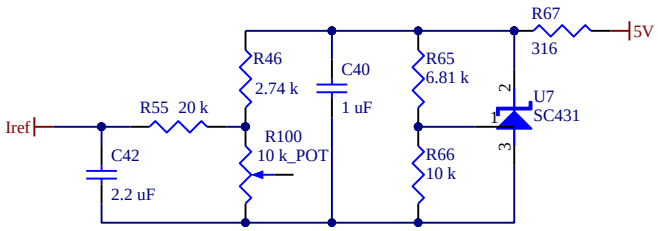

Fig. 5.2. Circuitry generating dimming signal

5.1.1 Balanced Loads

In practice, Cree's XLamp MX-3 LEDs is adopted as the load of this 2-stage LED driver. 28 Xlamp MX-3 LEDs are in series to form one LED string. 10 LED strings as the loads are shown in Fig. 5.3.

Fig. 5.3. Balanced Load of 2-stage LED driver: 10 LED strings with Cree XLamp MX-3 LEDs

(1) 2 LED Strings

There is only one transformer, and these 2 LED strings driven by this transformer have same LED number (28 LEDs/string). The output voltages and output currents these 2 LED strings under different dimming conditions are presented in Table 5.2.

Table 5.2. Output voltages and output currents (28 LEDs/string)

Dimming Ratio	I_{ref} (V)	Vo1 (V)	Vo2 (V)	Io1(A)	Io2(A)
1.00	3.001	90.00	90.87	0.303	0.303
0.50	1.510	85.36	86.15	0.153	0.153
0.19	0.597	80.09	80.72	0.057	0.057
0.05	0.191	75.42	75.86	0.016	0.016

The switching ripple of output current I_{o1} and I_{o2} from 5% dimming to full load for the case that these 2 LED string have 28 LEDs/string are presented in Fig. 5.4. The results are presented in Table 5.3.

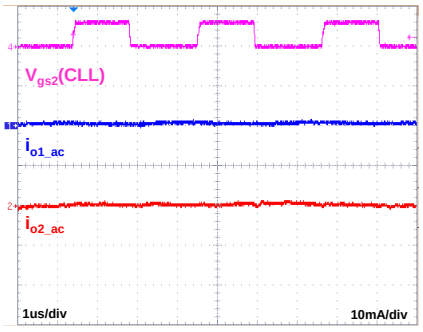

(a) 5% Dimming

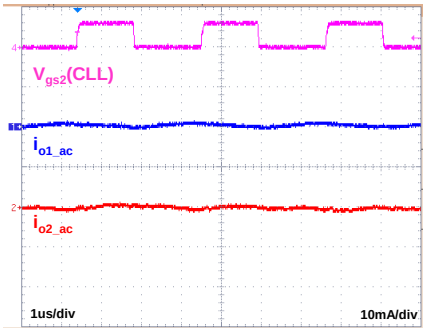

(b) 20% Dimming

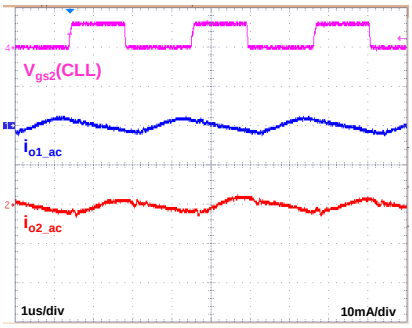

(c) 50% Dimming

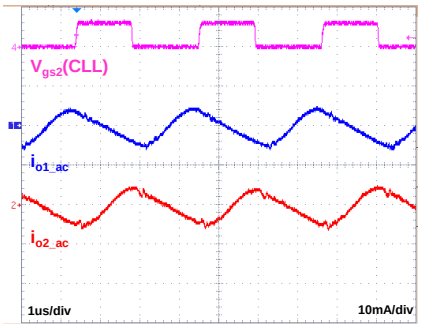

(d) Full Load

Fig. 5.4. Switching ripple of output current I_{o1} and I_{o2} (28 LEDs/string)

Table 5.3. Output currents' peak-peak switching ripple (28 LEDs/string)

Dimming Ratio	ΔIo1(mA)	ΔIo2(mA)
1.00	10.0	10.0
0.50	4.0	4.0
0.19	1.6	1.6
0.05	0.8	0.8

(2) 10 LED Strings

There are 5 transformers, and each string of these 10 LED strings has same LED number (28 LEDs/string). The output currents of these 10 LED strings under different dimming conditions are presented in Table 5.4. The waveforms of the output currents of three LED strings are presented in Fig. 5.5.

Table 5.4. Output currents of 10 LED strings (28 LEDs/string)

Dimming Ratio	Io1(A)	Io2(A)	Io3(A)	Io4(A)	Io5(A)	Io6(A)	Io7(A)	Io8(A)	Io9(A)	Io10(A)
1.00	0.303	0.303	0.301	0.301	0.300	0.300	0.299	0.299	0.298	0.298
0.50	0.152	0.151	0.150	0.150	0.148	0.149	0.147	0.147	0.147	0.147
0.19	0.058	0.058	0.056	0.056	0.055	0.055	0.054	0.054	0.053	0.054
0.05	0.016	0.016	0.014	0.014	0.013	0.013	0.012	0.012	0.012	0.012

The output currents' switching ripple of these 10 LED strings under different dimming conditions are presented in Table 5.5.

Table 5.5. Output currents' peak-peak switching ripple (28 LEDs/string)

Dimming Ratio	ΔIo1 (mA)	ΔIo2 (mA)	ΔIo3 (mA)	ΔIo4 (mA)	ΔIo5 (mA)	ΔIo6 (mA)	ΔIo7 (mA)	ΔIo8 (mA)	ΔIo9 (mA)	ΔIo10 (mA)
1.00	10.0	10.0	10.0	10.0	10.0	10.0	10.0	10.0	10.0	10.0
0.50	4.0	4.0	4.0	4.0	4.0	4.0	4.0	4.0	4.0	4.0
0.19	1.6	1.6	1.6	1.6	1.6	1.6	1.6	1.6	1.6	1.6
0.05	0.8	0.8	0.8	0.8	0.8	0.8	0.8	0.8	0.8	0.8

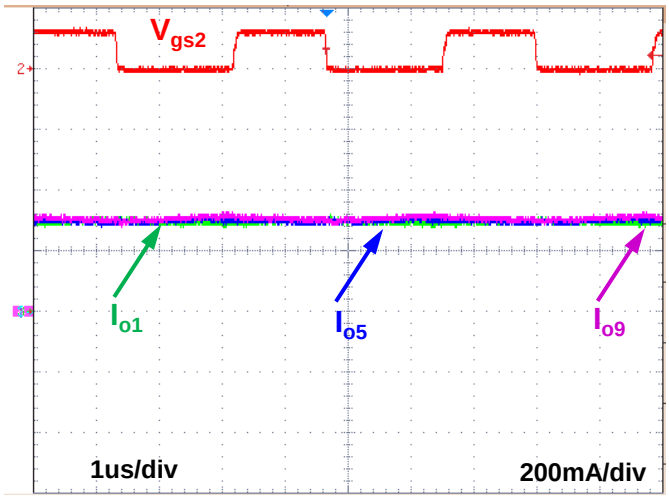

Fig. 5.5. Output currents of three LED strings (28 LEDs/string & full load)

5.1.2 Unbalanced Loads

Each LED string has 28 Xlamp MX-3 LEDs in series, as Fig. 5.3 shows. For unbalanced load condition, some LEDs in the LED strings will be shorted, as Fig. 5.6 shows.

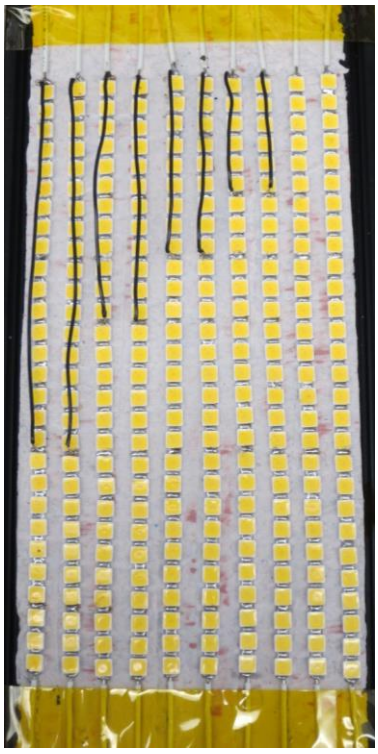

Fig. 5.6. Unbalanced Load of 2-stage LED driver: 10 LED strings with Cree XLamp MX-3 LEDs

(1) 4 LED Strings

There are 2 transformers. These 2 strings driven by #1 transformer has 28 LEDs for each string. The other 2 strings driven by #2 transformer has 10 LEDs for each string. The output voltages and output currents of these 4 LED strings under different dimming conditions are presented in Table 5.6. In contrast, those 2 string driven by #1 transformer has 10 LEDs for each string and the other 2 strings driven by #2 transformer has 28 LEDs for each string. The output voltages and output currents of these 4 LED strings under different dimming conditions are presented in Table 5.7.

Table 5.6. Output voltages and output currents of 4 LED strings (28, 10 LEDs/string)

Dimming Ratio	Vo1 (V)	Vo2 (V)	Vo3 (V)	Vo4 (V)	Io1(A)	Io2(A)	Io3(A)	Io4(A)
1.00	89.49	90.46	32.91	33.05	0.303	0.303	0.308	0.308
0.50	85.12	85.91	31.15	31.21	0.152	0.152	0.155	0.155
0.20	80.13	80.75	29.17	29.23	0.059	0.058	0.061	0.061
0.05	75.42	75.87	27.32	27.44	0.016	0.016	0.017	0.017

Table 5.7. Output voltages and output currents of 4 LED strings (10, 28 LEDs/string)

Dimming Ratio	Vo1 (V)	Vo2 (V)	Vo3 (V)	Vo4 (V)	Io1(A)	Io2(A)	Io3(A)	Io4(A)
1.00	32.42	32.50	92.00	91.86	0.303	0.303	0.298	0.298
0.50	30.57	30.68	86.79	86.59	0.152	0.152	0.148	0.148
0.19	28.64	28.75	81.19	80.96	0.058	0.058	0.055	0.055
0.05	26.85	26.99	75.99	75.83	0.016	0.016	0.014	0.014

The output currents' switching ripple of these 4 LED strings under different dimming conditions are presented in Table 5.8 and Table 5.9.

Table 5.8. Output currents' peak-peak switching ripple of 4 LED strings (28, 10 LEDs/string)

Dimming Ratio	ΔIo1(mA)	ΔIo2(mA)	ΔIo3(mA)	ΔIo4(mA)
1.00	10.0	10.0	10.0	10.0
0.50	4.0	4.0	4.0	4.0
0.20	1.6	1.6	1.6	1.6
0.05	0.8	0.8	0.8	0.8

Table 5.9. Output currents' peak-peak switching ripple of 4 LED strings (10, 28 LEDs/string)

Dimming Ratio	ΔIo1(mA)	ΔIo2(mA)	ΔIo3(mA)	ΔIo4(mA)
1.00	10.0	10.0	10.0	10.0
0.50	4.0	4.0	4.0	4.0
0.20	1.6	1.6	1.6	1.6
0.05	0.8	0.8	0.8	0.8

(2) 10 LED Strings

There are 5 transformers. 2 strings driven by #1, #2, #3, #4 and #5 transformer have 28, 22, 19, 16, 10 LEDs for each string respectively. The output currents of these 10 LED strings under different dimming conditions are presented in Table 5.10. In contrast, those 2 strings driven by #1, #2, #3, #4 and #5 transformer have 10, 16, 19, 22, 28 LEDs for each string respectively. The output currents of these 10 LED strings under different dimming conditions are presented in Table 5.11. The waveforms of the output currents of three LED strings are presented in Fig. 5.7.

Table 5.10. Output currents of 10 LED strings (28, 22, 19, 16, 10 LEDs/string)

Dimming Ratio	Io1(A)	Io2(A)	Io3(A)	Io4(A)	Io5(A)	Io6(A)	Io7(A)	Io8(A)	Io9(A)	Io10(A)
1.00	0.303	0.303	0.303	0.304	0.303	0.303	0.304	0.304	0.305	0.305
0.50	0.151	0.151	0.151	0.151	0.151	0.152	0.151	0.151	0.153	0.153
0.19	0.057	0.057	0.057	0.057	0.057	0.057	0.056	0.056	0.057	0.057
0.05	0.015	0.015	0.014	0.014	0.014	0.014	0.013	0.013	0.014	0.014

Table 5.11. Output currents of 10 LED strings (10, 16, 19, 22, 28 LEDs/string)

Dimming Ratio	Io1(A)	Io2(A)	Io3(A)	Io4(A)	Io5(A)	Io6(A)	Io7(A)	Io8(A)	Io9(A)	Io10(A)
1.00	0.303	0.303	0.299	0.300	0.298	0.298	0.296	0.296	0.294	0.295
0.50	0.151	0.150	0.148	0.148	0.146	0.146	0.145	0.145	0.143	0.144
0.19	0.058	0.058	0.057	0.057	0.056	0.056	0.055	0.055	0.055	0.055
0.05	0.016	0.016	0.014	0.014	0.013	0.013	0.012	0.012	0.012	0.012

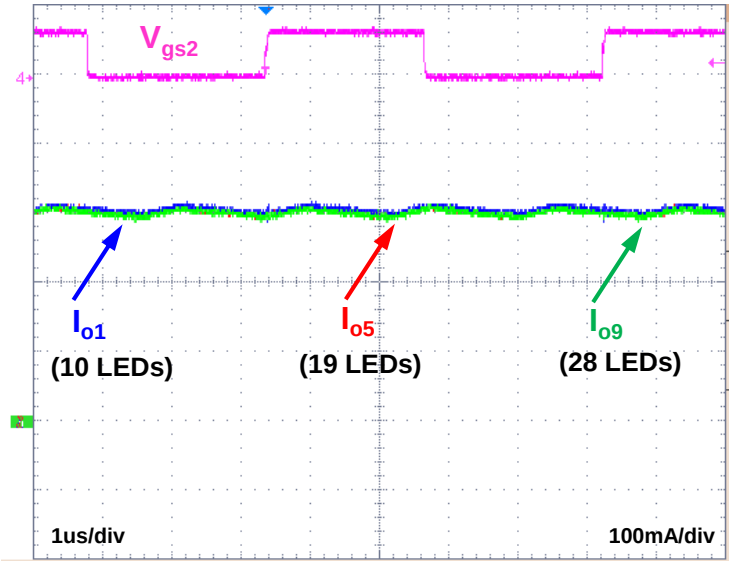

Fig. 5.7. Output currents of three LED strings (unbalanced load & full load)

The output currents' switching ripple of these 10 LED strings under different dimming conditions are presented in Table 5.12 and Table 5.13.

Table 5.12. Output currents' peak-peak switching ripple (28, 22, 19, 16, 10 LEDs/string)

Dimming Ratio	ΔIo1 (mA)	ΔIo2 (mA)	ΔIo3 (mA)	ΔIo4 (mA)	ΔIo5 (mA)	ΔIo6 (mA)	ΔIo7 (mA)	ΔIo8 (mA)	ΔIo9 (mA)	ΔIo10 (mA)
1.00	10.0	10.0	10.0	10.0	10.0	10.0	10.0	10.0	10.0	10.0
0.50	4.0	4.0	4.0	4.0	4.0	4.0	4.0	4.0	4.0	4.0
0.19	1.6	1.6	1.6	1.6	1.6	1.6	1.6	1.6	1.6	1.6
0.05	0.8	0.8	0.8	0.8	0.8	0.8	0.8	0.8	0.8	0.8

Table 5.13. Output currents' peak-peak switching ripple (10, 16, 19, 22, 28 LEDs/string)

Dimming Ratio	ΔIo1 (mA)	ΔIo2 (mA)	ΔIo3 (mA)	ΔIo4 (mA)	ΔIo5 (mA)	ΔIo6 (mA)	ΔIo7 (mA)	ΔIo8 (mA)	ΔIo9 (mA)	ΔIo10 (mA)
1.00	10.0	10.0	10.0	10.0	10.0	10.0	10.0	10.0	10.0	10.0
0.50	4.0	4.0	4.0	4.0	4.0	4.0	4.0	4.0	4.0	4.0
0.19	1.6	1.6	1.6	1.6	1.6	1.6	1.6	1.6	1.6	1.6
0.05	0.8	0.8	0.8	0.8	0.8	0.8	0.8	0.8	0.8	0.8

5.2 Conversion Efficiency

Since the CLL resonant converter is always working around the resonant frequency. It can achieve high efficiency within a wide load range. Meanwhile, the efficiency of buck converter can be optimized accordingly. Therefore, high efficiency of this 2-stage LED driver could be achieved.

5.2.1 Balanced Loads

(1) 2 LED Strings

The efficiencies of 2-stage LED driver and CLL resonant converter are tested from 5% dimming to full load condition with 1 transformer. At the same time, the LED number varies from 10 LEDs/string to 28 LEDs/string. The efficiencies of 2-stage LED driver and CLL resonant converter are presented in Fig. 5.8 and Fig. 5.9 respectively.

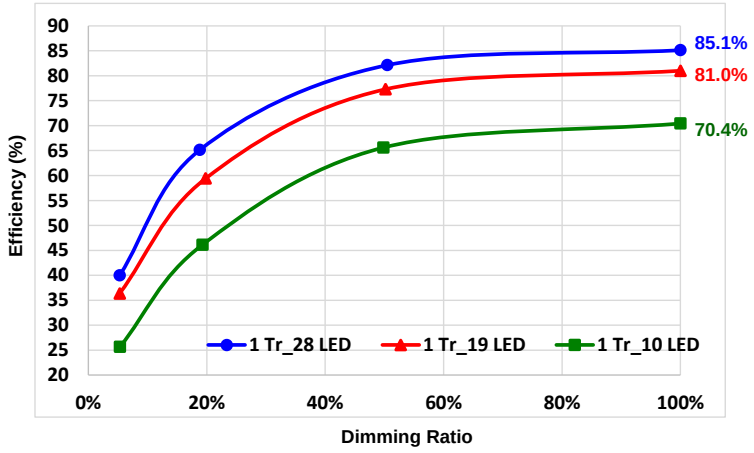

Fig. 5.8. Efficiency of 2-stage LED driver with 2 balanced LED strings

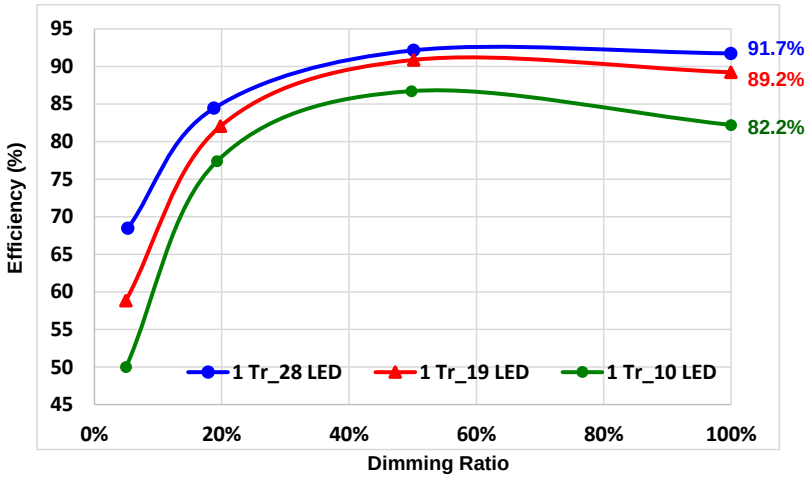

Fig. 5.9. Efficiency of CLL with 2 balanced LED strings

(3) 10 LED Strings

The efficiencies of 2-stage LED driver and CLL resonant converter are tested from 5% dimming to full load condition with 5 transformers. At the same time, the LED number varies from 10 LEDs/string to 28 LEDs/string. The efficiencies of 2-stage LED driver and CLL resonant converter are presented in Fig. 5.10 and Fig. 5.11 respectively.

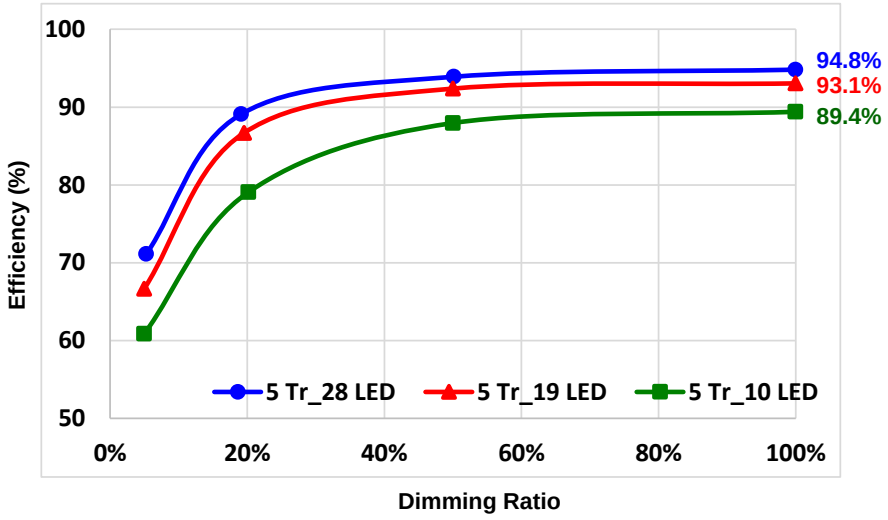

Fig. 5.10. Efficiency of 2-stage LED driver with 10 balanced LED string

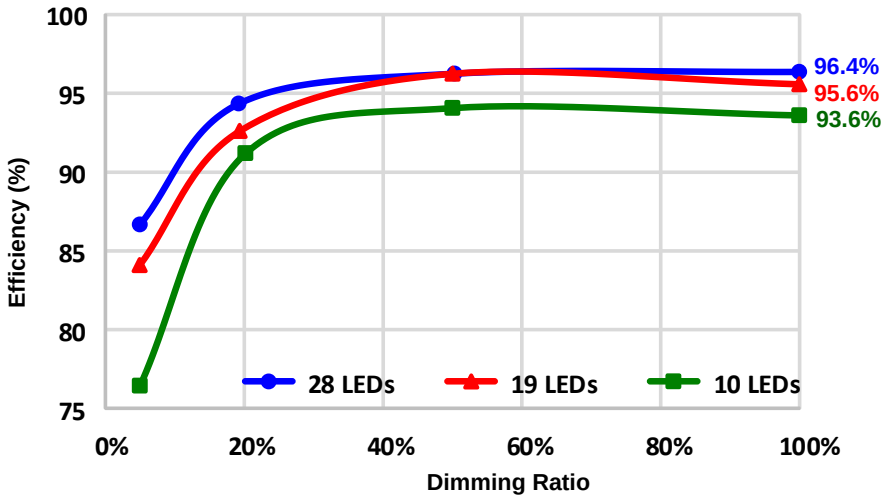

Fig. 5.11. Efficiency of CLL with 10 balanced LED strings

5.2.2 Unbalanced Loads

(1) 4 LED Strings

The efficiencies of 2-stage LED driver and CLL resonant converter are tested from 5% dimming to full load condition with 2 transformers. At the same time, the LED number of #1 transformer is 28 LEDs/string and the LED number of #2 transformer is 10 LEDs/string. In contrast, the LED number of #1 transformer is 10 LEDs/string and the LED number of #2 transformer is 28 LEDs/string. The efficiencies are also tested. The efficiencies of 2-stage LED driver and CLL resonant converter are presented in Fig. 5.12 and Fig. 5.13 respectively. For these 2 cases, the current of one LED string driven by #1 transformer is sensed for feedback control.

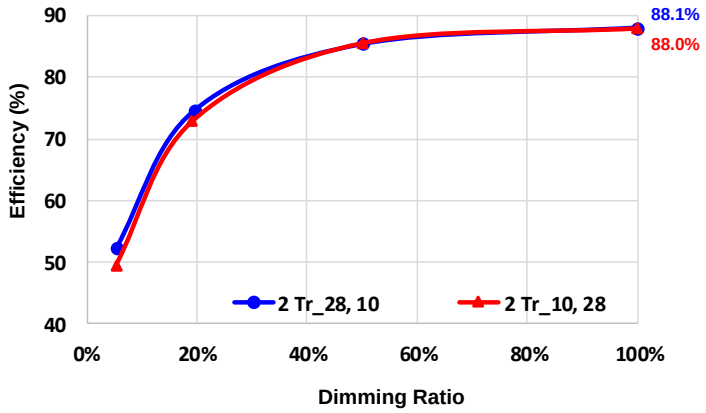

Fig. 5.12. Efficiency of 2-stage LED driver with 4 unbalanced LED string

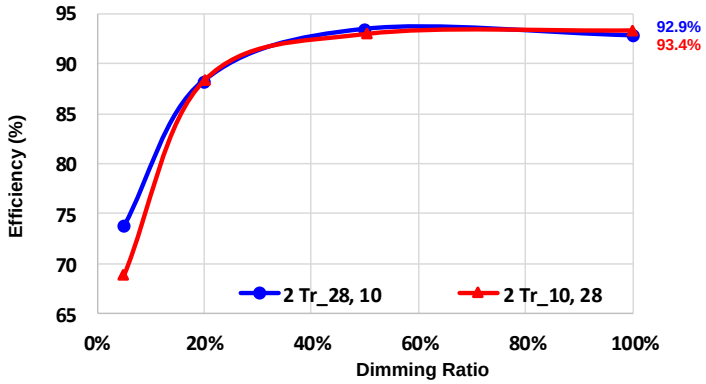

Fig. 5.13. Efficiency of CLL with 4 unbalanced LED string

(2) 10 LED Strings

The efficiencies of 2-stage LED driver and CLL resonant converter are tested from 5% dimming to full load condition with 5 transformers. At the same time, the LED number of #1, #2, #3, #4 and #5 transformer are 28, 22, 19, 16 and 10 LEDs/string respectively. In contrast, when the LED number of #1, #2, #3, #4 and #5 transformer are 10, 16, 19, 22 and 28 LEDs/string respectively, the efficiencies are also tested. The efficiencies of 2-stage LED driver and CLL resonant converter are presented in Fig. 5.14 and Fig. 5.15 respectively. For these 2 cases, the current of one LED string driven by #1 transformer is sensed for feedback control.

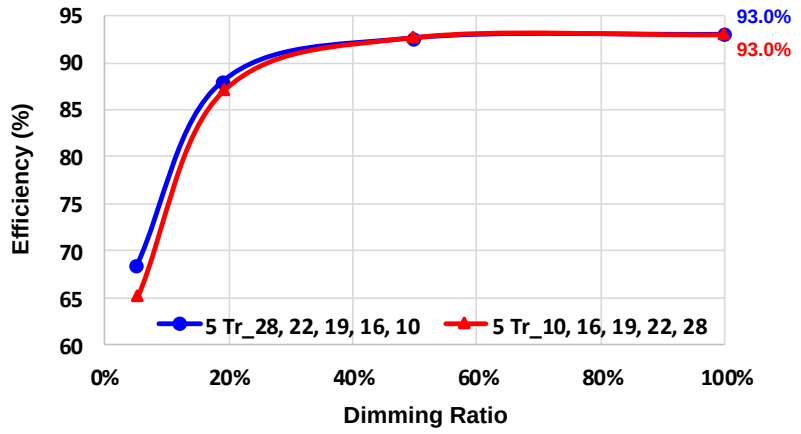

Fig. 5.14. Efficiency of 2-stage LED driver with 10 unbalanced LED strings

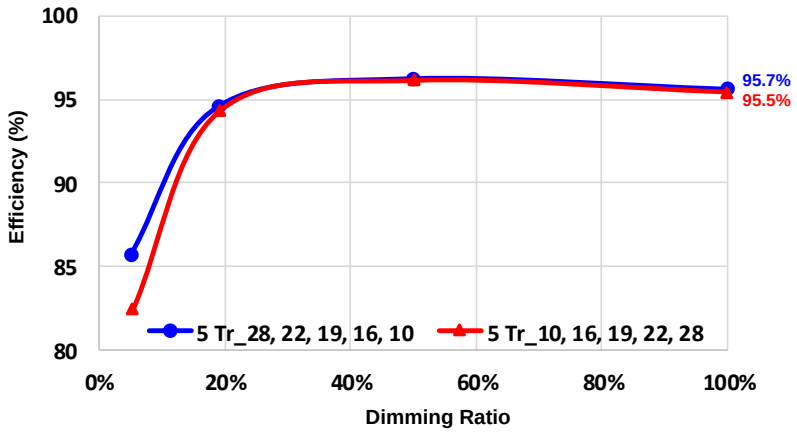

Fig. 5.15. Efficiency of CLL with 10 unbalanced LED strings

As the transformer module increases, the efficiency of the 2-stage LED driver goes up. When one transformer module is plugged in, it contributes extra core loss and winding loss resulting from transformer. Besides that, there is additional conduction loss from the secondary side rectifiers. Meanwhile, the loss caused by the resonant tank will rise as the transformer module increases. The winding loss of L_{e2} keeps the same, but the winding loss of L_{r1} will increase. The core losses of L_{r1} and L_{e2} will increase as the bus voltage rise. The conduction loss of the main switches on the primary side will be the same.

When the dimming ratio is lower like 5% dimming~20% dimming, the efficiency goes down. Working at the low dimming condition, the bus voltage will drop comparing with the full load condition. Therefore, complete ZVS of the primary-side main switches will be lost. It can only achieve partial ZVS. This will significantly impact the light load's efficiency.

If the LED number of each string is reduced, the efficiency of the 2-stage LED driver drops. Since the LED number is reduced, the forward voltage of LED string is also reduced. Finally, the bus voltage will drop. In this circumstance, only partial ZVS of the primary-side switches can be achieved. This will also impact the efficiency.

Since CLL resonant converter is working around the resonant frequency, the primary-side switches can achieve ZVS and the secondary-side rectifier diode can achieve ZCS. Soft switching is guaranteed within a wide load range. Its major loss is contributed by the conduction losses of the primary-side main switches and secondary-side rectifier when it is working under the full load condition. For buck converter, it is hard switching for the upper-side MOSFET. So the switching loss of the upper-side MOSFET is the dominant loss within a wide load range.

Chapter 6. Conclusion and Future Work

6.1 Conclusion

MC^3 CLL resonant converter is proposed for the multiple LED strings application. Its voltage gain characteristic and the operation principle are similar to the LLC's. However, its unique characteristics are investigated for driving LEDs. Larger magnetizing inductance Lm is good for current balance among LED strings, especially when the load is unbalanced. ZVS of primary side witches could be achieved by designing L_{r1} properly. Voltage gain of CLL at resonant frequency point is higher than one, which is useful for the voltage step-up application as well.

After investigate the characteristic of MC^3 CLL resonant converter, a prototype of two-stage LED driver with CLL resonant converter as the second stage is carefully designed. The complete design procedure of MC^3 CLL resonant converter is presented. The key point of the design procedure is how to design the resonant tank. First of all, the turns ratio of the transformer is determined according to the specification of the LED driver. Then the primary side switches, dead time t_d and L_p are set in order to achieve the lowest conduction loss. Finally, L_{r1} and L_{e2} are ascertained on account of the ZVS requirement. C_r is determined based on the resonant frequency. In the design process, the junction capacitors of the secondary-side rectifiers have significant influence on the ZVS achievement of the primary-side switches. Since the rectifiers' junction capacitors resonate with L_{e2} and output capacitors of the primary-side switches during dead time, it must be taken into account with the voltage step-up transformer.

In order to design an appropriate compensator for this two-stage LED driver, its small-signal model is derived and verified. The small-signal model of buck converter is presented based on Vatche Varperian's three-terminal switch model. And the small-signal model of MC^3 CLL

resonant converter is obtained according to Eric Yang's model for resonant converter. Combine these two small-signal together, the small-signal model for this two-stage LED driver is got. The derived model is verify with the simulation. It is accurate up the switching frequency of buck converter. The PI compensator is used for the feedback control and the control strategy is easy to implement. Just the current of one specific LED string is sensed for feedback control and the currents of other LED strings are cross-regulated. With respect of the electrical characteristics of the solid state light source, the start-up process of the LED driver is also investigated. A RC network is added into the loop of the dimming signal, and the soft start-up of the LED driver is achieved without current overshoot.

A prototype of two-stage LED driver is built in lab. Its current balance capability is illustrated under the balanced load and the severe unbalanced load condition. It guarantees good current balance among multiple LED strings regardless of the load condition. In addition, the efficiencies of the MC^3 CLL resonant converter and the two-stage LED driver are presented. Since the ZVS of the primary-side switches is achieved within a wide load range, high efficiencies of the MC^3 CLL resonant converter and the two-stage LED driver are attained from 20% dimming to full load condition.

6.2 Future Work

Beside voltage mode control, other advanced control strategies could be applied to this two-stage LED driver. For buck converter, current mode control is a good candidate to achieve better control performance. For CLL, the switching frequency could be fine-tuned around the resonant frequency according to the load condition to find the best efficiency point.

Besides the analog dimming method, which has been used for this two-stage LED driver, PWM dimming method is an alternative to achieve better dimming performance and higher efficiency, especially under the lower dimming condition. Additionally, digital controller could be applied to with more advanced control scheme, like the trajectory control.

Appendix A. Pre-resonance Between L_{e2} and C_{jp} Before Dead Time

Usually, when the CLL resonant converter is working around the resonant frequency, as shown in Fig. A.1, i_{Cr} is equal to i_{Lr1} at the beginning of the dead time and i_{Cr} is almost equal to i_{Lr1} at the end of the dead time. In a word, the operation during dead time has little impact on the normal CLL resonant process. However, the junction capacitor will take part in the dead time process, and the influence of the junction capacitor is significant especially when the value of C_{jp} is close to the value of C_{oss}. L_{e2} will resonate with C_{oss} and C_{jp} during the dead time. Therefore, when CLL resonant converter is still working around the resonant frequency, as shown in Fig. A.2, i_{Cr} is much less than i_{Lr1} at the end of the dead time due to the resonance during dead time. Therefore, the normal CLL resonance process will be impacted. As a result, $i_{Cr}=i_{Lr1}$ before the dead time and the CLL resonance ends earlier than expectation. Consequently, the operation process during dead time is also impacted since the initial conditions have been changed. Meanwhile, ZVS of the primary-side switches will be influenced as well.

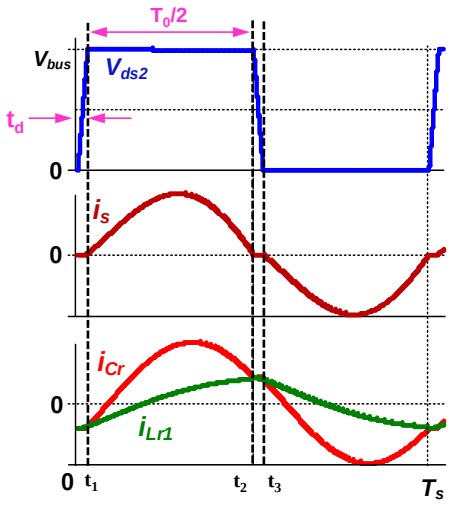

Fig. A.1 Waveforms of CLL resonant converter working at resonant frequency (W/O junction caps)

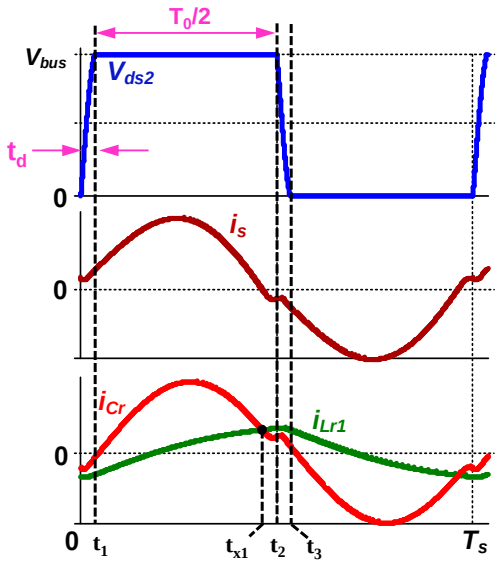

Fig. A.2. Waveforms of CLL resonant converter working at resonant frequency (W/ junction caps)

According to Fig. A.2, from t_1 to t_2, Q_1 is on and Q_2 is off. However, there will be two operation processes during this interval. During [t_1, t_{x1}], the energy is transferred from the primary side to the secondary side, as (a) of Fig. A.3 illustrates. When $t=t_{x1}$, $i_{Cr}=i_{Lr1}$. During [t_{x1}, t_2], Q_1 is still on and Q_2 is still off. However, L_{e2} and C_j starts to resonate when $t=t_{x1}$, as (b) of Fig. A.3 shows. This phase is not the normal operation of CLL resonance and there is no energy transfer from the primary side to the secondary side. The equivalent circuit during t_{x1} to t_1 is illustrated in Fig. A.4.

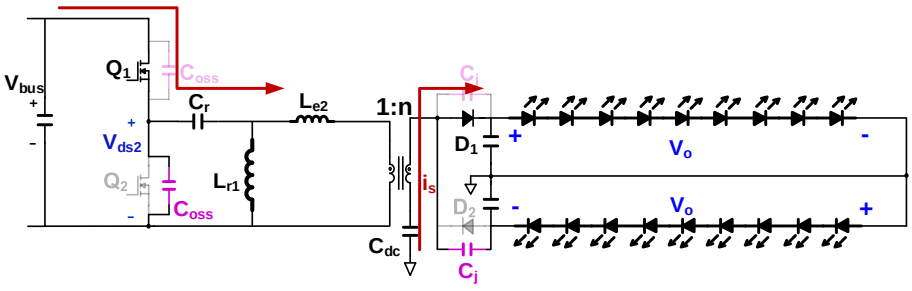

(a) Time interval from t_1 to t_{x1} (Q_1 is on and Q_2 is off)

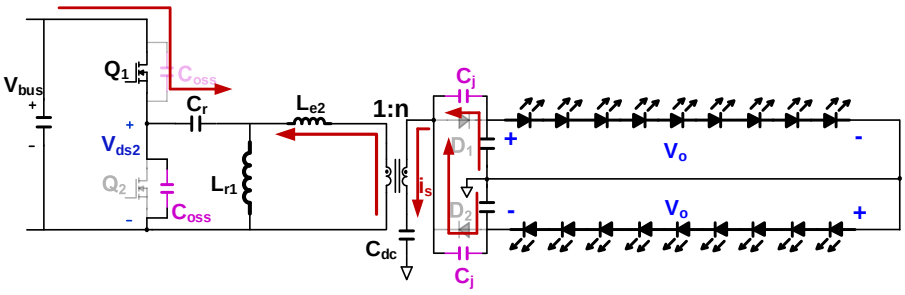

(b) Time interval from t_{x1} to t_2 (Q_1 is on and Q_2 is off)

Fig. A.3. Operation of CLL resonant converter during t_1 to t_2

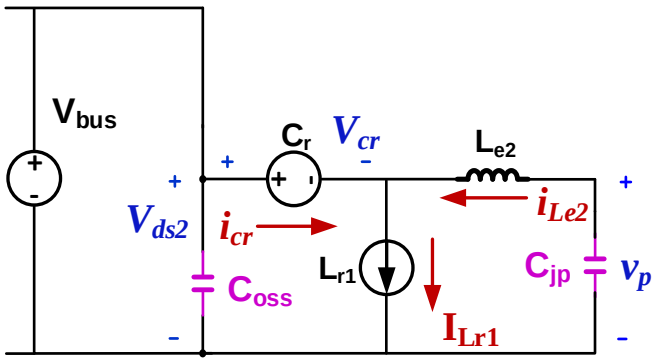

Fig. A.4. Equivalent circuit during t_{x1} to t_2

Take the case with five transformer modules as example, the state equations of the equivalent circuit during t_{x1} to t_2 are as follows

$$\frac{dv_p}{dt} = -\frac{i_{Le2}}{C_{jp}}, \tag{A.1}$$

$$\frac{di_{Le2}}{dt} = -\frac{1}{L_{e2}}(V_{ds2} - V_{cr} - v_p), \tag{A.2}$$

$$I_{Lr1} = i_{cr} + i_{Le2}. \tag{A.3}$$

The initial conditions for the phase during tx1 to t2 are as follows

$$I_{Lr1} \approx \frac{5V_o}{nL_{r1}} \cdot \frac{T_0}{4};$$

$V_{cr} = \frac{V_{bus}}{2} + \frac{n^2 v_p(0)}{5R_L} \cdot \frac{\pi}{2} \cdot \omega_0 L_{e2}$;

$v_{ds2}(0)=V_{bus}$;

$v_p(0)=5V_o/n$;

$i_{cr}(0)=I_{Lr1}$.

Solve the state equations with the initial conditions, we can get the following expressions in time domain

$$i_{Le2}(t) = \frac{A_1}{\omega_1}\sin(\omega_1 t). \tag{A.4}$$

$$i_{Cr}(t) = I_{Lr1} - \frac{A_1}{\omega_1}\sin(\omega_1 t). \tag{A.5}$$

$$v_p(t) = v_p(0) - \frac{A_1}{C_{jp}G_1}\left[1-\cos(\omega_1 t)\right]. \tag{A.6}$$

where $A_1 = \frac{v_p(0) + V_{Cr} - V_{bus}}{L_{e2}}$, $G_1 = \frac{1}{L_{e2}C_{jp}}$, $\omega_1 = \sqrt{G_1}$.

The coefficient of $i_{Le2}(t)$ is $\frac{A_1}{\omega_1} = \frac{v_p(0)}{5N^2R_o} \cdot \frac{\pi}{2} \cdot \omega_0 \sqrt{L_{e2}C_{jp}}$, which is proportional to $\sqrt{L_{e2}}$.

Meanwhile, the coefficient of $v_p(t)$ is $\frac{A_1}{C_{jp}G_1} = \frac{v_p(0)}{5N^2R_o} \cdot \frac{\pi}{2} \cdot \omega_0 L_{e2}$, which is proportional to L_{e2}.

$i_{Le2}(t)$ and $v_p(t)$ with different L_{e2} are presented in Fig. A.5. L_{e2} determines the resonant frequency of $i_{Le2}(t)$ and $v_p(t)$. The smaller L_{e2} is, the higher the resonant frequency will be. Meanwhile, L_{e2} also determines the oscillation amplitude of $i_{Le2}(t)$ and $v_p(t)$. The larger L_{e2} is, the larger the

oscillation amplitude will be. Therefore, with a smaller L_{e2}, the pre-resonance has little impact on the operation process during the dead time. As L_{e2} increases, the influence of pre-resonance becomes more significant.

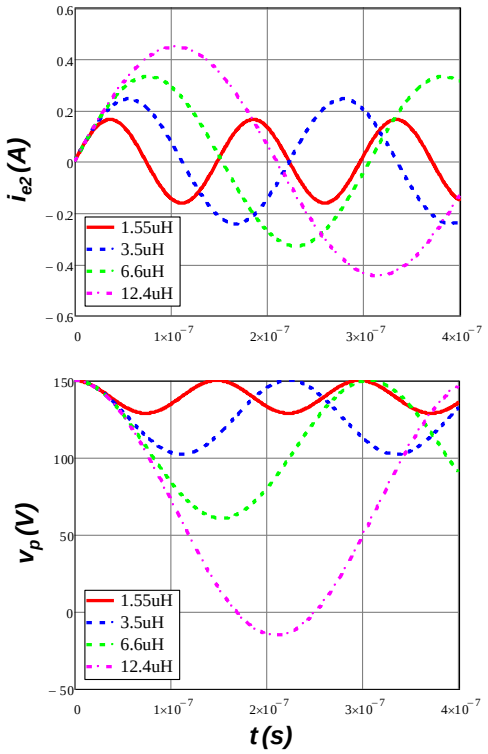

Fig. A.5. Pre-resonance waveforms of $i_{Le2}(t)$ and $v_p(t)$ with different L_{e2}

As the dead time interval starts, Q_1 and Q_2 are both turned off. L_{e2} will resonate with C_{oss} and C_{jp}. The equivalent circuit is presented in Fig. 3.15, which is the same as the case without pre-resonance. Therefore, the state equations of the equivalent circuit are also the same as (3.35) to (3.38). The difference comes from the initial conditions, which are influenced by the pre-resonance. The initial conditions are as follows

$$I_{pk} = \frac{5V_o}{nL_{r1}} \cdot \frac{T_0}{4};$$

$V_{cr} = \frac{V_{bus}}{2} + \frac{n^2 v_p(0)}{5R_L} \cdot \frac{\pi}{2} \cdot \omega_0 L_{e2}$;

$v_{ds2}(0)=V_{bus}$;

$v_p(0)= V_{p0}$;

$i_{Le2}(0)=I_{e20}$;

$i_{cr}(0)=I_{pk}-I_{e20}$.

Solve the state equations with the initial conditions, we can get the following expressions in time domain.

$$i_{Le2}(t) = \frac{D_2}{G} + 2V_2 \cos(\omega_d t + \theta_2). \tag{A.7}$$

$$i_{Cr}(t) = I_{pk} - \frac{D_2}{G} - 2V_2 \cos(\omega_d t + \theta_2). \tag{A.8}$$

$$v_p(t) = v_p(0) - \frac{D_2}{C_{jp}G} \cdot t - \frac{2V_2}{C_{jp}\omega_d}\left[\sin(\omega_d t + \theta_2) - \sin(\theta_2)\right]. \tag{A.9}$$

$$v_{ds2}(t) = v_{ds2}(0) - \frac{I_{pk}}{2C_{oss}} \cdot t + \frac{D_2}{2C_{oss}G} \cdot t + \frac{V_2}{C_{oss}\omega_d}\left[\sin(\omega_d t + \theta_2) - \sin(\theta_2)\right]. \tag{A.10}$$

where $A_2 = I_{e20}$,

$B_2 = \frac{v_p(0) + V_{Cr} - V_{bus}}{L_{e2}}$,

$D_2 = \frac{I_{pk}}{2C_{oss}L_{e2}}$,

$$G = \frac{2C_{oss} + C_{jp}}{2C_{oss}C_{jp}} \cdot \frac{1}{L_{e2}},$$

$$\omega_d = \sqrt{G},$$

$$V_2 = \frac{\sqrt{(A_2\omega_d^2 - D_2)^2 + (B_2\omega_d)^2}}{2G},$$

$$\cos(\theta_2) = \frac{A_2\omega_d^2 - D_2}{\sqrt{(A_2\omega_d^2 - D_2)^2 + (B_2\omega_d)^2}}.$$

For example, when L_{e2}=6.6uH and L_{r1}=95.6uH, C_r=45.6nF, the simulation waveforms of CLL resonant converter without pre-resonance and with pre-resonance are presented in Fig. A.6 and Fig. A.7 respectively. Due to the resonance between L_{e2} and C_{oss}, C_{jp} during the dead time, i_{Cr}<i_{Le2} at the end of the dead time. Therefore, the normal CLL resonance will be influenced when the primary-side switch turns on. As a result, the operation during the dead time will also be impacted, as Fig. A.7 shows.

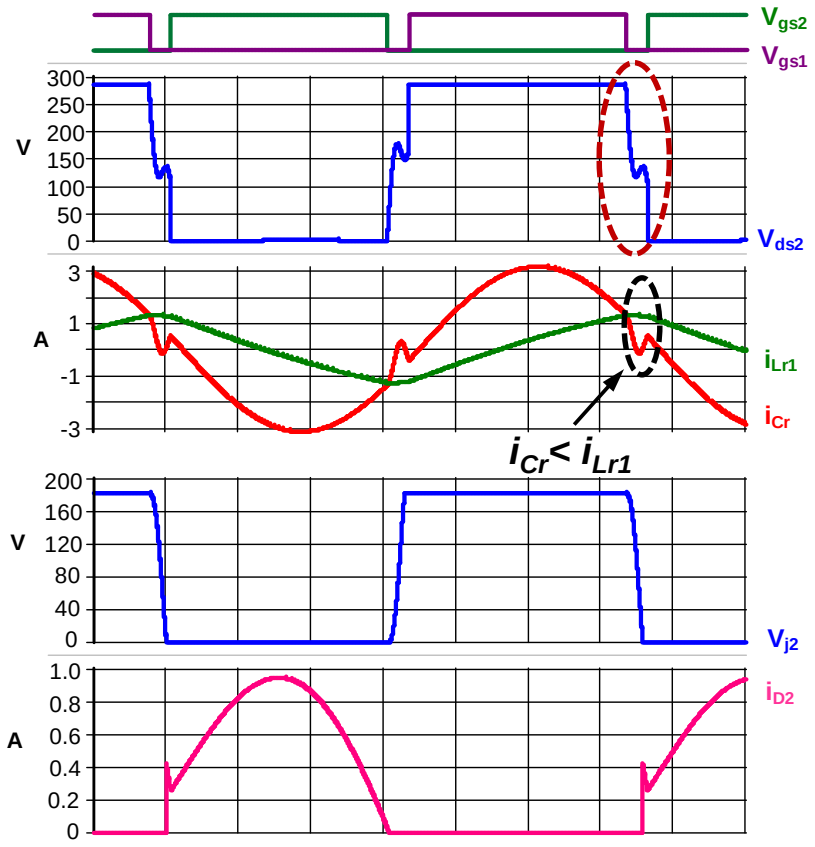

Fig. A.6. Waveforms of CLL resonant converter without pre-resonance

With the pre-resonance, the ZVS achievement of Q_1 and Q_2 will not comply with the conclusions based on the previous analysis. The total charge provided by i_{Cr} during dead time t_d can be obtained by the integration of (A.8), so it is

$$Q_{Cr2} = \int_0^{t_d} i_{Cr}(t)dt = I_{pk}t_d - \frac{D_2}{G}\cdot t_d - \frac{2V_2}{\omega_d}\left[\sin(\omega_d t_d + \theta) - \sin(\theta)\right]. \quad \text{(A.11)}$$

The coefficients of Q_{Cr2} are strongly related to L_{r1} and L_{e2}. When there are 10 LED strings and LEDs are working under full-load condition, the bus voltage is about 300V and the output capacitor of STB11NM60FD is about 150pF. The total charge needed for the ZVS achievement is given in (3.37).

If the ZVS of the primary-side switches could be achieved during dead time, the following inequality should be met.

$$Q_{Cr2} \geq Q_{oss} = 90nC. \tag{A.12}$$

The bottleneck for this method is to get the initial condition of i_{e2} and v_p for analyzing the dead time process. The concept of this method is also based on the charge needed for the ZVS achievement.

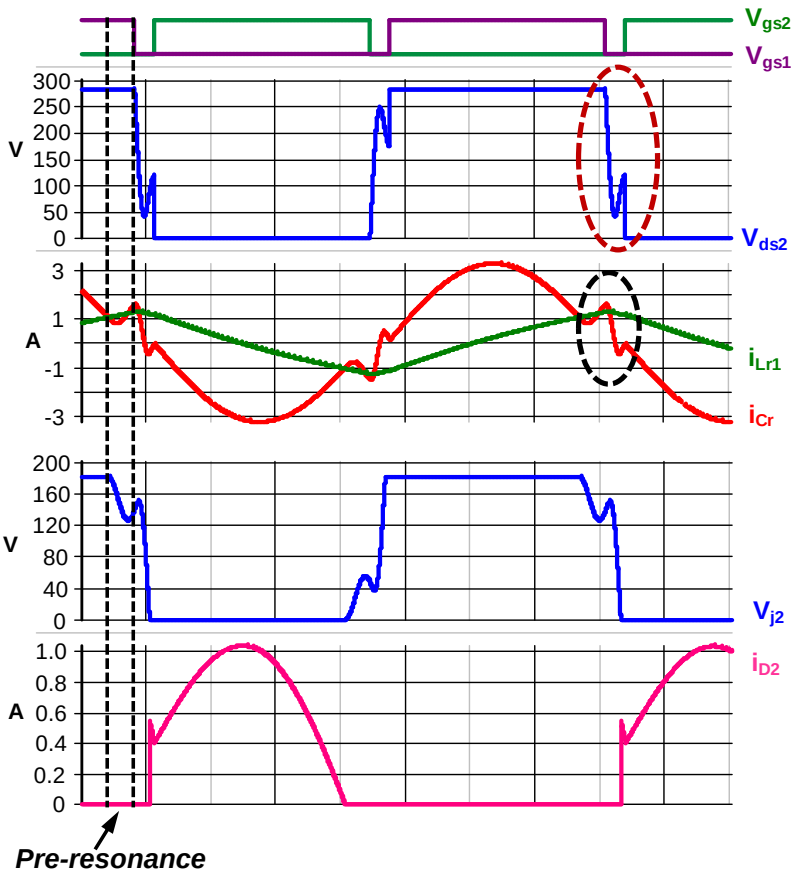

Fig. A.7. Waveforms of CLL resonant converter with pre-resonance

For example, when L_{r1}=95.6uH, the relationship between Q_{Cr} and L_{e2} is presented in Fig. 3.16. Under this circumstance, when L_{e2}=12.9uH, the ZVS requirement is not met because $Q_{Cr}<Q_{oss}$, as Fig. A.8 shows. With known L_{r1} and L_{e2}, C_r can be designed according to the resonant frequency.

In this case, C_r=25nF. The simulation results without pre-resonance are presented in Fig. A.9. The primary-side switches Q_1 and Q_2 can only achieve partial ZVS. However, when CLL resonant converter is working around the resonant frequency, there will be pre-resonance between L_{e2} and C_j before the dead time. The operation during the dead time will be influenced. The experiment results are presented in Fig. A.10. ZVS is achieved with the help of the pre-resonance.

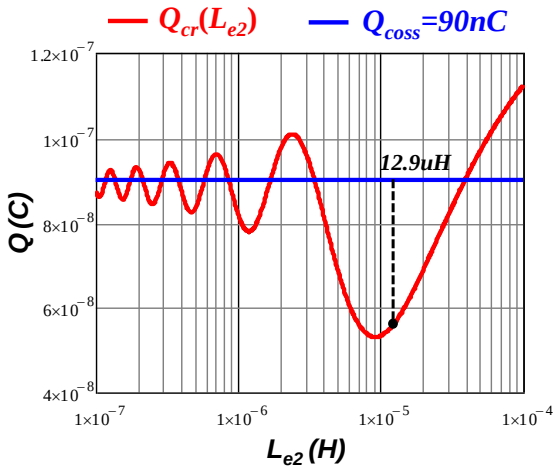

Fig. A.8. Q_{Cr}<Q_{oss} (L_{r1}=95.6uH, L_{e2}=12.9uH)

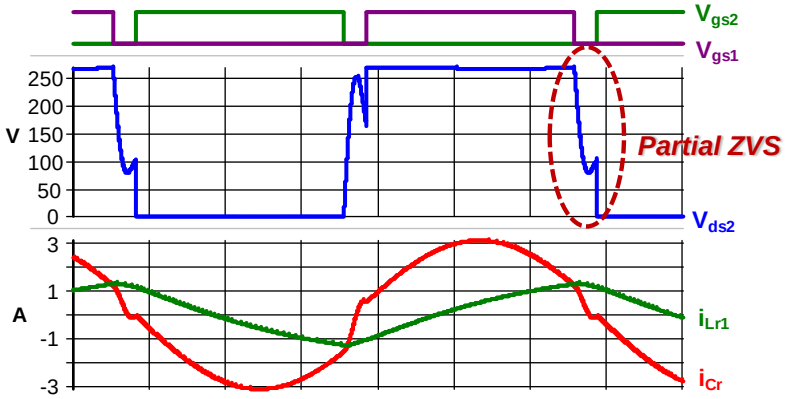

Fig. A.9. Simulation results without pre-resonance (L_{r1}=95.6uH, L_{e2}=12.9uH)

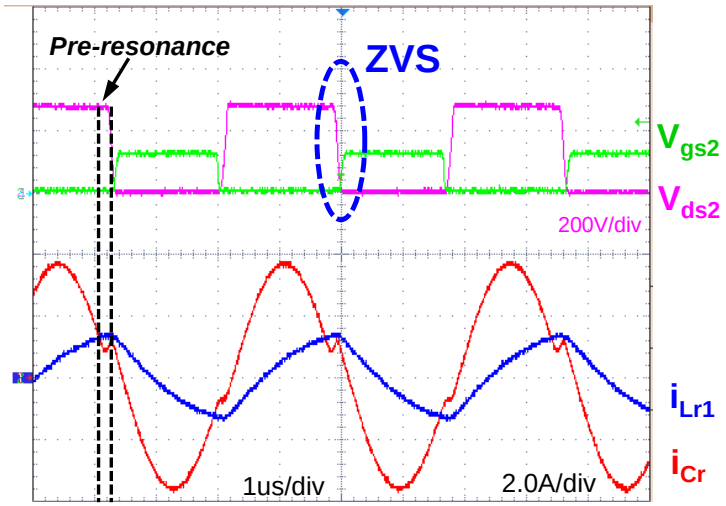

Fig. A.10. Simulation results with pre-resonance (L_{r1}=95.6uH & L_{e2}=12.9uH)

References

[1] Light-emitting diode [Online]. Available: http://en.wikipedia.org/wiki/Light-emitting_diode#Lighting.

[2] C. Chen, C. Wu, Y. Chen, and T. Wu, "Sequential color LED backlight driving system for LCD panels," *IEEE Trans. Power Electron.*, vol. 22, no. 3, pp. 919–925, May 2007.

[3] Y. Hu and M. M. Jovanovic, "LED driver with self-adaptive drive voltage," *IEEE Trans. Power Electron.*, vol. 23, no. 6, pp. 3116–3125, Nov. 2008.

[4] TI's Application Report, "Ballast Resistor Calculation-Current Matching in Parallel LEDs," April, 2009.

[5] K. I. Hwu and S. C. Chou, "A simple current-balancing converter for LED lighting," in *Proc. IEEE Appl. Power Electron. Conf. (APEC),* 2009, pp. 587-590.

[6] Y. Hu and M. M. Jovanovic, "A new current-balancing method for paralleled LED strings," in *Proc. IEEE Appl. Power Electron. Conf. (APEC),* 2011, pp. 705-712.

[7] S. Choi, P. Agarwal, T. Kim, J. Yang and B. Han, "Symmetric current balancing circuit for multiple DC loads," in *Proc. IEEE Appl. Power Electron. Conf. (APEC),* 2010, pp. 512-518.

[8] S. Ji, H. Wu and F. C. Lee, "Multi-channel constant current source and illumination source," U.S. Patent, US 2011/0291574 A1, May 24, 2011.

[9] S. Ji, H. Wu, X. Ren, and F. C. Lee, "Multi-channel constant current (MC^3) LED driver," in *Proc. IEEE Appl. Power Electron. Conf. (APEC),* 2011, pp. 718-722.

[10] Texas Instruments User's Guide, "UCC28810EVM-003 110-W multiple string LED driver with universal line input and PFC," Texas Instruments Incorporated, Dallas, Texas, Nov. 2010.

[11] J. Zhang, L. Xu, X. Wu and Z. Qian, "A precise passive current balancing method for multioutput LED drivers," *IEEE Trans. Power Electron.*, vol. 26, no. 8, pp. 2149–2159, Aug. 2011.

[12] J. Wang, J. Zhang, X. Huang and L. Xu, "A family of capacitive current balancing methods for multi-output LED driver," in *Proc. IEEE Appl. Power Electron. Conf. (APEC)*, 2011, pp. 2040-2046.

[13] J. Zhang, J. Wang and X. Wu, "A capacitor-isolated LED driver with inherent current balance capability," *IEEE Trans. Power Electron.*, vol. 59, no. 4, pp. 1708–1716, Apr. 2012.

[14] H. Wu, S. Ji, F. C. Lee, and X. Wu, "Multi-channel constant current (MC^3) LLC resonant LED driver," in *Proc. IEEE Energy Conv. Congr. Expo (ECCE)*, 2011, pp. 2568-2575.

[15] W. Feng and F. C. Lee, "Multi-channel two-stage controllable constant current source and illumination source," U.S. Patent, US 2013/0285565 A1, Oct. 31, 2013.

[16] X. Wu, J. Zhang, and Z. Qian, "A simple two-channel LED driver with automatic precise current sharing," *IEEE Trans. Ind. Electron.*, vol. 58, no. 10, pp. 4783-4788, Otc. 2011.

[17] D. J. Tschirhart and P. K. Jain, "A CLL resonant asymmetrical pulsewidth-modulated converter with improved efficiency," *IEEE Trans. Ind. Electron.*, vol. 55, no. 1, Jan. 2008.

[18] D. Huang, D. Fu, F. C. Lee, and P. Kong, "High-Frequency High-Efficiency CLL Resonant Converters with Synchronous Rectifiers," *IEEE Trans. Ind. Electron.*, vol. 58, no. 8, pp. 3461-3470, Aug. 2011.

[19] Ferroxcube, "Soft Ferrites and Accessories". Sep. 2008.

[20] *IPB65R280C6 Datasheet*, Infineon Technologies AG, Munich, Germany, 2010.

[21] B. Yang, F. C. Lee, A. J. Zhang, and G. Huang, "LLC resonant converter for front end DC/DC converter," in *Proc. IEEE Appl. Power Electron. Conf. (APEC)*, 2002, pp. 1108-1112.

[22] B. Lu, W. Liu, Y. Liang, F. C. Lee, and J. D. van Wyk, "Optimal design methodology for LLC resonant converter," in *Proc. IEEE Appl. Power Electron. Conf. (APEC),* 2006, pp. 533-538.

[23] W. Feng, P. Mattavelli, and F. C. Lee, "Pulsewidth locked loop (PWLL) for automatic resonant frequency tracking in LLC DC-DC transformer (LLC-DCX)," *IEEE Trans. Power Electron.*, vol. 28, no. 4, pp. 1862-1869, Apr. 2011.

[24] Y. Yang, D. Huang, F. C. Lee and Q. Li, "Transformer shielding technique for common mode noise reduction in isolated converters," in *Proc. IEEE Energy Conv. Congr. Expo. (ECCE),* 2013, pp. 4149-4153.

[25] Y. Yang, D. Huang, F. C. Lee and Q. Li, "Analysis and reduction of common mode EMI moise for resonant converter," in *Proc. IEEE Appl. Power Electron. Conf. (APEC),* 2014, pp. 566-571.

[26] H. Hsieh, L. Huwang, T. Lin and D. Chen, "Use of a C_z common-mode capacitor in two-wire and three-wire offline power supplies," *IEEE Trans. Ind. Electron.*, vol. 55, no. 3, pp. 1435-1443, Mar. 2008.

[27] V. Vorperian, "Simplified analysis of PWM converters using model of PWM switch part I: continuous conduction mode", *IEEE Transactions on Aerospace and Electronic System,* vol. 26, no. 3, pp. 490-496, May 1990.

[28] V. Vorperian, "Simplified analysis of PWM converters using model of PWM switch part II: discontinuous conduction mode", *IEEE Transactions on Aerospace and Electronic System,* vol. 26, no. 3, pp. 497-505, May 1990

[29] E. X. Yang, F. C. Lee and M. M. Jovanovic, “Small-signal modeling of series and parallel resonant converters”, in *Proc. IEEE Appl. Power Electron. Conf. (APEC),* 1992, pp. 785-792.

[30] E. X. Yang, “Extended describing function method for small-signal modeling of resonant and multi-resonant converters,” Ph. D. dissertation, Virginia Tech, Blacksburg, VA, 1994.